

DOXORUBICIN INHIBITS CARDIOMYOCYTE AUTOPHAGIC FLUX  
BY SUPPRESSING LYSOSOMAL ACIDIFICATION

APPROVED BY SUPERVISORY COMMITTEE

---

Joseph A. Hill, M.D., Ph.D. (Mentor)

---

Hesham A. Sadek, M.D., Ph.D. (Committee Chair)

---

Beth Levine, M.D.

---

James F. Amatruda, M.D., Ph.D.

## DEDICATION

To Dr. Joseph A. Hill, who has always been a wonderful mentor and role model. As a mentor, he provides insightful guidance while granting ample flexibility. As a clinician-scientist, his devotion and hard working ethics are more than inspiring. What I most hope to learn from him is his composure and perseverance in face of difficulties and setbacks. Without doubt I will continue to benefit from him as a role model in the years to come. Thanks Joe, I owe you a lot!

To Dr. Thomas Gillette, who taught me how to pipette correctly on my first day of lab rotation and who directly witnessed my greenest days in Graduate School. Thank you for your advice, suggestions, and your help in my growth as a young scientist.

To Drs. Zully Pedrozo and Zhao Wang, who have been encouraging and helpful, especially during the days when I was groping in the dark “tunnel” of my research work. Thank you for listening to my ideas and helping me to shape them better. Thank you for inspiring me with your passions for science.

To my committee members, who have set good examples of excellent scientists for me, who have provided their constructive advice and insightful criticisms, and who have been so supportive and helpful.

To my parents Yunbiao and Shuling, for their love, support and understanding. They provided me with the best educations; they supported me wholeheartedly even when they hold different opinions. Their love and confidence in me are the sources of my strength.

Finally, to my grandfather. The jokes that he told numerous times on summer nights were funny every single time when he told them; the smell of his jasmines was the best memories of my childhood; his adventures in youth were the very admirations in my school times. And without his trust and support, I probably would not land in Graduate School in face of everyone else’s objection. To me he is and will always be a symbol of bravery, independence and enlightenment.

DOXORUBICIN INHIBITS CARDIOMYOCYTE AUTOPHAGIC FLUX BY SUPPRESSING  
LYSOSOMAL ACIDIFICATION

by

Dan Li

DISSERTATION/THESIS

Presented to the Faculty of the Graduate School of Biomedical Sciences

The university of Texas Southwestern Medical Center at Dallas

In Partial Fulfillment of the Requirements

For the Degree of

DOCTOR OF PHILOSOPHY

The university of Texas Southwestern Medical Center at Dallas

May, 2015

Copyright

By

Dan Li, 2015

All Rights Reserved

## ABSTRACT

### DOXORUBICIN INHIBITS CARDIOMYOCYTE AUTOPHAGIC FLUX BY SUPPRESSING LYSOSOMAL ACIDIFICATION

DAN LI

THE UNIVERSITY OF TEXAS SOUTHWESTERN MEDICAL CENTER AT DALLAS, 2015

SUPERVISING MENTOR: JOSEPH A. HILL, M.D., PH.D.

The clinical use of doxorubicin is limited by cardiotoxicity. Dysregulation of autophagy in the myocardium has been implicated in a variety of cardiovascular diseases. However, the role of autophagy in doxorubicin cardiomyopathy remains poorly defined.

Most models of acute doxorubicin cardiotoxicity involve intraperitoneal injection of high-dose drug, which elicits lethargy, anorexia, weight loss, and peritoneal fibrosis, all of which confound the interpretation of autophagy. Given this, I first established a model that provokes modest and progressive cardiotoxicity without constitutional symptoms, and is reminiscent of the effects seen in patients of chronic doxorubicin cardiomyopathy. Next, via multiple assays I showed that doxorubicin blocks cardiomyocyte autophagic flux *in vivo* and in cardiomyocytes in culture. This block was accompanied by robust accumulation of undegraded autolysosomes. Moreover, I went on to localize the site of block as a defect in lysosome acidification. To test the

functional relevance of doxorubicin-triggered autolysosome accumulation, I studied animals with diminished autophagic activity due to haploinsufficiency for *Beclin 1*. *Beclin 1*<sup>+/-</sup> mice exposed to doxorubicin manifested restored cardiac autophagic flux, and were protected in terms of structural and functional changes within the myocardium. Conversely, animals over-expressing *Beclin 1* manifested an amplified cardiotoxic response, correlating with their aggravated accumulation of autolysosomes in cardiomyocytes after doxorubicin treatments.

In summary, I report here that doxorubicin blocks autophagic flux in cardiomyocytes by impairing lysosome acidification and lysosomal function. Further, reducing autophagy initiation may protect against doxorubicin cardiotoxicity.

## TABLE OF CONTENTS

ABSTRACT.....	v
TABLE OF CONTENTS.....	vii
PRIOR PUBLICATIONS.....	ix
LIST OF FIGURES AND TABLES.....	x
ABBREVIATIONS.....	xii

### CHAPTER 1. INTRODUCTION

Cardiovascular perils of anti-cancer therapies.....	2
Doxorubicin cardiomyopathy and heart failure.....	2
Models of doxorubicin cardiotoxicity.....	3
Mechanisms proposed for doxorubicin cardiomyopathy.....	5
Autophagy, a dynamic flux process.....	11
Assays for monitoring autophagic flux.....	13
Autophagy in cardiac diseases: friend or foe?.....	14
Autophagy's controversial role in doxorubicin cardiotoxicity - previous studies.....	17
Central Thesis.....	20
Chapter 1 References.....	22

### CHAPTER 2. DOXORUBICIN INHIBITS CARDIOMYOCYTE AUTOPHAGIC FLUX BY SUPPRESSING LYSOSOMAL ACIDIFICATION.....

Introduction.....	30
Results.....	31
A mouse model of doxorubicin cardiomyopathy reflects clinical scenario.....	31
Doxorubicin inhibits cardiomyocyte autophagic flux in vivo.....	31
Doxorubicin inhibits autophagic flux in cultured cardiomyocytes.....	34
mTORC1 activation is not required for doxorubicin-triggered block of autophagic flux.....	36
Doxorubicin inhibits lysosome function via elevating lysosomal pH.....	36
Doxorubicin inhibits V-ATPase-driven lysosome acidification.....	38
Doxorubicin alters subcellular lysosomal localization.....	40
Inhibition of ROS damage failed to rescue autophagic flux inhibition by doxorubicin.....	41

Figures and Tables .....	43
Methods .....	70
Chapter 2 References.....	78
<b>CHAPTER 3. ATTENUATED AUTOPHAGIC INITIATION AMELIORATES DOXORUBICIN CARDIOTOXICITY IN MICE .....</b>	<b>81</b>
Introduction .....	82
Results .....	83
Attenuated autophagy initiation restores autophagic flux after doxorubicin exposure .....	83
Attenuated autophagy initiation protects from doxorubicin-induced cardiotoxicity.....	84
Enhanced autophagy initiation exacerbates autolysosome accumulation by doxorubicin....	84
Enhanced autophagy initiation exacerbates doxorubicin cardiotoxicity .....	85
Modulation of autophagic initiation alters doxorubicin-elicited increase in ROS.....	86
Beclin1 modulates autophagic flux in the long term after doxorubicin treatment.....	86
Beclin1 levels and cardiac apoptotic activity in chronic doxorubicin cardiomyopathy.....	88
<i>In vitro</i> modulation of Beclin1 levels failed to affect doxorubicin cytotoxicity in NRVMs .....	88
Figures and Tables .....	90
Methods .....	108
Chapter 3 References.....	111
<b>CHAPTER 4. DISCUSSION .....</b>	<b>112</b>
Mouse model for chronic doxorubicin cardiomyopathy.....	113
Doxorubicin's impact on cardiomyocyte autophagic flux .....	115
Impaired lysosome function by doxorubicin.....	117
Lysosome V-ATPase and regulation of lysosomal pH.....	119
Impaired autophagy in doxorubicin cardiomyopathy .....	120
Autophagy, ROS and doxorubicin cardiomyopathy .....	123
Future directions in autophagic flux inhibition and doxorubicin cardiomyopathy .....	123
Conclusions .....	126
Figures .....	128
Chapter 4 References.....	132

## PRIOR PUBLICATIONS

Morselli E, Fuente-Martin E, Finan B, Kim M, Frank A, Garcia-Caceres C, Navas CR, Gordillo R, Neinast M, Kalainayakan SP, **Li DL**, Gao Y, Yi CX, Hahner L, Palmer BF, Tschöp MH, Clegg DJ. Hypothalamic PGC-1 $\alpha$  protects against high-fat diet exposure by regulating ER $\alpha$ . *Cell Rep*. 2014 Oct 23;9(2):633-45.

Wang ZV, Deng Y, Gao N, Pedrozo Z, **Li DL**, Morales CR, Criollo A, Luo X, Tan W, Jiang N, Lehrman MA, Rothermel BA, Lee AH, Lavandero S, Mammen PP, Ferdous A, Gillette TG, Scherer PE, Hill JA. Spliced X-box binding protein 1 couples the unfolded protein response to hexosamine biosynthetic pathway. *Cell*. 2014 Mar 13;156(6):1179-92.

Wang ZV, **Li DL**, Hill JA. Heart failure and loss of metabolic control. *J Cardiovasc Pharmacol*. 2014 Apr;63(4):302-13.

**Li DL**, Hill JA. Cardiomyocyte autophagy and cancer chemotherapy. *J Mol Cell Cardiol*. 2014 Jun;71:54-61.

## LIST OF FIGURES AND TABLES

Figure 2.1. A mouse model of chronic doxorubicin cardiomyopathy without systemic toxicity ...	43
Figure 2.2. Doxorubicin causes temporal changes of autophagy markers .....	46
Figure 2.3. Doxorubicin blocks autophagic flux in mouse heart. ....	47
Figure 2.4. Doxorubicin induces autolysosome accumulation in mouse heart. ....	49
Figure 2.5. Doxorubicin inhibits autophagic flux in cultured NRVMs .....	51
Figure 2.6. Doxorubicin inhibits autophagic flux in other <i>in vitro</i> models of cardiomyocytes. ....	53
Figure 2.7. Doxorubicin inhibits multiple autophagic genes in NRVMs. ....	54
Figure 2.8. Doxorubicin induces accumulation of autolysosomes in NRVMs. ....	54
Figure 2.9. Doxorubicin induces mTORC1 activation in NRVMs. ....	57
Figure 2.10. Inhibition of autophagic flux by doxorubicin in NRVMs is independent of mTORC1 activation. ....	58
Figure 2.11. Doxorubicin inhibits lysosomal function in NRVMs. ....	59
Figure 2.12. Doxorubicin inhibits lysosomal acidification in NRVMs. ....	61
Figure 2.13. Doxorubicin raises lysosomal pH in NRVMs. ....	62
Figure 2.14. Cardiomyocyte autophagy and lysosomal pH alterations by other cardiotoxic chemotherapeutics. ....	63
Figure 2.15. Doxorubicin inhibits v-ATPase-dependent lysosomal acidification. ....	64
Figure 2.16. Doxorubicin's effect on V-ATPase in NRVMs. ....	65
Figure 2.17. Doxorubicin alters subcellular lysosomal localization and mTOR recruitment to lysosomes .....	66
Figure 2.18. ROS scavengers do not rescue the inhibition of autophagic flux by doxorubicin ...	68
Figure 3.1. Attenuated autophagy initiation restores doxorubicin-blocked autophagic flux .....	90
Figure 3.2. Attenuated autophagy initiation is cardioprotective against doxorubicin. ....	93
Figure 3.3. Doxorubicin-induced autophagic flux inhibition is exacerbated in Beclin 1 Tg mice. ....	95
Figure 3.4. Doxorubicin cardiotoxicity is exacerbated in Beclin 1 Tg mice. ....	98
Figure 3.5. Modulation of autophagic initiation affects cardiac ROS levels elicited by doxorubicin. ....	100
Figure 3.6. Beclin1 levels modulate cardiac autophagic flux in the remodeling phase of chronic doxorubicin cardiomyopathy .....	102
Figure 3.7. Cardiac apoptotic activity in chronic doxorubicin cardiomyopathy model. ....	103

Figure 3.8. <i>In vitro</i> modulations of Beclin1 expression fail to affect doxorubicin-induced cell death .....	106
Figure 4.1. Doxorubicin-induced mitochondrial changes in hearts and NRVMs.....	128
Figure 4.2. The potential protective effect of TFEB in doxorubicin cardiotoxicity <i>in vitro</i> .....	129
Figure 4.3. Cardiomyocyte-specific TFEB transgenic mice develop heart failure .....	130
Figure 4.4. Working model.....	131
Table 2.1. Primers used in the study. ....	68
Table 3.1. Echocardiography of WT and <i>Beclin1</i> <sup>+/-</sup> .....	107
Table 3.2. Echocardiography of WT and Beclin1 Tg .....	107
Table 3.3. Primers used in the study .....	107

## LIST OF ABBREVIATIONS

ARVM: Adult Rat Ventricular Myocytes  
Atg5/7/12: Autophagy-related gene 5/7/12  
ANF: Atrial Natriuretic Factor  
BNP: Brain Natriuretic Peptide  
BafA1: Bafilomycin A1  
DHE: dihydroethidium  
DOX: Doxorubicin  
DXZ: Dexrazoxane  
GPx: Glutathione peroxidase  
LAMP-1: Lysosomal Associated Membrane Protein-1  
LAMP-2: Lysosomal Associated Membrane Protein-2  
LC3: Light Chain 3  
mPTP: mitochondrial Permeability Transition Pore  
mTORC1: mammalian Target Of Rapamycin Complex 1  
NRVM: Neonatal Rat Ventricular Myocytes  
Pac: Paclitaxel  
PI3K: Phosphoinositide 3-kinase  
ROS: Reactive Oxygen Species  
SOD: Superoxide dimutase  
Sun: Sunitinib  
TUNEL: Terminal deoxynucleotidyl transferase dUTP nick end labeling  
ULK1/2: Unc-51 like autophagy-activated kinase 1/2  
V-ATPase: vacuolar H<sup>+</sup>-ATPase

## **CHAPTER 1. INTRODUCTION**

### **Cardiovascular perils of anti-cancer therapies**

Owing to the progress in primary prevention, early diagnosis and effective new treatments, overall cancer mortality has been declining since the 1990s; in children, the mortality rate has continued to decrease since 1975 (1). With the increased survival and aging of the cancer patient population, long-term cardiovascular disease due to anti-cancer therapies has become an important concern for this population.

It has been shown that a host of chemotherapeutic and targeted therapies (2), as well as radiation therapies (3), can lead to acute, chronic or late-onset cardiac diseases. The cardiovascular complications can be local cardiac injury, including cardiomyopathy, heart failure, ischemic heart disease and arrhythmia, or secondary to systemic complications such as hypertension/hypotension or thrombotic events (2, 3). In fact, many cancer survivors now face a higher risk of cardiovascular disease than cancer recurrence (4). Therefore, prevention of anti-cancer treatments related cardiovascular complications is of critical importance in decreasing long-term morbidity and mortality in cancer survivors. However, long-term cardiovascular complications are hard to predict, and scant approaches exist for preventing anti-cancer therapy-related cardiac injury, due to our limited understanding of the molecular mechanisms.

### **Doxorubicin cardiomyopathy and heart failure**

Doxorubicin cardiomyopathy is a typical example of cardiotoxicity caused by anti-cancer therapies. Since its isolation from the bacteria *Streptococcus peucetius* in the 1960s, doxorubicin remains one of the most effective and widely used anti-cancer drugs in the oncologic armamentarium (5). In the 1970s the acute and chronic dose-dependent cardiotoxicity of doxorubicin was revealed, with the incidence of heart failure drastically increasing when the total dosage exceeds 550 mg/m<sup>2</sup> (6, 7). In the 1990s, late-onset cardiotoxicity caused by doxorubicin was uncovered in pediatric cancer survivors who presented with cardiac dysfunction and heart failure (8).

Three types of cardiotoxicity caused by doxorubicin have been described in patients: acute, chronic, and late onset (9). Acute cardiotoxicity is dose-independent and reversible; it usually occurs within 2-3 days and presents as EKG changes, arrhythmia, and occasionally heart failure (9). By contrast, chronic cardiotoxicity occurs within one year after doxorubicin therapy, and late-onset cardiomyopathy might present years or decades after doxorubicin exposure (8, 9). The latter two types of doxorubicin cardiotoxicity are dose-dependent and irreversible (9). The chronic and late cardiotoxicity of doxorubicin cannot be overlooked; the incidence of doxorubicin-related congestive heart failure is as high as 26% at a cumulative dosage of 550 mg/m<sup>2</sup>, and 48% at 650 mg/m<sup>2</sup> of total doxorubicin dosage (10). The single most important risk factor for developing doxorubicin cardiomyopathy and heart failure is cumulative dosage of doxorubicin exposure; other risk factors include age (patients younger than 4 or older than 65 years of age being more susceptible) (11), comorbidities such as hypertension, previous cardiac diseases and mediastinal radiation therapy.

At present, the only FDA-approved therapy to prevent doxorubicin cardiomyopathy is dexrazoxane (12). In addition, the beta-blocker carvedilol and angiotensin-converting enzyme (ACE) inhibitors have been shown to be protective in animal and pre-clinical studies, but still await confirmation from large clinical trials in the future (4).

### **Models of doxorubicin cardiotoxicity**

Since acute doxorubicin cardiotoxicity is of low incidence and always reversible (9), while chronic and late-onset doxorubicin cardiomyopathy is irreversible and poses significant health risks for cancer patients/survivors, a better understanding of chronic and late-onset doxorubicin cardiotoxicity is needed. However, chronic and late-onset doxorubicin cardiomyopathy models have proved difficult to establish in the laboratory.

Such a model system is essential in studying molecular mechanisms of doxorubicin cardiotoxicity, because it determines the translatability of findings from bench to bedside. Given

the numerous distinct models reported in the literature, it is not surprising that there exist many discrepancies among studies (examples will be discussed later).

The *in vitro* cell culture model is the most commonly used system for studying doxorubicin cardiotoxicity. Commonly used cell types include Neonatal Rat Ventricular Myocytes (NRVMs), Adult Rat Ventricular Myocytes (ARVMs) and H9c2 cells (13). As an isolated environment depleted of circulatory or neuro-hormonal influences, the *in vitro* system allows dissection of direct cellular responses upon doxorubicin exposure. In addition, the *in vitro* system offers the potential for more mechanistic insights at a molecular level. However, caveats are two fold: the limited time of drug exposure hinders the study of long-term effects of doxorubicin, and the differences in biologic features between cultured cells and cardiomyocytes in heart tissues raise concern for clinical relevance (14).

The concentration of doxorubicin utilized *in vitro* ranges from 0.1  $\mu\text{M}$  to 50  $\mu\text{M}$ , as reported in the literature (15-19). However, one must bear in mind that in human cancer patients, the peak and steady-state plasma concentrations of doxorubicin after one standard dose (30  $\text{mg}/\text{m}^2$ ) are 5  $\mu\text{M}$  and 25-250 nM, respectively (20). Therefore, doxorubicin concentrations higher than 1-2  $\mu\text{M}$  in *in vitro* studies may not reflect the clinical scenario (20).

The *ex vivo* model of doxorubicin cardiotoxicity has also been employed, which employs a Langendorff system to perfuse isolated animal hearts (21, 22). Doxorubicin can be directly added to the perfusion buffer. This model allows the examination of acute electrophysiologic changes as well as molecular changes of the heart in response to doxorubicin. The caveat also holds in that it is not a model for chronic doxorubicin cardiotoxicity.

The *in vivo* model remains the most important tool in the study of doxorubicin cardiotoxicity. Animal species used include mouse, normotensive rat, spontaneously hypertensive rat, rabbit, dog and pig (23, 24). Due to feasibility and manipulability reasons, mouse and rat (normotensive or spontaneously hypertensive) are the most commonly used animal models. One critical issue remains, however, in terms of the protocol of doxorubicin

administration. In patients, doxorubicin is administered via a venous route, in 30-75 mg/m<sup>2</sup> every 3-4 weeks (25). Cardiotoxicity increases significantly when the accumulative dose reaches 550 mg/m<sup>2</sup> (10). However, differences in pharmacokinetics and susceptibility to doxorubicin exist across species (23, 25, 26). Therefore, the drug delivery protocol in humans cannot simply be extrapolated to animal models. Doxorubicin administration protocols are usually based on individual experiences, aiming to attain reproducible and significant cardiac injury within a reasonable time frame. Many studies employ a single high dose of doxorubicin, which lead to acute cardiotoxicity within hours or days; however, models of chronic doxorubicin cardiotoxicity often involve lower drug concentrations, and cardiac injury might not be evident until weeks later (27). This suggests that lower drug doses and multiple injections should be employed in creating a meaningful model of chronic doxorubicin cardiomyopathy.

Another concern involving the *in vivo* model is the route of drug delivery. Doxorubicin is delivered to patients via *i.v.* infusion; in fact, doxorubicin extravasation causes local tissue damage. Consistently, other routes of delivering doxorubicin, including subcutaneous, intraperitoneal, and intramuscular administrations, all cause local tissue damage in animal models, leading to confounding bias and hindrance of doxorubicin tissue distribution (23). Therefore, *i.v.* administration should be chosen over other administration routes.

### **Mechanisms proposed for doxorubicin cardiomyopathy**

Numerous studies have probed molecular mechanisms of doxorubicin cardiomyopathy (28). As a result, a number of pathways have been implicated in the pathogenesis of doxorubicin cardiotoxicity, including DNA damage (17), transcriptome alterations (17), mitochondrial iron accumulation (18), mitochondrial damage (29), and accumulation of reactive oxygen species (ROS) (11). Here, the major models proposed will be described and discussed.

### Doxorubicin-topoisomerase II $\beta$ -DNA complex formation

Topoisomerase II is required for topological relaxation of DNA supercoils, a prerequisite step for DNA replication and gene transcription. It includes isoforms II $\alpha$  and II $\beta$ . Although the two isoforms share similar enzymatic activity, they have distinct expression patterns and biological significance. The II $\alpha$  isoform is highly expressed and active in proliferating cells and is essential for their survival, growth and proliferation. By contrast, the II $\beta$  isoform seems dispensable for most cellular activities except, under certain circumstances, for a few cases, including transcription of hormone-regulated genes (30).

Topoisomerase II relaxes DNA supercoils by generating transient DNA double strand breaks (DSBs), delivering a double helix through the cleaved site, followed by resealing the break. However, doxorubicin can intercalate into the interface between topoisomerase and DNA at the cleaved site, forming a doxorubicin-topoisomerase-DNA cleavage complex and preventing the resealing of DNA breaks by topoisomerase (30). In this way, doxorubicin “hijacks” topoisomerase to trigger DSBs without repairing them. Therefore, in rapidly proliferating cells such as cancer cells where topoisomerase II $\alpha$  is highly active, doxorubicin causes abundant DNA damage and inhibition of both cell cycle and protein biosynthesis, eventually leading to apoptosis. This is believed to be the primary molecular mechanism of doxorubicin’s anti-cancer effect.

Given the limited expression of Topoisomerase II $\alpha$  in adult cardiomyocytes, it has long been considered that doxorubicin causes cardiotoxicity independent of topoisomerase (11). However, Zhang et al. (17) demonstrated that Top II $\beta$  was required for doxorubicin cardiotoxicity. Mice with cardiomyocyte-specific deletion of Top II $\beta$  were protected from doxorubicin-induced mitochondrial damage, Reactive Oxygen Species (ROS) generation and reduction in cardiac contractility. These data not only highlight the importance of Topoisomerase II $\beta$  in the pathogenesis of doxorubicin cardiomyopathy, but also suggest that doxorubicin-

Topoisomerase II $\beta$ -DNA complex formation is upstream of doxorubicin-induced ROS production, which has been considered as an important culprit in doxorubicin cardiotoxicity.

### Oxidative stress

Despite controversies, excessive production of ROS remains widely accepted as the key factor contributing to doxorubicin cardiotoxicity (11). Oxidative stress is associated with the progression of heart failure (31). At a lower level, ROS can activate signaling pathways that lead to pathologic remodeling. At a higher level, ROS causes subcellular damage (lipid and protein peroxidation, DNA damage, etc.) and subsequent contractile dysfunction of cardiomyocytes (31). Additionally, chronic ROS leads to mitochondrial DNA damage and creates a vicious cycle of ROS generation (31).

The two major pathways of doxorubicin-induced ROS include redox cycling involving doxorubicin in a free form and doxorubicin-iron complex formation (32). Redox cycling can stem from the structure of the doxorubicin molecule, which is prone to accept electrons and to be reduced into a semiquinone radical. This is followed by donation of the electron to O<sub>2</sub> and formation of free radical  $\bullet\text{O}_2^-$ . Completion of the redox cycle requires donation of electrons from NAD(P)H (32). The major site for doxorubicin redox cycling occurs at complex I within mitochondria, obtaining electrons from NADH (33). This, and other effects of doxorubicin (34) on mitochondria might contribute to mitochondrial damage in cardiomyocytes. Indeed, alterations of mitochondrial morphology and function have been consistently reported in various models of doxorubicin cardiomyopathy (29, 34, 35); the severity of mitochondrial damage correlates with the decline in cardiac function (34, 35).

Another pathway of doxorubicin-induced ROS is through a doxorubicin-iron complex (32). Cycling between doxorubicin-Fe<sup>3+</sup> and doxorubicin-Fe<sup>2+</sup> could lead to robust  $\bullet\text{O}_2^-$  production by passing electrons to O<sub>2</sub>. Iron loading has been shown to exacerbate doxorubicin cardiotoxicity in animal models (36, 37). The iron chelator, dexrazoxane, protects against

doxorubicin cardiomyopathy in both animal models and patients (38). Ichikawa et al. recently further demonstrated that iron accumulation within mitochondria was of critical importance in doxorubicin cardiotoxicity, and the protective effect of dexrazoxane is at least partially due to its reduction of mitochondrial iron levels (18).

Moreover, doxorubicin might compromise the detoxifying system for ROS in cardiomyocytes. The endogenous cellular defense system against free radicals includes 3 scavenging enzymes: superoxide dismutase (SOD), glutathione peroxidase (GPx), and catalase (39). SOD is responsible for catalyzing the reduction of  $\bullet\text{O}_2^-$  to oxygen or hydrogen peroxide. GPx and catalase can further reduce hydrogen peroxide to oxygen and water. Interestingly, the abundance and activity of SOD and catalase in heart is much lower than liver while GPx is expressed at relatively high levels in heart (40). GPx may therefore play critical roles in cardiac protection against ROS (39, 40). Due to inconsistencies in literature it remains unclear whether doxorubicin affects the abundance and activities of these three enzymes. In various studies SOD activity is slightly decreased (41) or unchanged (42, 43). Catalase activity is reported modestly increased (43) or unchanged (41, 42), and GPx activity is either unchanged (42) or decreased (40, 41, 44). These discrepancies might derive from the different animal models (rat, mouse, rabbit), injection protocols, time of observation, etc.

A host of anti-oxidant drugs have been studied as potential prevention therapies for doxorubicin cardiomyopathy. Most of them yielded disappointing results, except dexrazoxane (DXZ) and carvedilol (32). DXZ reduces doxorubicin-induced ROS production by chelating iron in heart (45). However, DXZ is also a topoisomerase II inhibitor (45). Therefore, the cardioprotective effects might be multi-factorial. DXZ is the only clinically approved agent (in adult patients only) against doxorubicin cardiomyopathy (46). Moreover, DXZ has been recently shown to exert protective effects both in the short-term (46) and long-term (47) against doxorubicin cardiomyopathy in children with high-risk acute lymphoblastic leukemia. However,

important concerns remain, e.g. whether DXZ co-treatment with doxorubicin reduces doxorubicin's efficacy, and whether DXZ increases the risk for secondary malignancies (12).

Carvedilol is a beta-blocker that possesses anti-oxidant activities. Although not FDA-approved for treatment of doxorubicin cardiomyopathy, carvedilol has been shown to exert cardioprotective effects against doxorubicin in animal studies (48) and a small pre-clinical trial (49). However, the protective role of carvedilol remains to be further confirmed in future large randomized trials.

### Cell death

ROS production and mitochondrial damage, features of doxorubicin cardiotoxicity, can lead to calcium dysregulation, opening of mitochondrial permeability transition pore (mPTP), and eventually cell death (apoptosis or necrosis) (50) (13). However, caution needs to be exercised when interpreting the data, with the awareness of differences between neonatal and adult cardiomyocytes, as well as between *in vitro* and *in vivo* systems.

Cardiomyocyte apoptosis is the most commonly reported type of cell death triggered by doxorubicin. The models for *in vitro* studies are often H9c2 cells – embryonic myoblasts that proliferate in culture, and neonatal rat ventricular myocytes (NRVMs) (13). Adult rat ventricular myocytes (ARVMs), however, have significantly lower activities of caspases in comparison to NRVMs and H9c2 cells (13). This is at least partially due to the low expression of pro-apoptotic proteins such as apoptotic protease activating factor-1 (Apaf1) and procaspase-9 in adult cardiomyocytes (13). Consistently, Shi, et al showed a rapid down-regulation of a host of pro-apoptotic proteins (pro-caspase 3, 8, 9, Bax, Bak, Apaf1) and caspase activities in post-natal mouse hearts (51). The down-regulation of apoptotic proteins correlated with decreased apoptotic events in mouse hearts (51). Caspase 3 activity, while robust in the neonatal mouse heart, is no longer detectable in the heart by 3 weeks of age, both at baseline and after

doxorubicin (10 mg/kg) injection (51). These results suggest that doxorubicin may only be able to cause extremely low levels of cardiomyocyte apoptosis, if any.

Additionally, while many studies use the terminal deoxynucleotidyl transferase dUTP nick end labeling (TUNEL) assay to detect apoptosis in heart tissues, two caveats exist. First, the TUNEL assay does not specifically recognize apoptosis, but marks necrotic cells as well (52). Second, lack of co-staining with cardiomyocyte markers renders a high possibility of mistaking apoptotic signals in non-cardiomyocytes as cardiomyocytes. Zhang et al (53) pointed out that the TUNEL positive sites in their chronic doxorubicin cardiomyopathy rat model were confined to endothelial cells, interstitial cells and macrophages, but not cardiomyocytes. Therefore, doxorubicin-induced cardiomyocyte apoptosis, at least in a clinically relevant manner, is still debatable.

Some studies have reported that doxorubicin can induce cardiomyocyte necrosis (13, 54, 55). However, it is technically difficult to detect necrosis in doxorubicin-treated heart. Histologically, necrosis is characterized as rupture of plasma membrane and subsequent inflammation (50). In tissue culture systems, the plasma membrane rupture can be evaluated by various assays (e.g. LDH release assay, trypan blue incorporation assay etc.); however, other types of cell death in *in vitro* systems can also cause loss of plasma membrane integrity at late stages. In addition, lipid peroxidation can increase membrane permeability, which does not necessarily mean cell death (56). Under *in vivo* conditions, rupture of the cell membrane and loss of myocytes are difficult to detect unless in the scenario of myocardial infarction. While inflammation always accompanies necrosis in tissues, it is not a specific marker for necrosis. Mechanistically, opening of the mPTP is considered a key contributor to necrosis (50). ROS within mitochondria, along with calcium dysregulation by doxorubicin, are likely to cause mitochondrial calcium overload, opening of the mPTP, mitochondrial swelling and irreversible necrotic death (50). Opening of the mPTP was observed in doxorubicin-treated cardiomyocytes

cultured *in vitro* (55), hinting at necrosis as a possible mechanism of doxorubicin-caused cardiomyocyte loss; however, no conclusive evidence exists in *in vivo* studies.

Additionally, several groups suggested that doxorubicin caused “autophagic cell death” in cardiomyocytes (13, 57, 58). However, both the legitimacy of the concept of “autophagic cell death” and that doxorubicin upregulates autophagy in cardiomyocytes are controversial (59), which will be discussed in the following sections.

### **Autophagy, a dynamic flux process**

Autophagy, meaning “self-eating”, is a generic name for different routes of cytosolic material delivery to the lysosome for degradation, which includes macroautophagy, microautophagy and chaperone-mediated autophagy. Among them, macroautophagy is the major type and is the most extensively studied (referred to as autophagy hereafter).

Autophagy not only serves as pro-survival machinery in cellular starvation, but also is involved in the turnover and renovation of organelles, as well as degradation of protein aggregates during cell stress (60, 61). Defective autophagy leads to perinatal death due to energy deficiency before feeding commences (60); in later stages of life, defects in autophagy cause premature aging and reduction in life span with end stage organ damage (62-64). Additionally, dysregulation of autophagy has been shown to contribute to a variety of human diseases (60).

Autophagy is a dynamic process. It involves multiple steps: the formation of phagophores and autophagosomes, fusion between autophagosomes and lysosomes to generate autolysosomes, and finally degradation of internal cargo by lysosomal enzymes. Alteration of any step is likely to affect the execution of autophagy (60). That autophagy is a dynamic flow rather than a static reflection of “vacuoles” under the microscope has been increasingly appreciated in recent years, with “autophagic flux” often used to denote the dynamic nature of autophagy.

Regulation of the initiation process of autophagy has been intensively studied. It involves the cooperation of evolutionarily conserved proteins (60). The mammalian target of rapamycin complex 1 (mTORC1), a cellular “nutrient sensor”, is a major inhibitor of autophagy. mTORC1 suppresses autophagic induction mainly by phosphorylating ULK1/2, a component of the PI3-kinase (PI3K) complex that governs the phagophore nucleation. On the other hand, AMP-activated kinase (AMPK) activates autophagy both indirectly by inhibiting mTORC1 activity, and directly by phosphorylating Beclin 1 (65). Further, phosphorylation of Bcl-2 and Bcl-X<sub>L</sub> can disrupt the interaction with Beclin 1, leading to the release of Beclin 1 for autophagy induction (66, 67).

Autophagosome turnover is the second half of the autophagy process, but the molecular regulation is less well characterized. Autophagosome-lysosome fusion is a process that requires cellular membrane trafficking. Autophagosomes are often delivered to the perinuclear microtubule-organizing center (MTOC) where lysosomes are abundant (68). Disruption of microtubule assembly or impairment of dynein/dynactin-mediated retrograde transport decreases chances for autophagosome-lysosome fusion and leads to accumulation of autophagosomes (68). Rab7 is a small GTPase required for autophagosome trafficking, and recruitment of tethering complexes that mediate membrane fusion (69, 70). Other proteins shown to be required for the autophagosome-lysosome fusion process include Rab7 binding partners UV radiation resistance-associated gene (UVRAG) (71) and RUN domain protein as Beclin1 interacting and cysteine-rich containing (Rubicon) (72), Rab7 effector protein Pleckstrin homology domain containing protein family member 1 (PLEKHM1) (70), and soluble N-ethylmaleimide-sensitive factor attachment protein receptor (SNARE) complex components Syntaxin 17 (Stx17), SNAP-29 and VAMP8 (73, 74). Interestingly, SNAP-29 serves as a “nutrient sensor” to regulate the final fusion process via O-GlcNAcylation modification (74).

Lysosomal digestion of intra-autolysosomal cargo is the final step of autophagic flux. Transcription factor EB (TFEB) is a transcription factor that drives lysosomal gene expression

and lysosomal biogenesis (75). Overexpression of TFEB induces autophagic flux in mammalian cells (76). Derived from lysosomes, autolysosomes are equipped with a milieu of hydrolases that function optimally at pH 4.5-5.0 (77). Lysosomes/autolysosomes acquire an acidic environment via the activity of the vacuolar-ATPase (V-ATPase), a proton pump at the lysosomal membrane (78). The lysosomal membrane is protected by LAMP-1 and LAMP-2 - two glycosylated proteins - from being digested. The single lysosomal membrane creates a special compartment and separates the acidic lumen from the rest of the cell. A host of human diseases are associated with mutations of V-ATPase component genes, *Lamp-2*, various lysosomal enzyme genes, and other mutations affecting lysosomal functions, leading to blockage of autophagic flux in late stages of the process (79, 80).

### **Assays for monitoring autophagic flux**

Counting the number of autophagosomes has long been considered the gold standard to assess autophagy. However, a misconception exists that autophagosome number positively correlates with autophagic activity. The number of autophagic vacuoles is a balance between generation by autophagic initiation and turnover of autophagosomes/autolysosomes. Therefore, blocking of autophagy flux also displays an increase in autophagosome numbers. In order to discern between these two possibilities, assays to measure autophagic flux are imperative.

In comparison to electron microscopic studies for detecting autophagic vacuoles, Atg8/LC3 detection assays are technically more feasible, more reliable and less experience-dependent. The conversion of cytosolic LC3-I to phosphatidylethanolamine-conjugated LC3-II is used as a marker for autophagosome formation. Based on the relationship between LC3 and autophagic vacuoles, autophagic vacuole numbers can be monitored via either immunoblotting for LC3, or fluorescent microscopy detecting LC3 puncta. To monitor flux rather than taking snapshots of autophagy, these approaches can be aided by pharmaceutical manipulations to

block autophagic degradation in combination with autophagosome detection. E64D, PepstatinA, Chloroquine and bafilomycin A1 are commonly used for this purpose. A third method to quantify autophagic flux involves the usage of tandem mRFP/mCherry-GFP-LC3 fusion protein (81). The GFP signal is sensitive to pH change and will be quenched in lysosomes while mRFP/ mCherry signal is more stable in the acidic lysosomal compartment. Therefore, dual fluorescence can aid in differentiating autophagosomes and autolysosomes.

Measuring protein degradation by autophagy is another approach to monitor autophagic activity. The long-lived protein degradation assay was first developed in the 1970s, offering to measure the “bulk-degradation” rate by autophagy (82). However, one needs to be cautious whether the measurement is specific to autophagy or a mixture of autophagy and proteasomal degradation. Quality controls such as inhibition of autophagy and/or the proteasome pathway are therefore needed. In recent years, measurement of long-lived protein degradation has largely been replaced by monitoring the protein level of p62, a substrate protein in the autophagy pathway. In many cases, p62 levels inversely correlate with autophagic activity. However, one must be cautious that given this protein’s multiple biological functions (83, 84), transcriptional regulation by stresses (85), and decreased solubility in some contexts (86), p62 protein levels do not necessarily reflect autophagic flux in every scenario.

### **Autophagy in cardiac diseases: friend or foe?**

Cumulative evidence supports the importance of autophagy in cardiac physiology and pathophysiology, albeit controversies exist whether regarding autophagy is a friend or foe under various conditions.

*Autophagy is required for normal cardiac function*

Basal levels of autophagy in the heart play critical roles in recycling proteins and organelles, particularly mitochondria, so that homeostasis in cardiomyocytes can be maintained. The heart is a dynamic organ with a high metabolic rate, providing ATP for continuous cardiac muscle contraction to sustain the peripheral circulation. In the nutrient-rich state, autophagy is not required for energy provision in cardiomyocytes; however, during persistent fasting, lack of autophagy has been shown to be detrimental to cardiac performance (87).

On the other hand, the abundance of mitochondria and high oxidative phosphorylation levels render the heart at a higher risk of ROS injury and mitochondrial damage. Autophagy serves as an efficient housekeeper, digesting damaged mitochondria and oxidized proteins/organelles. Defective autophagy in heart could result in cardiomyopathy, such as heart failure (88) and early-onset cardiac aging (63). Danon disease in humans is another example in which defective autophagic flux due to LAMP-2 deficiency, leads to autophagic vacuole accumulation in cardiomyocytes and eventual heart failure (78).

Further, altered autophagic levels have been observed in various cardiac diseases (as discussed below). To date, whether autophagy is adaptive or maladaptive in cardiac diseases is still controversial, and depends on specific disease contexts and degrees of autophagic alteration.

#### *Accumulation of autophagic vacuoles in heart failure*

Increased numbers of autophagic vacuoles have been observed in heart samples from dilated cardiomyopathy and heart failure patients (89). However, due to limitations in assessing the dynamic autophagic process in human endomyocardial biopsy samples, it is not known if the increased vesicles are due to increased autophagic activity or defective lysosomal degradation of autophagic cargo. It is also unknown whether autophagy is a culprit in promoting cardiac decompensation, or merely a failed compensatory strategy to salvage defective energy production in cardiomyocytes during heart failure.

### Hypertensive cardiomyopathy

High blood pressure increases ventricular wall stress. According to Laplace's law, wall stress is negatively proportional to wall thickness. To ameliorate wall stress, the ventricle manifests hypertrophic growth by adding sarcomeres in parallel in cardiomyocytes. When hemodynamic stress persists, however, adaptive hypertrophy progresses and become maladaptive, eventually leading to heart failure. Despite extensive interest, the mechanisms governing the transition remain elusive. Autophagy has been implicated in both cardiac hypertrophy and decompensated heart failure. However, the exact role is still up for debate (88, 90). On one hand, Atg5 cardiomyocyte-specific knockout mice ( $\alpha$ MHC-Cre, Atg5 flox/flox) develop more robust cardiac hypertrophy and rapid progression to heart failure upon TAC (88). On the other hand, *Beclin 1*<sup>+/-</sup> mice are protected from severe TAC while cardiomyocyte-specific Beclin 1 transgenic mice develop heart failure upon TAC (90). This apparent contradiction could be explained by the different autophagy modulations in animal models: complete ablation of autophagy might be detrimental for cardiomyocytes under pressure overload stress, while partially reduced autophagy is protective.

### Ischemia/reperfusion injury

Myocardial infarction is a leading cause of death worldwide. Effective and timely reperfusion of the coronary artery is the most important approach to mitigate cardiac damage and improve clinical outcomes. Reperfusion, however, causes additional damage to the heart. This ischemia/reperfusion (I/R) injury is a subject for actively ongoing research. Rodent models of I/R recapitulate the clinical circumstance when a patient receives percutaneous intervention (PCI) and stenting, or thrombolytic agents. During ischemia, lack of oxygen and nutrients triggers a number of cellular responses including autophagy (91). Decker et al (91) showed that 40 minutes after ischemia in a rabbit model triggered an increase in both autophagosomes and

lysosomal activity in cardiomyocytes. However, autophagic changes during reperfusion are more controversial. In the same study, autophagic vacuoles strongly increased and the lysosomal degradation process was robustly enhanced upon reperfusion after 20 minutes of ischemia, which correlated with cell repair. However, during reperfusion after 40 minutes of ischemia, autophagosomes still increased, but appear less frequently in hearts compared to those recovering after 20 minutes of ischemia. Instead, large membrane-bound vacuoles without lysosomal reaction product were observed. These observations raise the possibility that while shorter ischemic time triggers autophagy during reperfusion and subsequent cardiomyocyte repair, longer ischemic duration might cause defects in autophagic flux. In accordance with this, it was shown that in an I/R mouse model, autophagic flux is initially activated in ischemia but blocked during reperfusion (92). Functionally, accumulating evidence suggests that induction of autophagy offers cardioprotection against ischemia/reperfusion injury (93). Enhanced autophagy in cardiomyocytes is correlated with cell survival in a porcine model of chronic ischemic cardiac disease (93). Additionally, Xie et al. reported that HDAC inhibitor's protection against I/R injury was associated with upregulation of autophagic flux in mouse and rabbit models (94).

### **Autophagy's controversial role in doxorubicin cardiotoxicity - previous studies**

In recent years, a number of studies have emerged, focusing on the role of autophagy in doxorubicin-induced cardiotoxicity. However, studies employing either *in vitro* or *in vivo* platforms have generated conflicting results. Overcoming the challenges inherent to experimental models of doxorubicin cardiotoxicity is required to facilitate the emergence of new clinically relevant insights.

#### *In vitro studies*

Involvement of autophagy in doxorubicin cardiotoxicity has been tested in a variety of cell types *in vitro*, including neonatal rat ventricular myocytes (NRVMs), adult rat ventricular myocytes (ARVMs), and H9c2 cells (rat embryonic myoblast cell line) (19, 58, 95). In general, ratios of LC3-II/LC3-I and p62 protein abundance were evaluated as the major criteria of autophagic activation. Kobayashi et al (58) and Dimitrakis et al (19) reported an increase of autophagy in doxorubicin treated NRVMs (1  $\mu$ M for 18 hours) and ARVMs (10  $\mu$ M for 48 hours) respectively. In contrast, Sishi et al reported that LC3-II/LC3-I ratios in H9c2 cells were not altered by doxorubicin treatment (3  $\mu$ M for 24 hours) (95). One caveat of these studies is the lack of evaluation of autophagic flux. Thus, the role of autophagy in doxorubicin-exposed cardiomyocytes and cardiomyocyte-like cell lines remains inconclusive.

Several *in vitro* studies have yielded conflicting data regarding whether autophagy alters the cardiomyocyte response to doxorubicin. Kobayashi et al suggested that autophagy activation increased cell injury and death of NRVMs by doxorubicin (58). However, Sishi et al reported opposite results in H9c2 cells (95). Discrepancies observed among these studies might be explained by: 1) different treatment strategies; 2) off-target effects of compounds used to modulate autophagy. The commonly used autophagy modulators, such as rapamycin, 3-MA, chloroquine, bafilomycin A1, etc., all have biological targets other than autophagy, such as mTORC1, PI3K (59), and the lysosome (59). Therefore, further work with rigorous controls is required to clarify the puzzle.

From a different point of view, discrepancies observed in multiple studies may also reflect the complexity of studying drug-induced cardiotoxicity. Currently, there are no cell lines that optimally mimic human cardiac biology (96). H9c2 cells do not resemble cardiomyocytes morphologically, and they actively proliferate; hence, they could be more prone to doxorubicin-induced cytotoxicity and cell death. NRVMs, although widely used and well characterized, differ from adult cardiomyocytes in many ways. Doxorubicin of 1-3  $\mu$ M, a concentration used in many

*in vitro* studies and reflective of plasma drug concentrations in patients receiving doxorubicin, triggers robust cell death in NRVMs and H9c2 cells within 24 hours, but a much higher concentration of doxorubicin ( $> 20 \mu\text{M}$ ) is required to induce cell death in ARVMs (97). Indeed, acute cardiomyocyte death is not a common event in animal hearts even after exposure to lethal-dose doxorubicin, suggesting that cell death measurements may not be the best assay to accurately assess doxorubicin-induced cardiotoxicity.

### *In vivo studies*

*In vivo* studies of autophagy in doxorubicin-induced cardiomyopathy have employed rabbits, rodents, and zebrafish. In general, two modes of drug administration have been studied in rodent models: high-dose (10 mg/kg-20 mg/kg, 1-2 injections) and chronic exposure to serial low-dose drug (1-5 mg/kg, 3-15 injections) (57, 98-100). While early studies employed intravenous (*i.v.*) injections, more recent studies have employed intraperitoneal (*i.p.*) injections, largely for sake of convenience. As discussed earlier, one limitation of *i.p.* doxorubicin exposure is local tissue damage, which can alter bowel function and food intake, confounding not only tissue distributions of doxorubicin, but also the evaluation of autophagy.

Multiple *in vivo* studies arrived at dissimilar conclusions regarding how autophagy is regulated by doxorubicin in animal hearts. Several studies reported increases in LC3-II/LC3-I ratios in heart tissue after doxorubicin exposure, yet autophagic flux was not rigorously evaluated (57, 98, 99). In contrast, Kawaguchi et al (100) reported that whereas steady state levels of LC3-II/LC3-I increased, inhibition of downstream lysosomal processing with bafilomycin A1 failed to increase those ratios further, suggesting a defect in autophagosome processing. Interestingly, early studies reported that chronic doxorubicin exposure resulted in a decrease in the sedimentable activity of cathepsin D (101), which highlights the importance of evaluating autophagosome turnover and lysosome function in doxorubicin-treated hearts.

In a zebrafish model of doxorubicin cardiomyopathy (102), steady state LC3-II levels increased acutely upon doxorubicin exposure and later declined. The autophagic response may differ in the acute phase relative to later phases. In aggregate, it is still debated whether cardiac autophagy is upregulated or rather blocked by doxorubicin.

The functional role of autophagy in the pathogenesis of doxorubicin cardiotoxicity has been explored in multiple *in vivo* studies, albeit with conflicting conclusions. Lu et al (57) reported that 3-MA treatment reduced mitochondrial damage and preserved cardiac function after exposure to high-dose doxorubicin. However, several studies have reported that boosting autophagy by either rapamycin or fasting was protective of doxorubicin-induced cardiac dysfunction (95,100). Others reported correlations between autophagic levels and the severity of doxorubicin cardiotoxicity (98, 99). Further, in light of mTORC1's regulation of autophagy, two studies evaluated the role of mTORC1 in doxorubicin cardiotoxicity in rodents and zebrafish, respectively, with conflicting results (98, 102).

While maladaptive autophagy exacerbates cardiac function under stress (90), perturbation of downstream autophagosome processes will also lead to cellular damage resulting from the accumulation of damaged mitochondria as well as ROS-damaged proteins (60). At present, a consensus has not emerged regarding how cardiomyocyte autophagy is altered by doxorubicin or its possible role in the pathogenesis of anthracycline cardiomyopathy.

To address this, it is critical to probe autophagic flux by inhibiting lysosomal processing, especially given that p62 expression can be induced by oxidative stress (85). In addition, tandem fluorescence probes can be informative (81). For *in vivo* models, it is critical to avoid the systemic effects of doxorubicin exposure, including lethargy, anorexia, and weight loss, as these are likely to alter autophagy secondarily. Further, detailed time course analysis is needed, as acute responses may differ from chronic events.

**Central Thesis**

The clinical use of doxorubicin is limited by cardiotoxicity. Histopathologic changes include increased myocardial interstitial fibrosis and appearance of vacuolated cardiomyocytes. Whereas past decades have witnessed numerous mechanisms proposed, the mechanism of doxorubicin cardiomyopathy is not well defined. Additionally, lack of approaches to prevent or treat doxorubicin cardiomyopathy calls for better understanding of mechanisms untaking doxorubicin cardiotoxicity.

Autophagy plays a critical role in cardiac physiology; dysregulation of autophagy in the myocardium has been implicated in a variety of cardiovascular diseases. However, the role of autophagy in doxorubicin cardiomyopathy remains poorly defined. To explore the role of autophagy in doxorubicin cardiomyopathy, I designed experiments to examine 1) how autophagic flux is altered in cardiomyocytes upon doxorubicin exposure, and 2) how alteration of autophagic flux affects the outcome of doxorubicin cardiotoxicity.

## CHAPTER 1 REFERENCES

1. Jemal, A., Simard, E.P., Dorell, C., Noone, A.M., Markowitz, L.E., Kohler, B., Ehemann, C., Saraiya, M., Bandi, P., Saslow, D., et al. 2013. Annual Report to the Nation on the Status of Cancer, 1975-2009, featuring the burden and trends in human papillomavirus(HPV)-associated cancers and HPV vaccination coverage levels. *J Natl Cancer Inst* 105:175-201.
2. Albin, A., Pennesi, G., Donatelli, F., Cammarota, R., De Flora, S., and Noonan, D.M. 2010. Cardiotoxicity of anticancer drugs: the need for cardio-oncology and cardio-oncological prevention. *J Natl Cancer Inst* 102:14-25.
3. Darby, S.C., Ewertz, M., McGale, P., Bennet, A.M., Blom-Goldman, U., Bronnum, D., Correa, C., Cutter, D., Gagliardi, G., Gigante, B., et al. 2013. Risk of ischemic heart disease in women after radiotherapy for breast cancer. *N Engl J Med* 368:987-998.
4. Khakoo, A.Y., and Yeh, E.T. 2008. Therapy insight: Management of cardiovascular disease in patients with cancer and cardiac complications of cancer therapy. *Nat Clin Pract Oncol* 5:655-667.
5. Tacar, O., Sriamornsak, P., and Dass, C.R. 2013. Doxorubicin: an update on anticancer molecular action, toxicity and novel drug delivery systems. *J Pharm Pharmacol* 65:157-170.
6. Lefrak, E.A., Pitha, J., Rosenheim, S., and Gottlieb, J.A. 1973. A clinicopathologic analysis of adriamycin cardiotoxicity. *Cancer* 32:302-314.
7. Von Hoff, D.D., Layard, M.W., Basa, P., Davis, H.L., Jr., Von Hoff, A.L., Rozenzweig, M., and Muggia, F.M. 1979. Risk factors for doxorubicin-induced congestive heart failure. *Ann Intern Med* 91:710-717.
8. Lipshultz, S.E., Colan, S.D., Gelber, R.D., Perez-Atayde, A.R., Sallan, S.E., and Sanders, S.P. 1991. Late cardiac effects of doxorubicin therapy for acute lymphoblastic leukemia in childhood. *N Engl J Med* 324:808-815.
9. Sereno, M., Brunello, A., Chiappori, A., Barriuso, J., Casado, E., Belda, C., de Castro, J., Feliu, J., and Gonzalez-Baron, M. 2008. Cardiac toxicity: old and new issues in anti-cancer drugs. *Clin Transl Oncol* 10:35-46.
10. Swain, S.M., Whaley, F.S., and Ewer, M.S. 2003. Congestive heart failure in patients treated with doxorubicin: a retrospective analysis of three trials. *Cancer* 97:2869-2879.
11. Singal, P.K., and Iliskovic, N. 1998. Doxorubicin-induced cardiomyopathy. *N Engl J Med* 339:900-905.
12. van Dalen, E.C., van den Berg, H., Raphael, M.F., Caron, H.N., and Kremer, L.C. 2011. Should anthracyclines and dexrazoxane be used for children with cancer? *Lancet Oncol* 12:12-13.
13. Zhang, Y.W., Shi, J., Li, Y.J., and Wei, L. 2009. Cardiomyocyte death in doxorubicin-induced cardiotoxicity. *Arch Immunol Ther Exp (Warsz)* 57:435-445.
14. Lipshultz, S.E., Cohen, H., Colan, S.D., and Herman, E.H. 2006. The relevance of information generated by in vitro experimental models to clinical doxorubicin cardiotoxicity. *Leuk Lymphoma* 47:1454-1458.
15. Spallarossa, P., Altieri, P., Aloj, C., Garibaldi, S., Barisione, C., Ghigliotti, G., Fugazza, G., Barsotti, A., and Brunelli, C. 2009. Doxorubicin induces senescence or apoptosis in rat neonatal cardiomyocytes by regulating the expression levels of the telomere binding factors 1 and 2. *Am J Physiol Heart Circ Physiol* 297:H2169-2181.
16. Menna, P., Salvatorelli, E., and Minotti, G. 2007. Doxorubicin degradation in cardiomyocytes. *J Pharmacol Exp Ther* 322:408-419.
17. Zhang, S., Liu, X., Bawa-Khalife, T., Lu, L.S., Lyu, Y.L., Liu, L.F., and Yeh, E.T. 2012. Identification of the molecular basis of doxorubicin-induced cardiotoxicity. *Nat Med* 18:1639-1642.

18. Ichikawa, Y., Ghanefar, M., Bayeva, M., Wu, R., Khechaduri, A., Naga Prasad, S.V., Mutharasan, R.K., Naik, T.J., and Ardehali, H. 2014. Cardiotoxicity of doxorubicin is mediated through mitochondrial iron accumulation. *J Clin Invest* 124:617-630.
19. Dimitrakis, P., Romay-Ogando, M.I., Timolati, F., Suter, T.M., and Zuppinger, C. 2012. Effects of doxorubicin cancer therapy on autophagy and the ubiquitin-proteasome system in long-term cultured adult rat cardiomyocytes. *Cell Tissue Res* 350:361-372.
20. Minotti, G., Menna, P., Salvatorelli, E., Cairo, G., and Gianni, L. 2004. Anthracyclines: molecular advances and pharmacologic developments in antitumor activity and cardiotoxicity. *Pharmacol Rev* 56:185-229.
21. Tokarska-Schlattner, M., Zaugg, M., da Silva, R., Lucchinetti, E., Schaub, M.C., Wallimann, T., and Schlattner, U. 2005. Acute toxicity of doxorubicin on isolated perfused heart: response of kinases regulating energy supply. *Am J Physiol Heart Circ Physiol* 289:H37-47.
22. Aksentijevic, D., Zervou, S., Faller, K.M., McAndrew, D.J., Schneider, J.E., Neubauer, S., and Lygate, C.A. 2014. Myocardial creatine levels do not influence response to acute oxidative stress in isolated perfused heart. *PLoS One* 9:e109021.
23. Herman, E.H., and Ferrans, V.J. 1998. Preclinical animal models of cardiac protection from anthracycline-induced cardiotoxicity. *Semin Oncol* 25:15-21.
24. Simunek, T., Klimtova, I., Kaplanova, J., Mazurova, Y., Adamcova, M., Sterba, M., Hrdina, R., and Gersl, V. 2004. Rabbit model for in vivo study of anthracycline-induced heart failure and for the evaluation of protective agents. *Eur J Heart Fail* 6:377-387.
25. Gustafson, D.L., Rastatter, J.C., Colombo, T., and Long, M.E. 2002. Doxorubicin pharmacokinetics: Macromolecule binding, metabolism, and excretion in the context of a physiologic model. *J Pharm Sci* 91:1488-1501.
26. Yesair, D.W., Schwartzbach, E., Shuck, D., Denine, E.P., and Asbell, M.A. 1972. Comparative pharmacokinetics of daunomycin and adriamycin in several animal species. *Cancer Res* 32:1177-1183.
27. Gianni, L., Herman, E.H., Lipshultz, S.E., Minotti, G., Sarvazyan, N., and Sawyer, D.B. 2008. Anthracycline cardiotoxicity: from bench to bedside. *J Clin Oncol* 26:3777-3784.
28. Octavia, Y., Tocchetti, C.G., Gabrielson, K.L., Janssens, S., Crijns, H.J., and Moens, A.L. 2012. Doxorubicin-induced cardiomyopathy: from molecular mechanisms to therapeutic strategies. *J Mol Cell Cardiol* 52:1213-1225.
29. Suliman, H.B., Carraway, M.S., Ali, A.S., Reynolds, C.M., Welty-Wolf, K.E., and Piantadosi, C.A. 2007. The CO/HO system reverses inhibition of mitochondrial biogenesis and prevents murine doxorubicin cardiomyopathy. *J Clin Invest* 117:3730-3741.
30. Pendleton, M., Lindsey, R.H., Jr., Felix, C.A., Grimwade, D., and Osheroff, N. 2014. Topoisomerase II and leukemia. *Ann N Y Acad Sci* 1310:98-110.
31. Ohta, Y., Kinugawa, S., Matsushima, S., Ono, T., Sobirin, M.A., Inoue, N., Yokota, T., Hirabayashi, K., and Tsutsui, H. 2011. Oxidative stress impairs insulin signal in skeletal muscle and causes insulin resistance in postinfarct heart failure. *Am J Physiol Heart Circ Physiol* 300:H1637-1644.
32. Sterba, M., Popelova, O., Vavrova, A., Jirkovsky, E., Kovarikova, P., Gersl, V., and Simunek, T. 2013. Oxidative stress, redox signaling, and metal chelation in anthracycline cardiotoxicity and pharmacological cardioprotection. *Antioxid Redox Signal* 18:899-929.
33. Davies, K.J., and Doroshov, J.H. 1986. Redox cycling of anthracyclines by cardiac mitochondria. I. Anthracycline radical formation by NADH dehydrogenase. *J Biol Chem* 261:3060-3067.
34. Wallace, K.B. 2003. Doxorubicin-induced cardiac mitochondrionopathy. *Pharmacol Toxicol* 93:105-115.

35. Singal, P.K., Deally, C.M., and Weinberg, L.E. 1987. Subcellular effects of adriamycin in the heart: a concise review. *J Mol Cell Cardiol* 19:817-828.
36. Panjra, G.S., Patel, V., Valdiviezo, C.I., Narula, N., Narula, J., and Jain, D. 2007. Potentiation of Doxorubicin cardiotoxicity by iron loading in a rodent model. *J Am Coll Cardiol* 49:2457-2464.
37. Miranda, C.J., Makui, H., Soares, R.J., Bilodeau, M., Mui, J., Vali, H., Bertrand, R., Andrews, N.C., and Santos, M.M. 2003. Hfe deficiency increases susceptibility to cardiotoxicity and exacerbates changes in iron metabolism induced by doxorubicin. *Blood* 102:2574-2580.
38. Simunek, T., Sterba, M., Popelova, O., Adamcova, M., Hrdina, R., and Gersl, V. 2009. Anthracycline-induced cardiotoxicity: overview of studies examining the roles of oxidative stress and free cellular iron. *Pharmacol Rep* 61:154-171.
39. Tsutsui, H., Kinugawa, S., and Matsushima, S. 2011. Oxidative stress and heart failure. *Am J Physiol Heart Circ Physiol* 301:H2181-2190.
40. Doroshov, J.H., Locker, G.Y., and Myers, C.E. 1980. Enzymatic defenses of the mouse heart against reactive oxygen metabolites: alterations produced by doxorubicin. *J Clin Invest* 65:128-135.
41. Li, T., and Singal, P.K. 2000. Adriamycin-induced early changes in myocardial antioxidant enzymes and their modulation by probucol. *Circulation* 102:2105-2110.
42. Robison, T.W., Giri, S.N., and Wilson, D.W. 1989. Effects of chronic administration of doxorubicin on myocardial creatine phosphokinase and antioxidant defenses and levels of lipid peroxidation in tissues and plasma of rats. *J Biochem Toxicol* 4:87-94.
43. Gustafson, D.L., Swanson, J.D., and Pritsos, C.A. 1993. Modulation of glutathione and glutathione dependent antioxidant enzymes in mouse heart following doxorubicin therapy. *Free Radic Res Commun* 19:111-120.
44. Revis, N.W., and Marusic, N. 1978. Glutathione peroxidase activity and selenium concentration in the hearts of doxorubicin-treated rabbits. *J Mol Cell Cardiol* 10:945-951.
45. Hasinoff, B.B., and Herman, E.H. 2007. Dexrazoxane: how it works in cardiac and tumor cells. Is it a prodrug or is it a drug? *Cardiovasc Toxicol* 7:140-144.
46. Lipshultz, S.E., Rifai, N., Dalton, V.M., Levy, D.E., Silverman, L.B., Lipsitz, S.R., Colan, S.D., Asselin, B.L., Barr, R.D., Clavell, L.A., et al. 2004. The effect of dexrazoxane on myocardial injury in doxorubicin-treated children with acute lymphoblastic leukemia. *N Engl J Med* 351:145-153.
47. Lipshultz, S.E., Scully, R.E., Lipsitz, S.R., Sallan, S.E., Silverman, L.B., Miller, T.L., Barry, E.V., Asselin, B.L., Athale, U., Clavell, L.A., et al. 2010. Assessment of dexrazoxane as a cardioprotectant in doxorubicin-treated children with high-risk acute lymphoblastic leukaemia: long-term follow-up of a prospective, randomised, multicentre trial. *Lancet Oncol* 11:950-961.
48. Matsui, H., Morishima, I., Numaguchi, Y., Toki, Y., Okumura, K., and Hayakawa, T. 1999. Protective effects of carvedilol against doxorubicin-induced cardiomyopathy in rats. *Life Sci* 65:1265-1274.
49. Kalay, N., Basar, E., Ozdogru, I., Er, O., Cetinkaya, Y., Dogan, A., Inanc, T., Oguzhan, A., Eryol, N.K., Topsakal, R., et al. 2006. Protective effects of carvedilol against anthracycline-induced cardiomyopathy. *J Am Coll Cardiol* 48:2258-2262.
50. Orogo, A.M., and Gustafsson, A.B. 2013. Cell death in the myocardium: my heart won't go on. *IUBMB Life* 65:651-656.
51. Shi, J., Zhang, L., Zhang, Y.W., Surma, M., Mark Payne, R., and Wei, L. 2012. Downregulation of doxorubicin-induced myocardial apoptosis accompanies postnatal heart maturation. *Am J Physiol Heart Circ Physiol* 302:H1603-1613.
52. Grasl-Kraupp, B., Ruttkey-Nedecky, B., Koudelka, H., Bukowska, K., Bursch, W., and Schulte-Hermann, R. 1995. In situ detection of fragmented DNA (TUNEL assay) fails to

- discriminate among apoptosis, necrosis, and autolytic cell death: a cautionary note. *Hepatology* 21:1465-1468.
53. Zhang, J., Clark, J.R., Jr., Herman, E.H., and Ferrans, V.J. 1996. Doxorubicin-induced apoptosis in spontaneously hypertensive rats: differential effects in heart, kidney and intestine, and inhibition by ICRF-187. *J Mol Cell Cardiol* 28:1931-1943.
  54. Lim, C.C., Zuppinger, C., Guo, X., Kuster, G.M., Helmes, M., Eppenberger, H.M., Suter, T.M., Liao, R., and Sawyer, D.B. 2004. Anthracyclines induce calpain-dependent titin proteolysis and necrosis in cardiomyocytes. *J Biol Chem* 279:8290-8299.
  55. Dhingra, R., Margulets, V., Chowdhury, S.R., Thliveris, J., Jassal, D., Fernyhough, P., Dorn, G.W., 2nd, and Kirshenbaum, L.A. 2014. Bnip3 mediates doxorubicin-induced cardiac myocyte necrosis and mortality through changes in mitochondrial signaling. *Proc Natl Acad Sci U S A* 111:E5537-5544.
  56. Wong-Ekkabut, J., Xu, Z., Triampo, W., Tang, I.M., Tieleman, D.P., and Monticelli, L. 2007. Effect of lipid peroxidation on the properties of lipid bilayers: a molecular dynamics study. *Biophys J* 93:4225-4236.
  57. Lu, L., Wu, W., Yan, J., Li, X., Yu, H., and Yu, X. 2009. Adriamycin-induced autophagic cardiomyocyte death plays a pathogenic role in a rat model of heart failure. *Int J Cardiol* 134:82-90.
  58. Kobayashi, S., Volden, P., Timm, D., Mao, K., Xu, X., and Liang, Q. 2010. Transcription factor GATA4 inhibits doxorubicin-induced autophagy and cardiomyocyte death. *J Biol Chem* 285:793-804.
  59. Kroemer, G., and Levine, B. 2008. Autophagic cell death: the story of a misnomer. *Nat Rev Mol Cell Biol* 9:1004-1010.
  60. Levine, B., and Kroemer, G. 2008. Autophagy in the pathogenesis of disease. *Cell* 132:27-42.
  61. Mizushima, N., and Komatsu, M. 2011. Autophagy: renovation of cells and tissues. *Cell* 147:728-741.
  62. Hara, T., Nakamura, K., Matsui, M., Yamamoto, A., Nakahara, Y., Suzuki-Migishima, R., Yokoyama, M., Mishima, K., Saito, I., Okano, H., et al. 2006. Suppression of basal autophagy in neural cells causes neurodegenerative disease in mice. *Nature* 441:885-889.
  63. Taneike, M., Yamaguchi, O., Nakai, A., Hikoso, S., Takeda, T., Mizote, I., Oka, T., Tamai, T., Oyabu, J., Murakawa, T., et al. 2010. Inhibition of autophagy in the heart induces age-related cardiomyopathy. *Autophagy* 6:600-606.
  64. Masiero, E., Agatea, L., Mammucari, C., Blaauw, B., Loro, E., Komatsu, M., Metzger, D., Reggiani, C., Schiaffino, S., and Sandri, M. 2009. Autophagy is required to maintain muscle mass. *Cell Metab* 10:507-515.
  65. Kim, J., Kim, Y.C., Fang, C., Russell, R.C., Kim, J.H., Fan, W., Liu, R., Zhong, Q., and Guan, K.L. 2013. Differential regulation of distinct Vps34 complexes by AMPK in nutrient stress and autophagy. *Cell* 152:290-303.
  66. Pattingre, S., Tassa, A., Qu, X., Garuti, R., Liang, X.H., Mizushima, N., Packer, M., Schneider, M.D., and Levine, B. 2005. Bcl-2 antiapoptotic proteins inhibit Beclin 1-dependent autophagy. *Cell* 122:927-939.
  67. Maiuri, M.C., Le Toumelin, G., Criollo, A., Rain, J.C., Gautier, F., Juin, P., Tasdemir, E., Pierron, G., Troulinaki, K., Tavernarakis, N., et al. 2007. Functional and physical interaction between Bcl-X(L) and a BH3-like domain in Beclin-1. *EMBO J* 26:2527-2539.
  68. Kimura, S., Noda, T., and Yoshimori, T. 2008. Dynein-dependent movement of autophagosomes mediates efficient encounters with lysosomes. *Cell Struct Funct* 33:109-122.

69. Jager, S., Bucci, C., Tanida, I., Ueno, T., Kominami, E., Saftig, P., and Eskelinen, E.L. 2004. Role for Rab7 in maturation of late autophagic vacuoles. *J Cell Sci* 117:4837-4848.
70. McEwan, D.G., Popovic, D., Gubas, A., Terawaki, S., Suzuki, H., Stadel, D., Coxon, F.P., Miranda de Stegmann, D., Bhogaraju, S., Maddi, K., et al. 2014. PLEKHM1 Regulates Autophagosome-Lysosome Fusion through HOPS Complex and LC3/GABARAP Proteins. *Mol Cell*.
71. Liang, C., Lee, J.S., Inn, K.S., Gack, M.U., Li, Q., Roberts, E.A., Vergne, I., Deretic, V., Feng, P., Akazawa, C., et al. 2008. Beclin1-binding UVRAG targets the class C Vps complex to coordinate autophagosome maturation and endocytic trafficking. *Nat Cell Biol* 10:776-787.
72. Matsunaga, K., Saitoh, T., Tabata, K., Omori, H., Satoh, T., Kurotori, N., Maejima, I., Shirahama-Noda, K., Ichimura, T., Isobe, T., et al. 2009. Two Beclin 1-binding proteins, Atg14L and Rubicon, reciprocally regulate autophagy at different stages. *Nat Cell Biol* 11:385-396.
73. Itakura, E., Kishi-Itakura, C., and Mizushima, N. 2012. The hairpin-type tail-anchored SNARE syntaxin 17 targets to autophagosomes for fusion with endosomes/lysosomes. *Cell* 151:1256-1269.
74. Guo, B., Liang, Q., Li, L., Hu, Z., Wu, F., Zhang, P., Ma, Y., Zhao, B., Kovacs, A.L., Zhang, Z., et al. 2014. O-GlcNAc-modification of SNAP-29 regulates autophagosome maturation. *Nat Cell Biol* 16:1215-1226.
75. Sardiello, M., Palmieri, M., di Ronza, A., Medina, D.L., Valenza, M., Gennarino, V.A., Di Malta, C., Donaudy, F., Embrione, V., Polishchuk, R.S., et al. 2009. A gene network regulating lysosomal biogenesis and function. *Science* 325:473-477.
76. Settembre, C., Di Malta, C., Polito, V.A., Garcia Arencibia, M., Vetrini, F., Erdin, S., Erdin, S.U., Huynh, T., Medina, D., Colella, P., et al. 2011. TFEB links autophagy to lysosomal biogenesis. *Science* 332:1429-1433.
77. Pillay, C.S., Elliott, E., and Dennison, C. 2002. Endolysosomal proteolysis and its regulation. *Biochem J* 363:417-429.
78. Forgac, M. 2007. Vacuolar ATPases: rotary proton pumps in physiology and pathophysiology. *Nat Rev Mol Cell Biol* 8:917-929.
79. Nixon, R.A., and Yang, D.S. 2012. Autophagy and neuronal cell death in neurological disorders. *Cold Spring Harb Perspect Biol* 4.
80. Tanaka, Y., Guhde, G., Suter, A., Eskelinen, E.L., Hartmann, D., Lullmann-Rauch, R., Janssen, P.M., Blanz, J., von Figura, K., and Saftig, P. 2000. Accumulation of autophagic vacuoles and cardiomyopathy in LAMP-2-deficient mice. *Nature* 406:902-906.
81. Kimura, S., Noda, T., and Yoshimori, T. 2007. Dissection of the autophagosome maturation process by a novel reporter protein, tandem fluorescent-tagged LC3. *Autophagy* 3:452-460.
82. Mizushima, N., Yoshimori, T., and Levine, B. 2010. Methods in mammalian autophagy research. *Cell* 140:313-326.
83. Linares, J.F., Duran, A., Yajima, T., Pasparakis, M., Moscat, J., and Diaz-Meco, M.T. 2013. K63 polyubiquitination and activation of mTOR by the p62-TRAF6 complex in nutrient-activated cells. *Mol Cell* 51:283-296.
84. Komatsu, M., Kurokawa, H., Waguri, S., Taguchi, K., Kobayashi, A., Ichimura, Y., Sou, Y.S., Ueno, I., Sakamoto, A., Tong, K.I., et al. 2010. The selective autophagy substrate p62 activates the stress responsive transcription factor Nrf2 through inactivation of Keap1. *Nat Cell Biol* 12:213-223.
85. Jain, A., Lamark, T., Sjøttem, E., Larsen, K.B., Awuh, J.A., Overvatn, A., McMahon, M., Hayes, J.D., and Johansen, T. 2010. p62/SQSTM1 is a target gene for transcription

- factor NRF2 and creates a positive feedback loop by inducing antioxidant response element-driven gene transcription. *J Biol Chem* 285:22576-22591.
86. Klionsky, D.J., Abdalla, F.C., Abeliovich, H., Abraham, R.T., Acevedo-Arozena, A., Adeli, K., Agholme, L., Agnello, M., Agostinis, P., Aguirre-Ghiso, J.A., et al. 2012. Guidelines for the use and interpretation of assays for monitoring autophagy. *Autophagy* 8:445-544.
  87. Kanamori, H., Takemura, G., Maruyama, R., Goto, K., Tsujimoto, A., Ogino, A., Li, L., Kawamura, I., Takeyama, T., Kawaguchi, T., et al. 2009. Functional significance and morphological characterization of starvation-induced autophagy in the adult heart. *Am J Pathol* 174:1705-1714.
  88. Nakai, A., Yamaguchi, O., Takeda, T., Higuchi, Y., Hikoso, S., Taniike, M., Omiya, S., Mizote, I., Matsumura, Y., Asahi, M., et al. 2007. The role of autophagy in cardiomyocytes in the basal state and in response to hemodynamic stress. *Nat Med* 13:619-624.
  89. Shimomura, H., Terasaki, F., Hayashi, T., Kitaura, Y., Isomura, T., and Suma, H. 2001. Autophagic degeneration as a possible mechanism of myocardial cell death in dilated cardiomyopathy. *Jpn Circ J* 65:965-968.
  90. Zhu, H., Tannous, P., Johnstone, J.L., Kong, Y., Shelton, J.M., Richardson, J.A., Le, V., Levine, B., Rothermel, B.A., and Hill, J.A. 2007. Cardiac autophagy is a maladaptive response to hemodynamic stress. *J Clin Invest* 117:1782-1793.
  91. Decker, R.S., Poole, A.R., Crie, J.S., Dingle, J.T., and Wildenthal, K. 1980. Lysosomal alterations in hypoxic and reoxygenated hearts. II. Immunohistochemical and biochemical changes in cathepsin D. *Am J Pathol* 98:445-456.
  92. Ma, X., Liu, H., Foyil, S.R., Godar, R.J., Weinheimer, C.J., Hill, J.A., and Diwan, A. 2012. Impaired autophagosome clearance contributes to cardiomyocyte death in ischemia/reperfusion injury. *Circulation* 125:3170-3181.
  93. Yan, L., Vatner, D.E., Kim, S.J., Ge, H., Masurekar, M., Massover, W.H., Yang, G., Matsui, Y., Sadoshima, J., and Vatner, S.F. 2005. Autophagy in chronically ischemic myocardium. *Proc Natl Acad Sci U S A* 102:13807-13812.
  94. Xie, M., Kong, Y., Tan, W., May, H., Battiprolu, P.K., Pedrozo, Z., Wang, Z.V., Morales, C., Luo, X., Cho, G., et al. 2014. Histone deacetylase inhibition blunts ischemia/reperfusion injury by inducing cardiomyocyte autophagy. *Circulation* 129:1139-1151.
  95. Sishi, B.J., Loos, B., van Rooyen, J., and Engelbrecht, A.M. 2013. Autophagy upregulation promotes survival and attenuates doxorubicin-induced cardiotoxicity. *Biochem Pharmacol* 85:124-134.
  96. Force, T., and Kolaja, K.L. 2011. Cardiotoxicity of kinase inhibitors: the prediction and translation of preclinical models to clinical outcomes. *Nat Rev Drug Discov* 10:111-126.
  97. Konorev, E.A., Vanamala, S., and Kalyanaraman, B. 2008. Differences in doxorubicin-induced apoptotic signaling in adult and immature cardiomyocytes. *Free Radic Biol Med* 45:1723-1728.
  98. Ma, Y., Zhang, X., Bao, H., Mi, S., Cai, W., Yan, H., Wang, Q., Wang, Z., Yan, J., Fan, G., et al. 2012. Toll-like receptor (TLR) 2 and TLR4 differentially regulate doxorubicin induced cardiomyopathy in mice. *PLoS One* 7:e40763.
  99. Zhang, Y., Kang, Y.M., Tian, C., Zeng, Y., Jia, L.X., Ma, X., Du, J., and Li, H.H. 2011. Overexpression of Nr1h3 in the heart exacerbates doxorubicin-induced cardiac dysfunction in mice. *PLoS One* 6:e21104.
  100. Kawaguchi, T., Takemura, G., Kanamori, H., Takeyama, T., Watanabe, T., Morishita, K., Ogino, A., Tsujimoto, A., Goto, K., Maruyama, R., et al. 2012. Prior starvation mitigates acute doxorubicin cardiotoxicity through restoration of autophagy in affected cardiomyocytes. *Cardiovasc Res* 96:456-465.

101. Singal, P.K., Segstro, R.J., Singh, R.P., and Kutryk, M.J. 1985. Changes in lysosomal morphology and enzyme activities during the development of adriamycin-induced cardiomyopathy. *Can J Cardiol* 1:139-147.
102. Ding, Y., Sun, X., Huang, W., Hoage, T., Redfield, M., Kushwaha, S., Sivasubbu, S., Lin, X., Ekker, S., and Xu, X. 2011. Haploinsufficiency of target of rapamycin attenuates cardiomyopathies in adult zebrafish. *Circ Res* 109:658-669.

**CHAPTER 2.**  
**DOXORUBICIN INHIBITS CARDIOMYOCYTE AUTOPHAGIC FLUX**  
**BY SUPPRESSING LYSOSOMAL ACIDIFICATION**

## INTRODUCTION

Doxorubicin is a commonly used chemotherapeutic drug. However, its clinical use has been limited due to dose-dependent cardiotoxicity (1, 2). While controversy exists about the proposed initial events driving the pathogenesis of doxorubicin cardiomyopathy, accumulation of reactive oxygen species (ROS) (3) and mitochondrial damage (4) are considered key contributors. The relatively low levels of antioxidant enzymes (5) and high autophagic flux (6) in heart raise the possibility that autophagy serves as an important defense mechanism against ROS and organelle damage.

Autophagy is a dynamic process that entails a relay of multiple steps to deliver cytosolic materials to lysosomes for degradation (7). While autophagosome formation is critical for the autophagy process, later steps including autophagosome turnover and internal cargo degradation by lysosomes are also critical for ensuring the completion of autophagy as a dynamic process. Disruption of the relay in any of these steps might block autophagic flux, leading to cell injury and increased fragility to stress (8-11).

Previous studies have shown that autophagy plays an important role in cardiac physiology (8); dysregulation of autophagy contributes to the pathogenesis of various cardiovascular diseases, leading to cardiomyopathy and heart failure (8, 9, 12).

Autophagy serves as a robust system protecting the heart from redox injury and internal organelle damage (4, 8, 13), yet still, doxorubicin causes progressive cardiac toxicity. Either this is because the mitochondrial damage and accumulation of ROS overwhelm the defensive systems or the defense system, *i.e.* autophagy, is compromised by doxorubicin. In order to accurately assess doxorubicin's effect on cardiac autophagy, I developed a mouse model of chronic doxorubicin cardiotoxicity that avoided doxorubicin's systematic toxicity and non-cardiac lethality. My data further show that doxorubicin inhibits cardiomyocyte autophagic flux by altering lysosomal pH and function *in vitro*.

## RESULTS

### ***A mouse model of doxorubicin cardiomyopathy reflects the clinical scenario.***

Patients who develop chronic cardiomyopathy attributed to doxorubicin exposure typically manifest slowly progressive cardiomyopathy. Further, initial exposure to the drug is relatively well tolerated. In contrast, most preclinical models reported in the literature involve high-dose doxorubicin delivered intraperitoneally and are marked by systemic toxicity, including malaise, lethargy, anorexia, and weight loss. These effects outside the myocardium do not reflect the clinical toxicity experienced by patients. Further, they are likely to confound the interpretation of doxorubicin effects on cardiomyocyte autophagy. Therefore, I first developed a chronic doxorubicin cardiomyopathy model that is not marked by these constitutional events.

Intravenous administration of low-dose doxorubicin (5 mg/kg) in a regime of four once-per-week injections was employed (**Figure 2.1A**). Left ventricular systolic function, tracked by serial echocardiography, was marked by progressive declines, reminiscent of clinical observations. Cardiac function remained depressed when measured four weeks after the last dose was given (**Figure 2.1B, C**). Meanwhile, mice appeared healthy, consumed normal quantities of food (**Figure 2.1D**), and gained weight normally (**Figure 2.1E**). In addition, this protocol did not cause mortality at 7 weeks; by contrast, other acute and chronic models of doxorubicin cardiomyopathy that I tested have resulted in lethality (heart failure irrelevant) before the end of the study (**Figure 2.1F, G**).

### ***Doxorubicin inhibits cardiomyocyte autophagic flux in vivo***

To evaluate autophagic flux, I quantified markers of autophagy in control and treated hearts. Steady state levels of the autophagy marker LC3-II showed an increase at 24 hours post-doxorubicin injection, persisted to day 3, and eventually returned to baseline by 7 days (**Figure 2.2A**). The protein level of another marker of autophagy p62/SQSTM1 also increased

by 24 hours, but returned to baseline by the third day (**Figure 2.2A**). However, mRNA abundance of several autophagy-related genes, including *p62/Sqstm1* (but not *Lc3b*), increased 24 hours after doxorubicin injection making it hard to interpret changes in autophagy with this specific marker (**Figure 2.2B**). I reasoned that these transcript changes likely reflect a stress response to doxorubicin.

Increases in steady state LC3-II levels may derive from increased autophagic activation or a downstream block of autophagosome processing resulting in decreased turnover of LC3-II. To distinguish between these two possibilities, I treated mice with *i.p.* injection of bafilomycin A1 (BafA1), a late stage inhibitor of autophagy. Further, mice were caged individually without food for the last 2 hours before sacrifice, and were sacrificed at the same time of the day, in order to eliminate possible confounding factors affecting autophagy. Treatment of the animals with BafA1 for 2 hours resulted in a significant increase in LC3-II levels, consistent with normal autophagic flux (**Figure 2.3A**). However, doxorubicin-treated animals showed no further increase in LC3-II levels with BafA1 treatment (**Figure 2.3A**). BafA1 treatment appeared less effective in increasing p62 protein levels in heart in my experiments (**Figure 2.3A**), and therefore I conclude that the protein might be less reliable in evaluating autophagic flux in this context. Similar findings of LC3-II were observed after the full 4-week course of serial doxorubicin injections (**Figure 2.3B**). These data suggest that the accumulation of LC3-II in doxorubicin-treated animals stems from an inhibition of LC3-II turnover and indicate a block in autophagic flux.

Next, I tested whether starvation, a robust trigger of autophagic flux, could rescue the apparent block in autophagy caused by doxorubicin. As expected, starvation triggered a strong increase in autophagic flux in the control group, as measured by LC3-II accumulation, and yet this flux was not observed in doxorubicin-treated mice (**Figure 2.3A**). Here starvation-induced autophagic flux was also reflected in the change of p62 levels, since bafA1 induced p62

accumulation upon starvation; however, the accumulation of p62 by bafA1 was also not observed in the doxorubicin group. These data provide additional evidence that doxorubicin inhibits autophagy by targeting distal events in the flux cascade.

Interestingly, the blockage of autophagic flux appeared to be reversible. Accumulation of LC3-II in doxorubicin-treated hearts appeared after 24 hours, persisted at 72 hours, but then LC3-II protein level returned back to normal baseline (**Figure 2.2A**). In addition, although autophagy was inhibited in mouse hearts 24 hours after the fourth serial doxorubicin injection (**Figure 2.3B**), it was restored, and even increased at late stage - 4 weeks after chronic doxorubicin injections (**Figure 2.3C**). Since heart is an organ that relies on high autophagy levels (6), frequent short-term inhibitions of autophagic flux might lead to cardiomyocyte dysfunction even at the basal level; furthermore, lack of autophagic flux might compromise cardiomyocytes' ability to diminish the damaged organelles by doxorubicin. Therefore, although the evidence indicated that the inhibition of autophagic flux might be temporary and reversible, the cumulative injuries caused by inhibition of autophagic flux accompanied with every injection of doxorubicin might be significant.

Autophagy is a multi-step, dynamic process. To map the specific step within the autophagic cascade inhibited by doxorubicin, I employed an autophagic flux reporter mouse model, which harbors an RFP-GFP-LC3 transgene expressed driven by the universally expressed promoter CAG (14). As RFP (pKa 4.5) fluorescence is stable in an acidic environment, whereas GFP (pKa 5.9) fluorescence is quenched in the acidic lysosomal compartment, autophagosomes (GFP/RFP) can be distinguished from autolysosomes (RFP only), and flux can be tested directly.

With the autophagic flux reporter mice, I examined hearts after doxorubicin treatment. Surprisingly, doxorubicin elicited an increase in autolysosomes in the heart, with no significant change in autophagosome numbers (**Figure 2.4A, B**). Furthermore, BafA1, which inhibits autophagosome-lysosome fusion, induced comparable increases of autophagosomes in both

normal saline- and doxorubicin-treated groups; however, there remained a trend of increased autolysosomes in doxorubicin-treated group than control group (**Figure 2.4A, B**).

The indications of these findings are two fold. Firstly, the comparable increase of autophagosomes after BafA1 treatment in both groups excluded the possibility that autolysosomal accumulation by doxorubicin was due to increased efficiency of autophagosome maturation and autophagosome-lysosome fusion – henceforth, increased autophagy. Secondly, accumulation of autolysosomes rather than autophagosomes by doxorubicin suggests that the defect in LC3-II turnover induced by doxorubicin occurs at a point downstream of autophagosome-lysosome fusion. Doxorubicin-treated hearts were marked by accumulation of vesicles containing electron-dense content on electron microscopy (**Figure 2.4C**), again consistent with increased numbers of lysosomes/autolysosomes. These data are consistent with a model in which doxorubicin blocks autophagic flux by inhibiting autolysosome turnover.

### ***Doxorubicin inhibits autophagic flux in cultured cardiomyocytes***

To test the effects of doxorubicin directly in cardiomyocytes, I treated neonatal rat ventricular myocytes (NRVMs) with doxorubicin. Suppression of autophagic flux – shown as the lack of BafA1-induced accumulation of both LC3-II and p62 - by doxorubicin was dose-dependent (**Figure 2.5A**). It has been suggested that doxorubicin concentrations greater than 2  $\mu\text{M}$  do not reflect the clinically relevant context (15), so I employed doxorubicin at 1  $\mu\text{M}$ . Treatment of NRVMs with doxorubicin resulted in a decrease in autophagic flux as measured by LC3-II levels within 6 hours with the maximum effect by 18 hours (**Figure 2.5B**). Doxorubicin decreased both p62 protein and *p62/Sqstm1* transcript levels (**Figure 2.5A, B, Figure 2.7A**), contrary to *in vivo* changes. As a secondary assessment of autophagy I looked at long-lived protein degradation by pulse chase analysis. Stimulation of autophagy by starvation increases long-lived protein turnover in NRVMs and this increase is inhibited in doxorubicin-treated cells

(**Figure 2.5C**). Interestingly, unlike the complete blockage of BafA1-inhibitable LC3-II turnover, that I observed in the western blotting analysis, doxorubicin only partially blocked wholesale turnover of long-lived proteins when compared to BafA1. This suggests that doxorubicin-induced inhibition of lysosomal degradation may not be complete. Regardless, these data are consistent with an ability of doxorubicin to inhibit autophagic flux *in vitro*.

To test for generalizability beyond NRVMs, I evaluated autophagic flux in other cell types commonly used for studying cardiomyocyte biology. I found that overnight treatment with doxorubicin inhibited autophagic flux in adult rat cardiomyocytes, cardiomyocyte-like cells differentiated from human embryonic stem cells, and H9c2 cells (**Figure 2.6A-C**). By contrast, doxorubicin did not alter autophagic flux in the skeletal myoblast cell line C2C12 (**Figure 2.6C**).

I noticed that in contrast to my *in vivo* observations, cardiomyocytes did not present with an accumulation of LC3-II after doxorubicin exposure, even though autophagic flux is still abolished. I reasoned that in cultured cardiomyocytes, the initiation of autophagy might also be compromised. Consistent with this, I found that doxorubicin decreased the transcript abundance of several of autophagic genes (**Figure 2.7A, B**) in cultured cardiomyocytes (NRVMs and ARVMs).

I next employed the tandem fluorescence RFP-GFP-LC3 reporter system (described earlier), introduced by lentivirus infection, as an additional monitor of autophagic flux in NRVMs. Consistent with the *in vivo* data, a significant increase in autolysosome numbers, without changes in autophagosome numbers, was observed after doxorubicin exposure (**Figure 2.8A**). Transmission electron microscopy revealed an accumulation of autolysosomes in doxorubicin-treated cardiomyocytes (**Figure 2.8B**). In aggregate, my data lend strong credence to a model in which doxorubicin inhibits autophagic flux in cultured cardiomyocytes at a point downstream of autolysosomal fusion.

***mTORC1 activation is not required for doxorubicin-triggered block of autophagic flux***

It is well established that mTORC1 activation inhibits autophagy initiation by phosphorylating ULK1 (16). Furthermore, it has been reported that mTORC1 activity also affects lysosomal biogenesis and lysosomal function (17). For these reasons, I examined whether doxorubicin alters mTORC1 activity in cardiomyocytes. Western analysis of known mTORC1 targets (S6K, S6 and 4EBP1) in hearts from doxorubicin-treated mice (**Figure 2.9A**) and in doxorubicin-treated cardiomyocytes (**Figure 2.9B**) both suggest significant stimulation of mTORC1 activity with doxorubicin treatment. Therefore, I next examined whether mTOR activity *per se* was required for the inhibition of autophagic flux by doxorubicin. To test for a requirement of mTORC1 activation, I treated the NRVMs with torin 1, a robust and specific inhibitor of mTORC1. As expected, in control group torin 1 blunted mTORC1 activity (**Figure 2.10A**) and increased the LC3-II/LC3-I ratio (**Figure 2.10B, C**), suggesting an increase of autophagy. However, torin 1 failed to rescue the inhibition of autophagic flux elicited by doxorubicin (**Figure 2.10B, C**). This suggests that even though doxorubicin activates mTORC1, inhibition of autophagy by doxorubicin is not dependent on up-regulation of mTORC1 activity.

***Doxorubicin inhibits lysosome function by elevating lysosomal pH***

My data demonstrate that doxorubicin blocks cardiomyocyte autophagic flux and promotes accumulation of autolysosomes, suggesting that doxorubicin impairs the lysosomal degradation at a point downstream of fusion. This observation, coupled with the decrease in long-lived protein turnover in doxorubicin treated cells, led us to examine lysosomal proteolysis in these cells. To pursue this, I measured the activities of cathepsin B and cathepsin L, two important lysosomal enzymes in NRVMs, using substrate-based cathepsin assays. Cresyl Violet (CV) fluorogenic substrates CV-(Arg-Arg)<sub>2</sub> and CV-(Phe-Arg)<sub>2</sub> harbor dipeptides targeted by cathepsin B and cathepsin L, respectively. Non-fluorescent themselves, both substrates are

converted to red fluorescent forms after hydrolysis of the two peptide sequences. Using flow cytometry, I was able to separate the red fluorescence signal elicited by doxorubicin from red fluorescence resulting from substrate cleavage (**Figure 2.11A**). By quantifying the signal from substrate cleavage, I found that doxorubicin triggered decreased activities of both enzymes (**Figure 2.11B**). By contrast, when I measured cathepsin B/L activities in pre-made reaction buffer (50 mM sodium acetate, 8 mM EDTA, 8 mM dithiothreitol, pH 5.0), I found no significant decrease in enzyme activities after doxorubicin treatment (**Figure 2.11C**). Next, I evaluated lysosome abundance by immunostaining for LAMP-1 and LAMP-2, two lysosome-specific markers. I observed that doxorubicin did not alter the intensity of LAMP-1 or LAMP-2 staining (**Figure 2.11D**), suggesting that doxorubicin did not alter lysosome numbers in NRVMs. These data suggest that the decreased enzyme activity was not due to declines in lysosome numbers or enzyme abundance/dysfunction, but rather due to changes in the lysosomal environment.

Next, I stained lysosomes with LysoTracker Red, a fluorescent dye that labels acidic organelles in live cells. I observed that doxorubicin treatment significantly decreased the numbers of LysoTracker Red puncta (**Figure 2.12A**). Similar results were seen using Acridine Orange, another dye that fluoresces red in an acid compartment (**Figure 2.12B**). Together, these data suggest that doxorubicin alters lysosome acidification. To test this further, I measured lysosomal pH qualitatively using lysosensor DND-189 and flow cytometry. DND-189 emits green fluorescence, the intensity of which increases within an acidic environment. Doxorubicin decreased DND-189 fluorescence in a time-dependent manner, suggesting that doxorubicin decreases lysosome acidity in NRVMs (**Figure 2.12C**). Comparable results were noted with a short-term treatment with BafA1 or NH<sub>4</sub>Cl (**Figure 2.12C**), which are well established to decrease lysosome acidity of the lysosome (18, 19).

In order to assess lysosomal pH quantitatively, I measured lysosome pH in cardiomyocytes directly using Dextran, Oregon Green 514, a fluorescent dye conjugated to

dextran. It can be excited by light of both 488 and 440 nm wavelength; its fluorescence when excited by 488 nm wavelength of light robustly increases when pH decreases, while the fluorescence excited by 440 nm wavelength of light remains stable. Therefore, an internal loading control can be achieved with utilization of Dextran, Oregon Green 514. This reagent provides a reliable standard curve of pH within the range of 4.0 to 6.5 (**Figure 2.13A**). As positive controls, brief treatment with BafA1 or NH<sub>4</sub>Cl increased lysosomal pH, as expected (**Figure 2.13B**). Next, I quantified lysosome pH following doxorubicin treatment, observing that doxorubicin increased lysosomal pH in NRVMs from 4.6 to 5.2 (**Figure 2.13B**). Together, these data suggest strongly that doxorubicin impairs lysosome acidification.

To test whether changes in lysosome function are specific to doxorubicin or derive nonspecifically from cytotoxicity, I first examined two other chemotherapeutic agents known to cause cardiotoxicity: sunitinib and paclitaxel. In NRVMs exposed to either drug overnight, I noted either no change (paclitaxel) or slight increases (sunitinib) in autophagic flux (**Figure 2.14A**). Using drug concentrations that are more clinically relevant (20, 21), I tested their effects on lysosomal pH, using both DND-189 and Dextran, Oregon Green 514. Neither drug caused an increase in DND-189 signals (**Figure 2.14B**); using dextran, Oregon Green 514 to measure lysosomal pH, I found that sunitinib decreased lysosomal pH, while paclitaxel raised it slightly (from 4.6 to 4.8), yet still within the normal range of lysosomal pH (**Figure 2.14C**). Given the differences in both autophagic changes and lysosomal pH alterations, I excluded the possibility that doxorubicin affects lysosomal pH and autophagic flux in cardiomyocytes similarly as other chemotherapeutic drugs such as sunitinib and paclitaxel.

### ***Doxorubicin inhibits V-ATPase-driven lysosome acidification***

The activities of most lysosomal enzymes are tightly regulated by pH (22). The acidic luminal environment of the lysosome is mainly attributed to the activity of the vacuolar H<sup>+</sup>-

ATPase (V-ATPase) (23), a multi-subunit protein on the surface of the lysosome. To test possible effects of doxorubicin on V-ATPase-mediated lysosome acidification, lysosomes were loaded with pH-sensitive dextran and treated with doxorubicin or normal saline (NS) overnight. First, lysosomes were transiently alkalinized by  $\text{NH}_4\text{Cl}$ -containing buffer, which acts by generating  $\text{NH}_3$ , which then rapidly diffuses across cytoplasmic membrane and into lysosomes, where it is protonated and trapped as ammonium ion (19). Next, re-acidification was initiated by removal of  $\text{NH}_4\text{Cl}$  and concomitant provision of magnesium-containing buffer.

Upon withdrawal of  $\text{NH}_4\text{Cl}$ , an early recovery of lysosome pH is observed due to the release of hydrogen ions by  $\text{NH}_4^+$  within the lysosome (**Figure 2.15A**). However, further recovery of lysosomal pH depends on V-ATPase activity. This is consistent with the observation that lysosomes rapidly re-acidified to baseline in NS-treated cardiomyocytes. By contrast, concanamycin A (CcA)-treated cells displayed an initial decrease in lysosomal pH, followed by a failure to re-acidify due to inhibition of V-ATPase (**Figure 2.15A, B**). Consistent with my previous pH measurements, doxorubicin-treated NRVMs displayed increased lysosome pH under baseline conditions. Further, failure of lysosomes to re-acidify after  $\text{NH}_4\text{Cl}$  washout was observed (**Figure 2.15A, B**).

These observations suggest that doxorubicin inhibits lysosome acidification through suppression of V-ATPase activity. The V-ATPase complex comprises fourteen subunits, assembled into an ATP-hydrolytic domain (V1) and a proton-translocation domain (V0). Energy from ATP hydrolysis within the V1 domain is used to transport protons into the lysosomal lumen through the V0 domain. The association/dissociation of V1 and V0 domains on lysosomes is an important regulatory mechanism of V-ATPase activity (23). To test whether doxorubicin affects the assembly of the domains on lysosomes, I isolated the lysosome-rich fraction from NRVMs and examined the presence of several subunit proteins of V1 and V0 domains. However, I

detected no changes in the amounts of these proteins on lysosomes, suggesting doxorubicin might not affect the assembly of V1V0 domains (**Figure 2.16A**).

Doxorubicin continued to induce mTORC1 activation, even in the setting of starvation (**Figure 2.16B**). Published work suggests that ATP hydrolysis at the V1 domain of the V-ATPase is essential for amino acid activation of mTORC1 (24). I observed that silencing specific V-ATPase subunits using siRNA abolished the activation of mTORC1 by doxorubicin (**Figure 2.16C**). This evidence suggests that ATPase hydrolysis is likely intact and argues that uncoupling of V1V0 domains or dysfunction of the V0 domain may underlie suppression of V-ATPase activity in doxorubicin-treated cells.

### ***Doxorubicin alters subcellular lysosomal localization***

Additionally, I found that doxorubicin alters lysosomal subcellular localizations in NRVMs. Using LAMP-2 as a marker of lysosomes, I observed that doxorubicin-treated NRVMs have more dispersed lysosomal localizations within the cell while more lysosomes localize to the perinuclear region in control cardiomyocytes (**Figure 2.17A,B**). The subcellular localization pattern of lysosomes between control and doxorubicin-treated NRVMs was more pronounced upon starvation treatment: starvation induced perinuclear localization of lysosomes, which was blunted by doxorubicin treatment (**Figure 2.17A-C**).

Moreover, I found that in NRVMs, mTOR closely colocalized with LAMP-2 under basal conditions; further, doxorubicin increased mTOR and LAMP-2 colocalization both under basal conditions (**Figure 2.17D**) and upon starvation (**Figure 2.17D**, increased trend), consistent with the previous observation that doxorubicin increased mTORC1 activity, since mTOR recruitment to the lysosome is essential for its activation (25). Because mTOR did not show changes in subcellular distribution upon doxorubicin treatment (data not shown), it is

possible that the increased colocalization of mTOR and LAMP-2 was due to the increased lysosomal localization to peripheral areas of the cell.

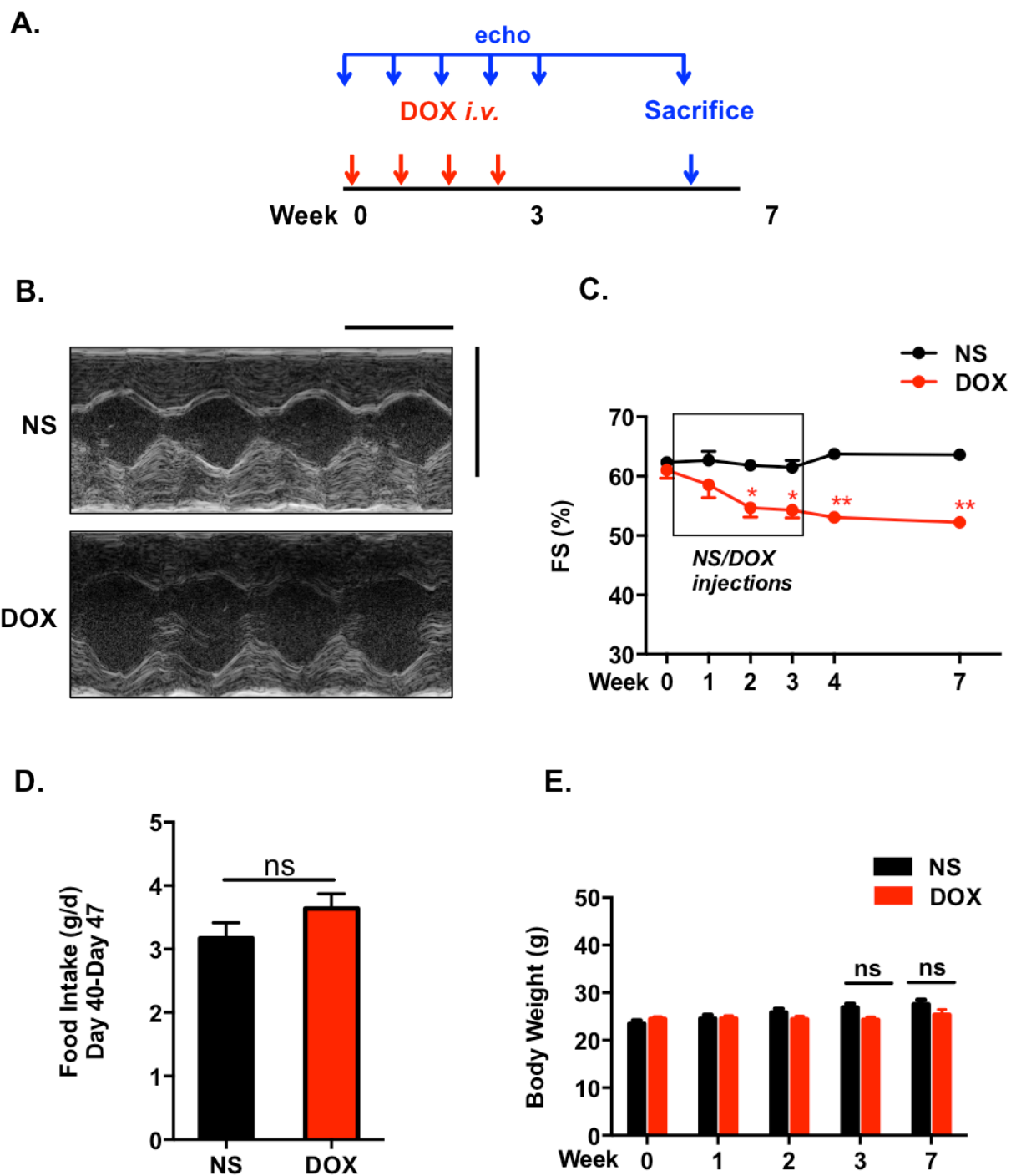
Korolchuk et al. (26) reported that lysosomal positioning regulates mTOR activity: activation of mTORC1 correlated with peripheral distribution of lysosomes. Disruption of lysosomal movement abolished mTORC1 activation. Here I observed that doxorubicin activated mTORC1, and the activation of mTORC1 appeared to require the presence of V-ATPase. On the other hand, mTORC1 activation by doxorubicin correlates with a more peripheral distribution of lysosomes. It is not clear yet in this case whether the altered lysosomal positioning had any causal relationship with the change in lysosomal pH. Furthermore, the trafficking of autophagosomes and lysosomes to perinuclear region promotes autophagosome-lysosome fusion (27). Conversely, the movement of lysosomes to peripheral areas has been reported to decrease autophagosome-lysosome fusion (26). However in my case, autophagosome accumulation was not observed, meaning autophagosome-lysosome fusion was not affected. Therefore, the alteration of lysosomal localization by doxorubicin might partially explain its activation of mTORC1, but it seems inadequate to explain the accumulation of autolysosomes, but not autophagosomes, observed in the study.

### ***Inhibition of ROS damage failed to rescue autophagic flux inhibition by doxorubicin***

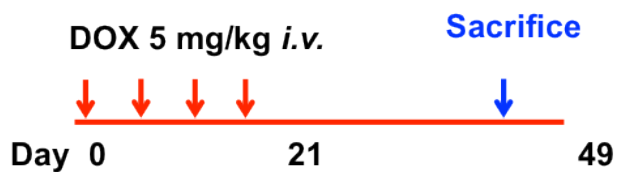
Since ROS production is deemed an important contributor to doxorubicin-induced cardiotoxicity, I set out to examine whether ROS production plays a role in doxorubicin-induced autophagic flux inhibition in cultured NRVMs. Dexrazoxane (DXZ) - an iron-chelator and FDA-approved therapeutic for doxorubicin cardiomyopathy, and trolox – an analogue of vitamin E, are potent ROS scavengers and inhibitors of ROS damage. However, co-treatment of NRVMs with either compound along with doxorubicin failed to rescue the blockage of autophagic flux caused by doxorubicin (**Figure 2.18A, B**). These data suggest that ROS production is less likely

to be the cause of autophagic alteration by doxorubicin in NRVMs. However, whether ROS scavengers could rescue the autophagic flux inhibition *in vivo* is not known and warrants further studies in the future.

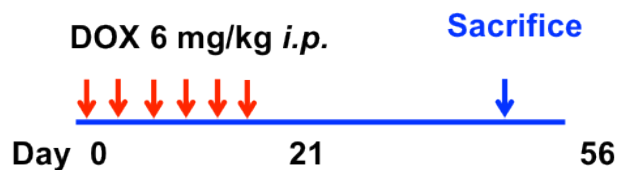
Figure 2.1



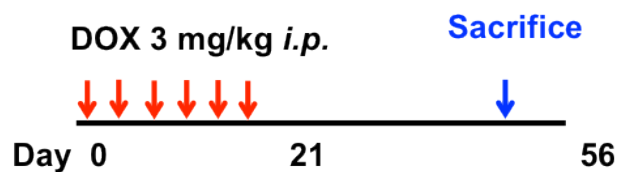
F.



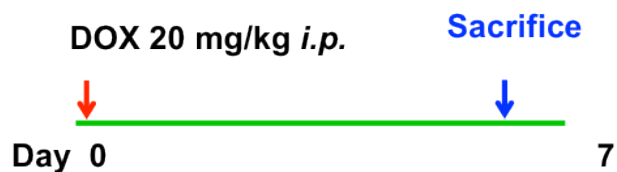
Protocol 0 (current in use)



Protocol 1 (total dose 36 mg/kg)



Protocol 2 (total dose 18 mg/kg)



Protocol 3 (total dose 20 mg/kg)

G.

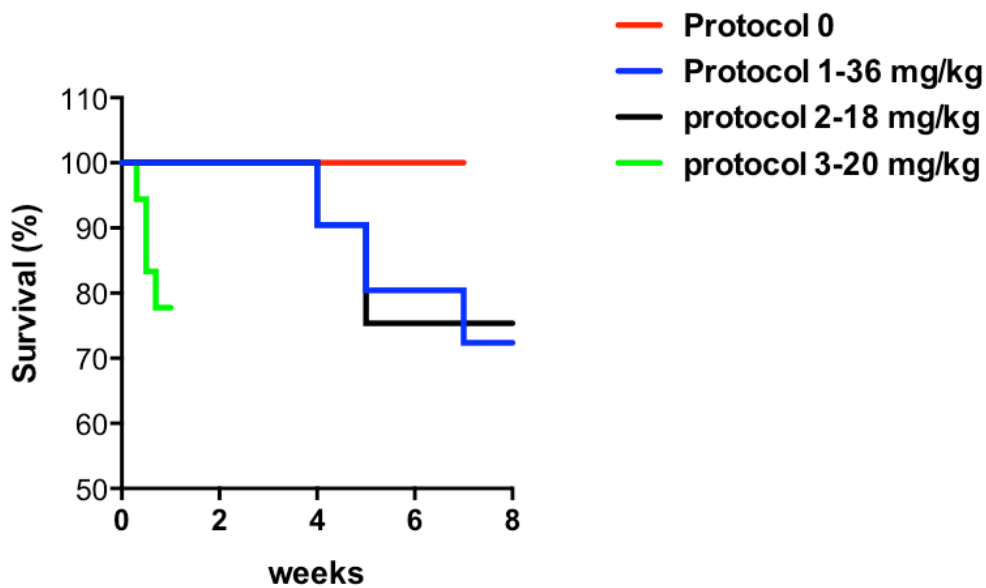


**Figure 2.1. A mouse model of chronic doxorubicin cardiomyopathy without systemic toxicity.** (A) Schematic of chronic doxorubicin administration protocol. C57BL/6 mice of 8 to 9-week-old were subjected to four serial doxorubicin (5 mg/kg) injections weekly via tail vein. Echocardiography was used to examine cardiac function in week 0, 1, 2, 3, 4 and 7. Mice were sacrificed on day 49, 7 weeks after the initial injection (4 weeks after the last injection). (B) Doxorubicin-treated mice developed dilated cardiomyopathy after serial doxorubicin injections. (C) Cardiac function declined continuously with serial injections of doxorubicin. N = 10 per group. (D) Food intake after treatment was not reduced in doxorubicin group. An average of food intake from day 41 to day 47 was calculated for each mouse. N = 8 mice per group. (E) Doxorubicin did not affect significantly body weight following the protocol. N = 10-13 in each group. (F) Comparison of the current protocol with other chronic and acute doxorubicin cardiotoxicity models. (G) All the other three protocols listed caused significant (non-cardiac) lethality in mice. N = 10-20 per group. FS, Fractional Shortening. \*,  $p < 0.05$  versus control; ns, not significant.

Figure 2.2

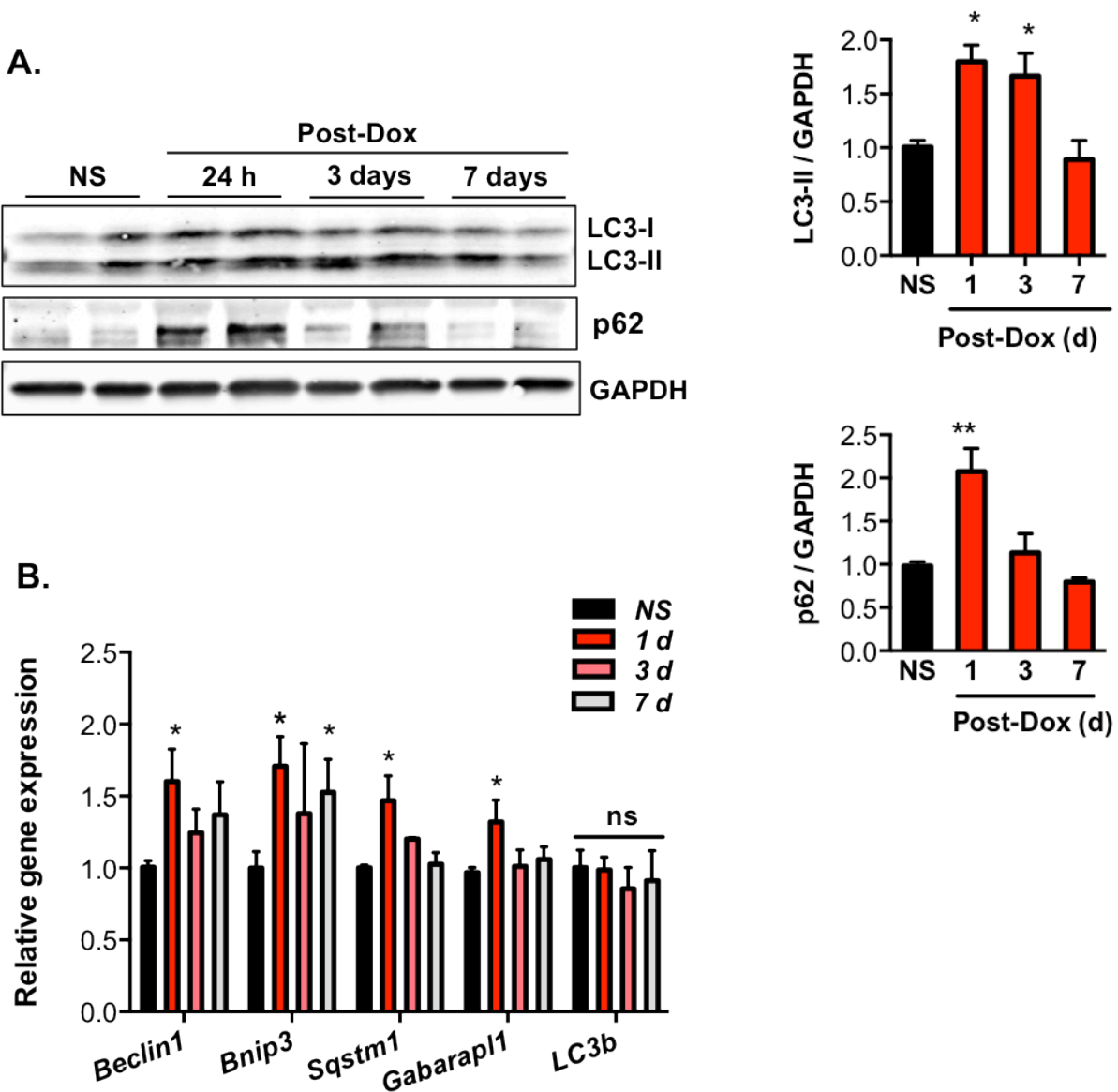


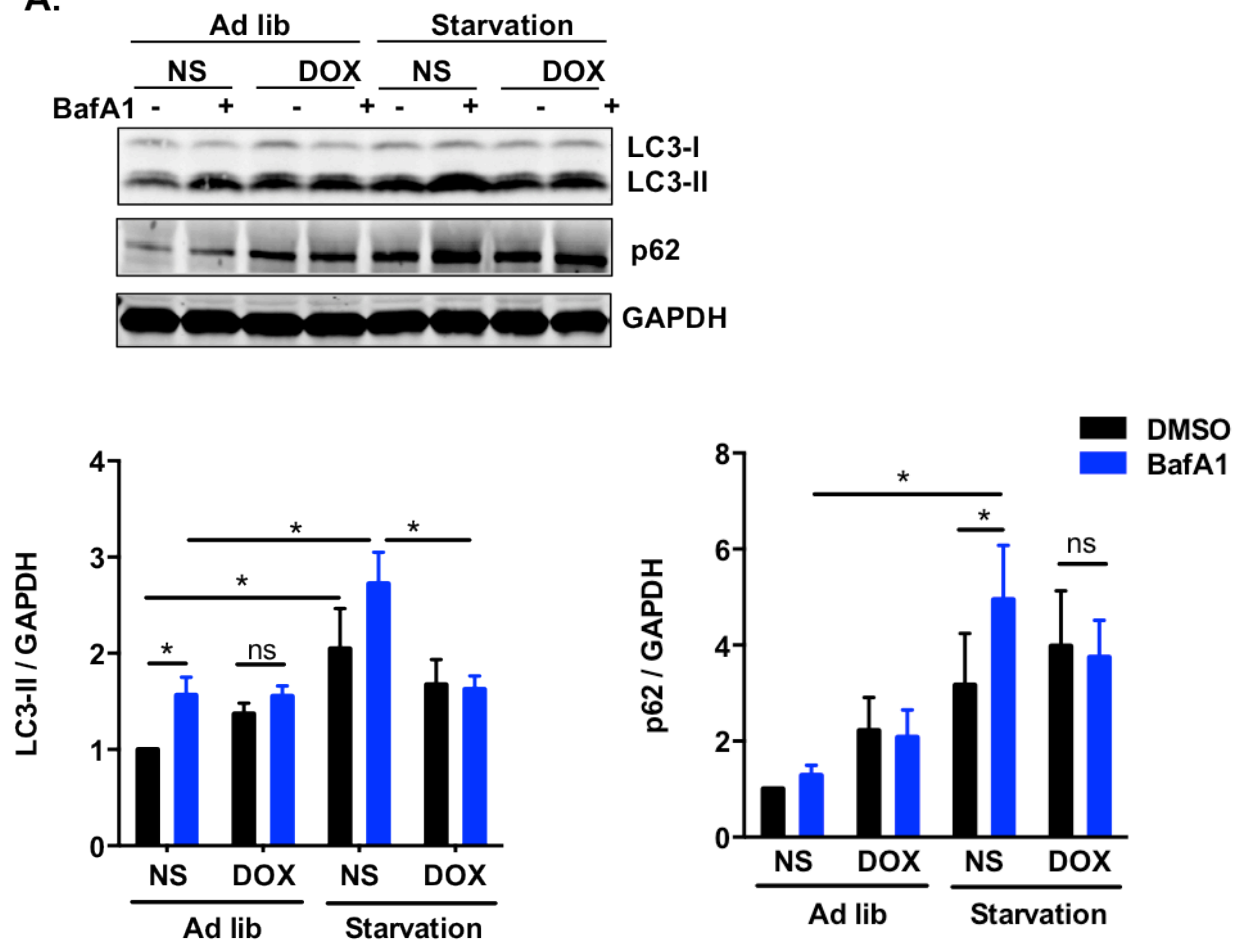
**Figure 2.2. Doxorubicin causes temporal changes of autophagy markers.**

(A) Temporal changes of LC3-II and p62 protein levels after one dose of doxorubicin. Hearts were harvested at different time points after *i.v.* injection of doxorubicin (5 mg/kg, DOX) or normal saline (NS). N = 3-5 mice per group.

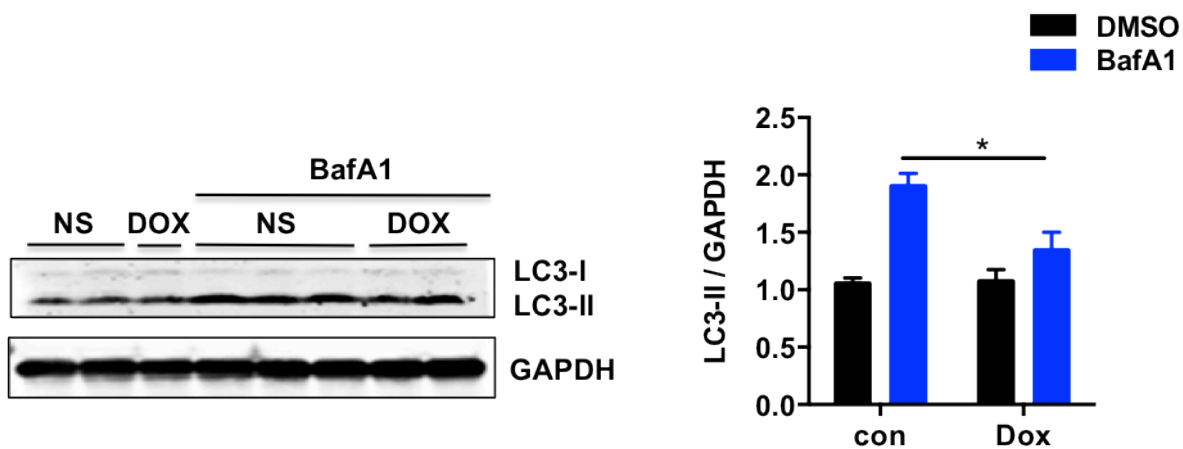
(B) Quantification of transcript levels of multiple autophagy-related genes (including *p62/Sqstm1*) at different time points after doxorubicin treatment. N = 3-6 mice per group. NS, normal saline. DOX, doxorubicin. \*,  $p < 0.05$ ; ns, not significant.

Figure 2.3

A.



B.



C.

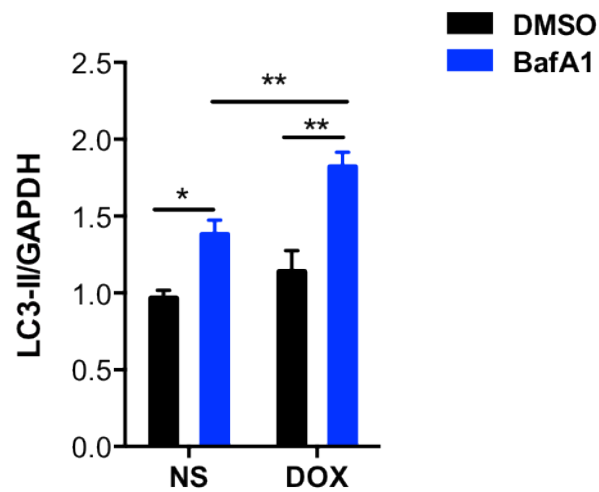
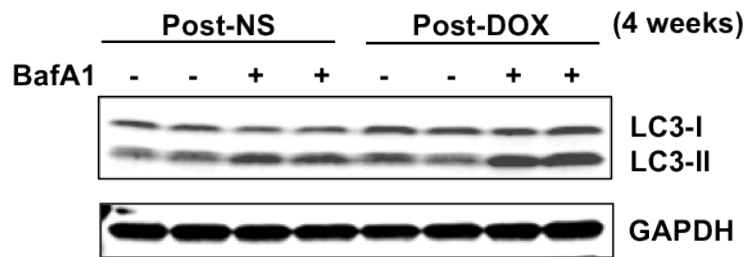
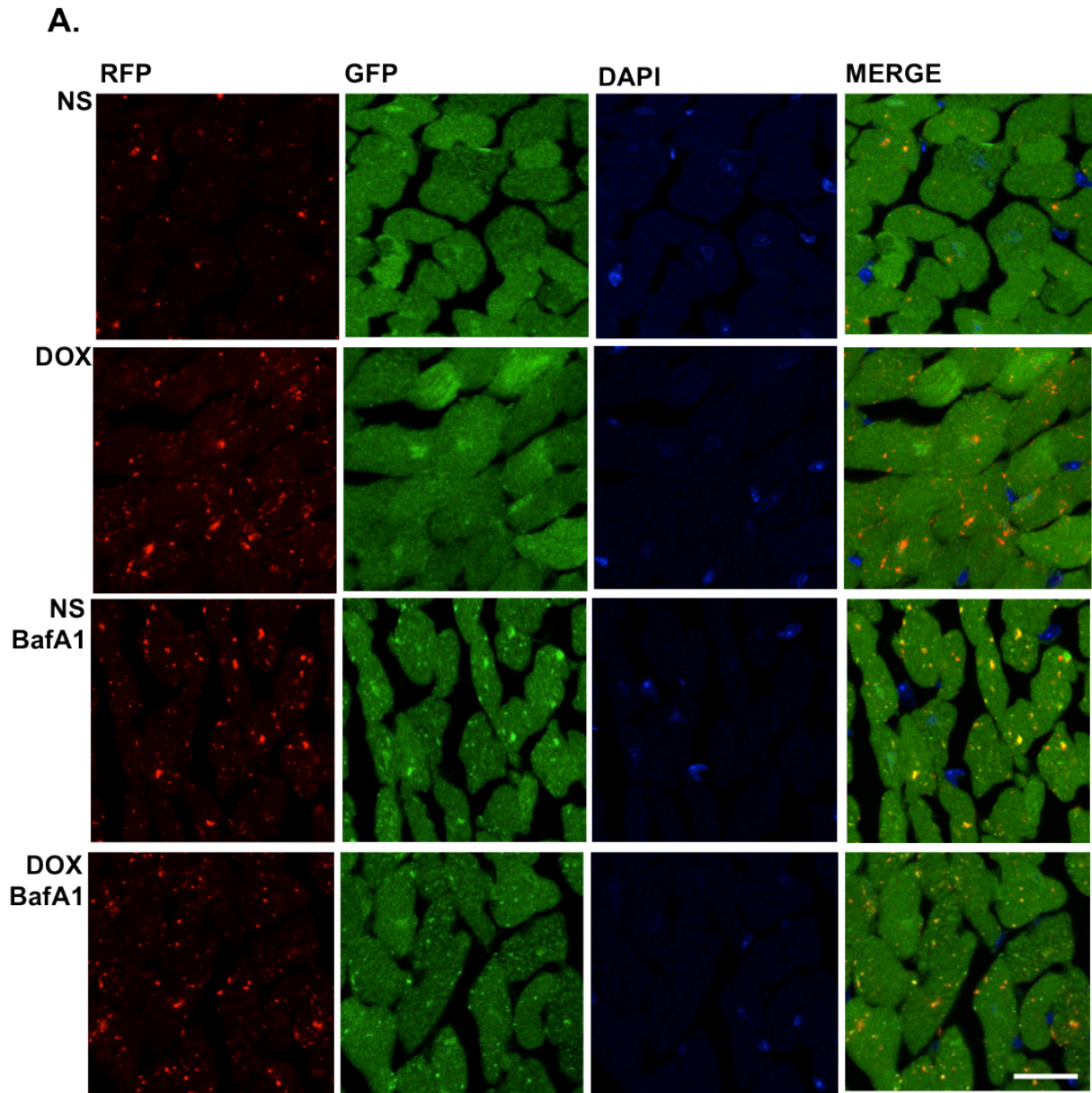
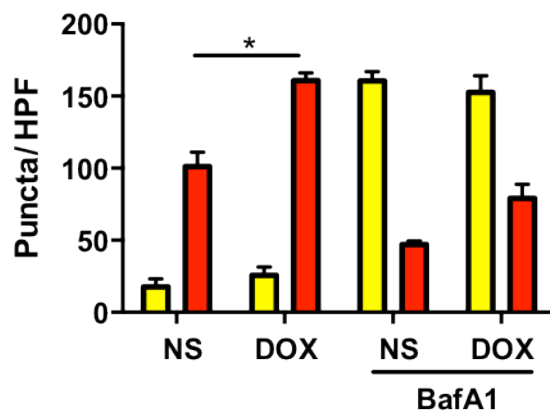


**Figure 2.3. Doxorubicin blocks autophagic flux in mouse heart.** (A) Doxorubicin inhibited cardiac autophagic flux. Mice were treated with DOX, then subjected to 24-hour starvation. Bafilomycin A1 (1.5 mg/kg, BafA1) was injected intraperitoneally 2 hours before sacrifice. N = 4 per group. (B) Autophagic flux was still inhibited in mouse hearts 24 hours after the fourth weekly injections of DOX or NS. N = 3-5 per group. (C) Autophagic flux was increased in mouse hearts four weeks after the last injection of DOX or NS. N = 6 per group. NS, normal saline. DOX, doxorubicin. \*,  $p < 0.05$ ; \*\*,  $p < 0.01$ ; ns, not significant.

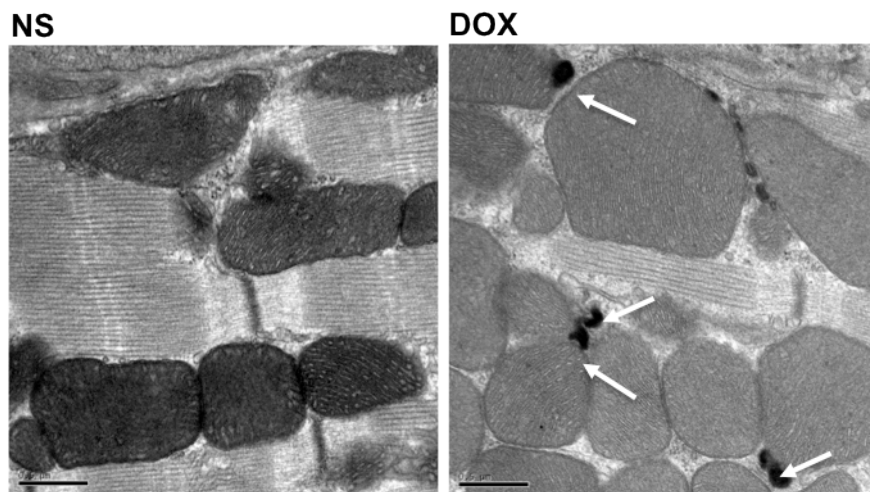
Figure 2.4



B.



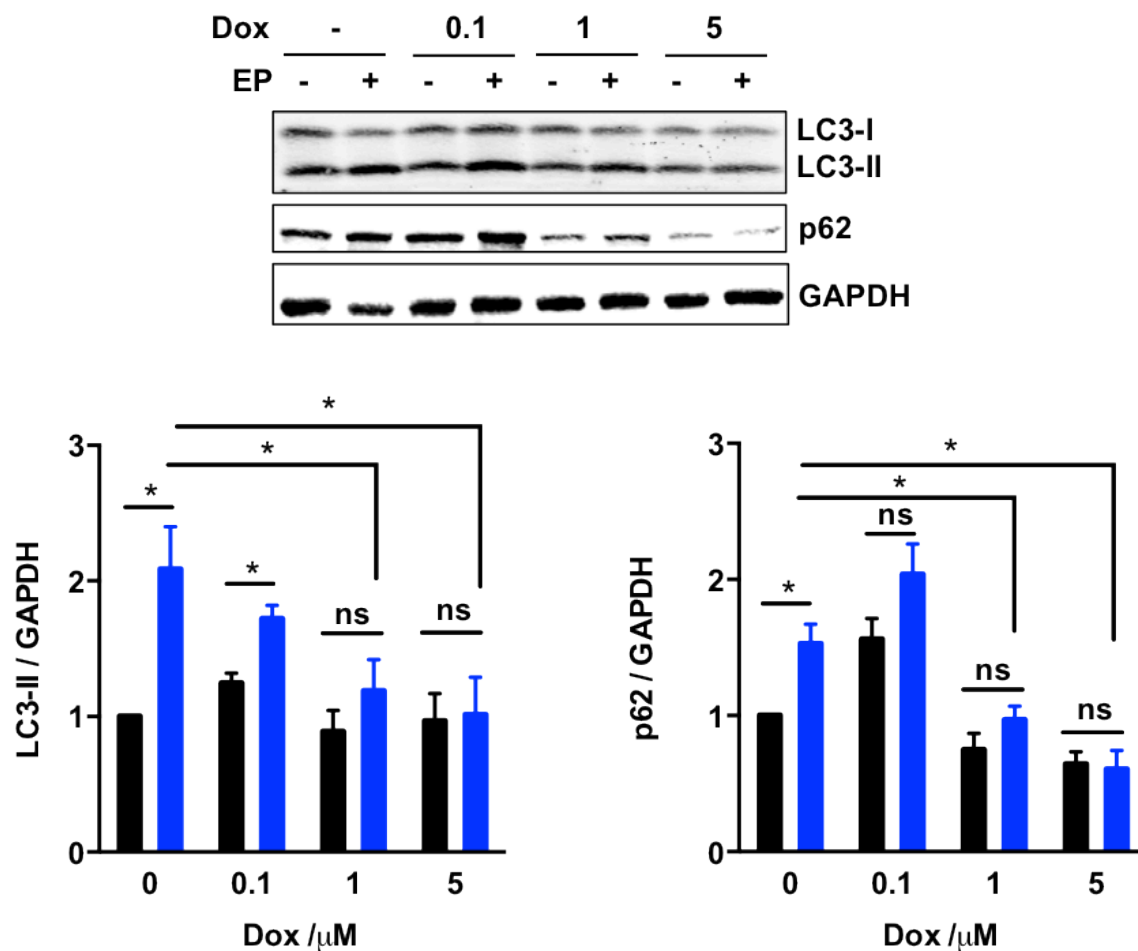
C.



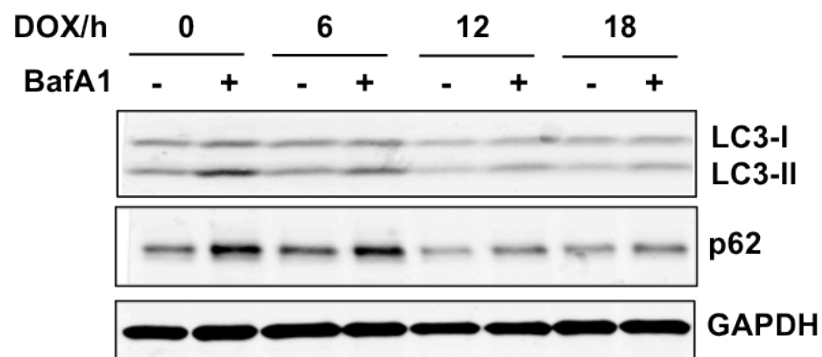
**Figure 2.4. Doxorubicin induces autolysosome accumulation in mouse heart.** (A) Representative fluorescent images of heart tissue sections from CAG-RFP-GFP-LC3 transgenic mice 24 hours after DOX injection, with or without BafA1 injection 2 hours before heart harvesting. (B) Autophagosome (yellow puncta) and autolysosome (red puncta) numbers in heart after DOX/NS treatment were calculated. N = 5 hearts per group with 6 microscopic fields (14,000  $\mu\text{m}^2$ ) per heart section analyzed. Scale bar, 20  $\mu\text{m}$ . \*,  $p < 0.05$ . (C) Representative transmission electron microscopy images of hearts from mice 24 hours after 5 mg/kg DOX or NS treatment. Doxorubicin-treated heart showed increased numbers of intracytoplasmic vacuoles with electron-dense contents (white arrows). Scale bar, 0.5  $\mu\text{m}$ . DOX, doxorubicin. NS, Normal Saline.

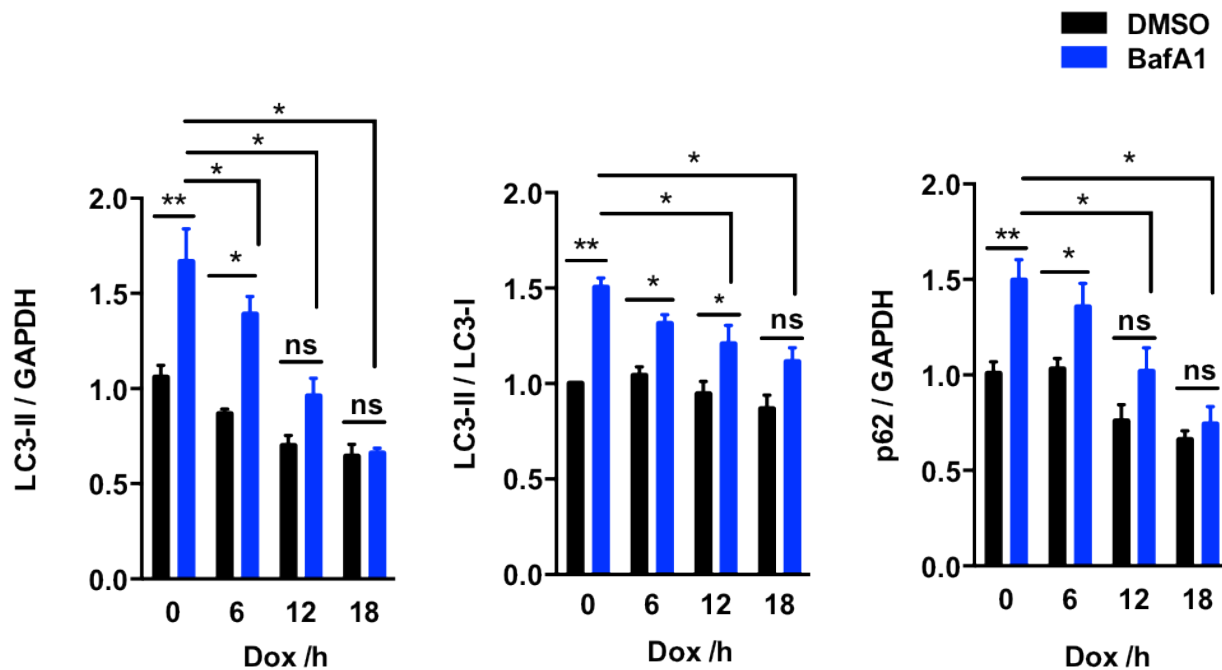
Figure 2.5

A.

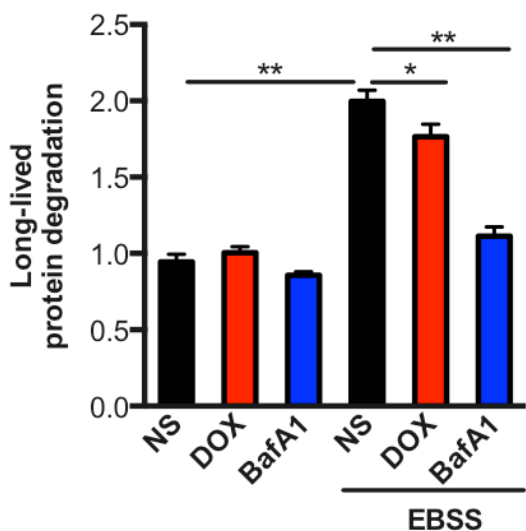


B.



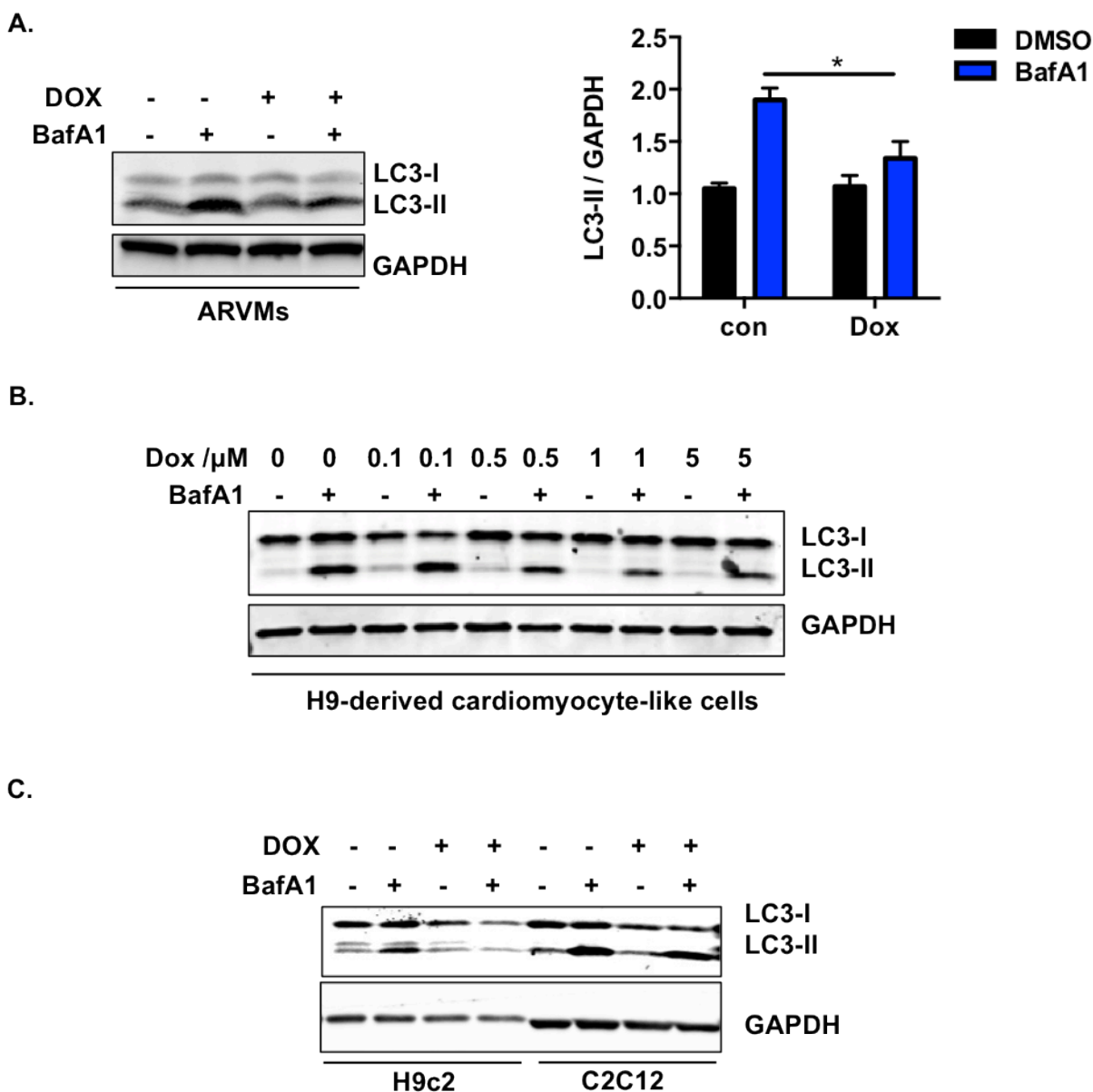


C.



**Figure 2.5. Doxorubicin inhibits autophagic flux in cultured Neonatal Rat Cardiomyocytes (NRVMs).** (A) Dose-dependent inhibition of autophagic flux by doxorubicin (24 hours) in NRVMs, examined by immunoblotting of LC3 and p62. N = 3 independent experiments. E64d (10  $\mu$ g/ml) and pepstatin A (10  $\mu$ g/ml) were added for 2 hours to block lysosomal degradation. (B) Time-dependent blockage of autophagic flux by doxorubicin. N = 3. (C) Long-lived protein degradation assay showed that doxorubicin decreased autophagic protein degradation in NRVMs. N = 3 in duplicates. \*,  $p < 0.05$ ; \*\*,  $p < 0.01$ ; ns, not significant.

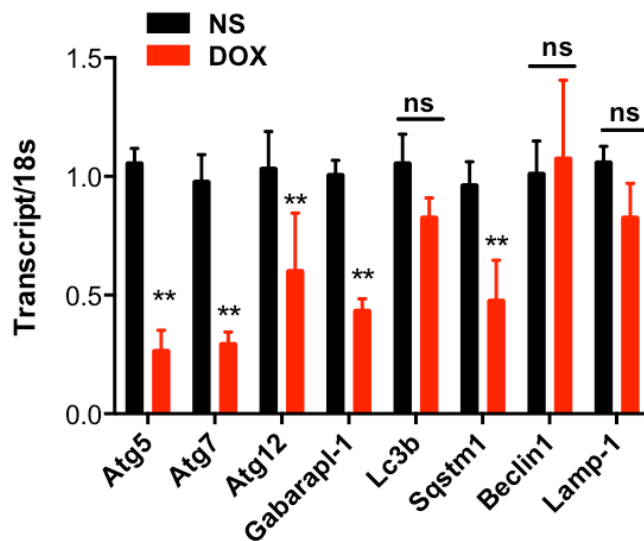
## Figure 2.6



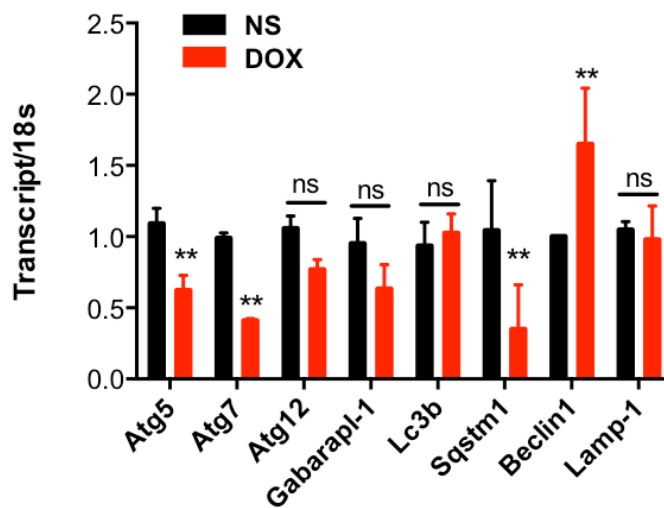
**Figure 2.6. Doxorubicin inhibits autophagic flux in other *in vitro* models of cardiomyocytes.** (A) Doxorubicin (1  $\mu$ M, 24 hours) inhibited autophagic flux in Adult Rat Ventricular Myocytes (ARVMs) examined by immunoblotting of LC3. N = 3. (B) Overnight treatments of doxorubicin at different concentrations inhibited autophagic flux in cardiomyocyte-like cells differentiated from H9 human embryonic stem cells. (C) Doxorubicin (1  $\mu$ M, 24 hours) inhibited autophagic flux in H9c2 cells but not in C2C12 cells (myoblasts). \*,  $p < 0.05$ .

Figure 2.7

A.



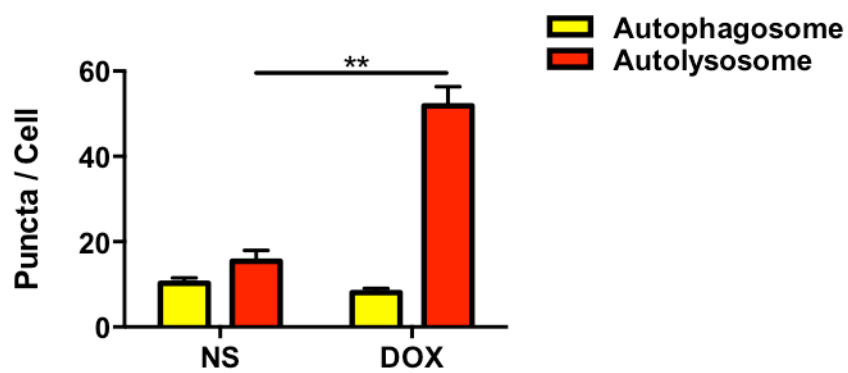
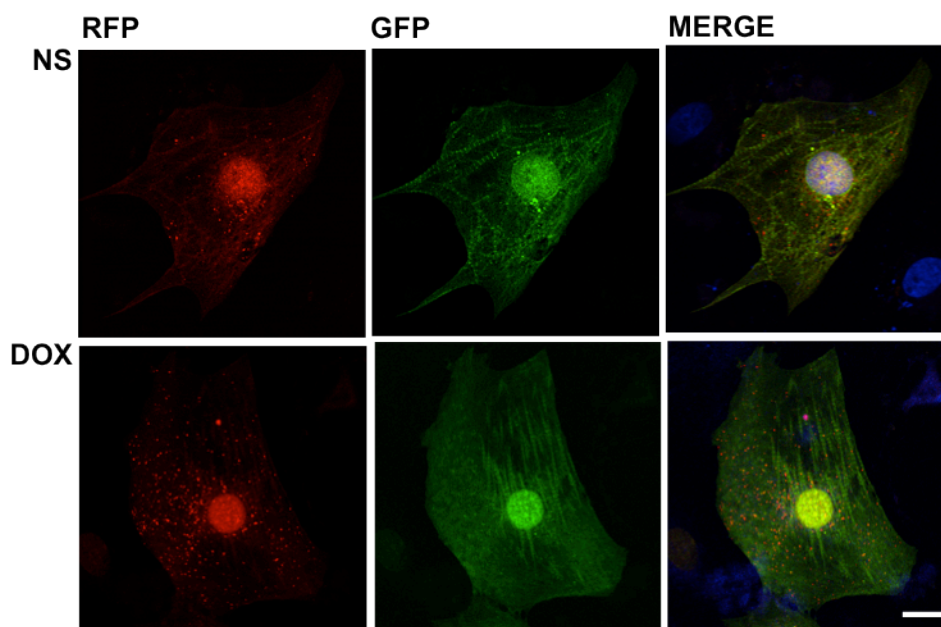
B.



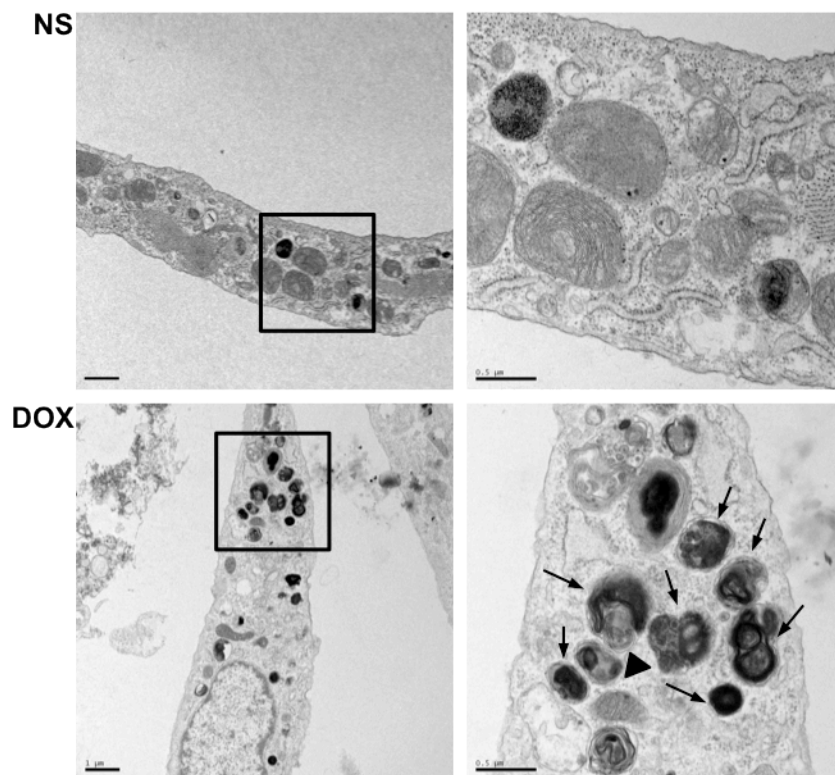
**Figure 2.7. Doxorubicin inhibits multiple autophagic genes in NRVMs.** (A) Doxorubicin (1  $\mu$ M, 18 hours) inhibited multiple autophagic gene transcripts in NRVMs. N = 6. (B) Doxorubicin (1  $\mu$ M, 18 hours) inhibited multiple autophagic gene transcripts in ARVMs. N = 4. \*\*,  $p < 0.01$ ; ns, not significant.

**Figure 2.8**

A.

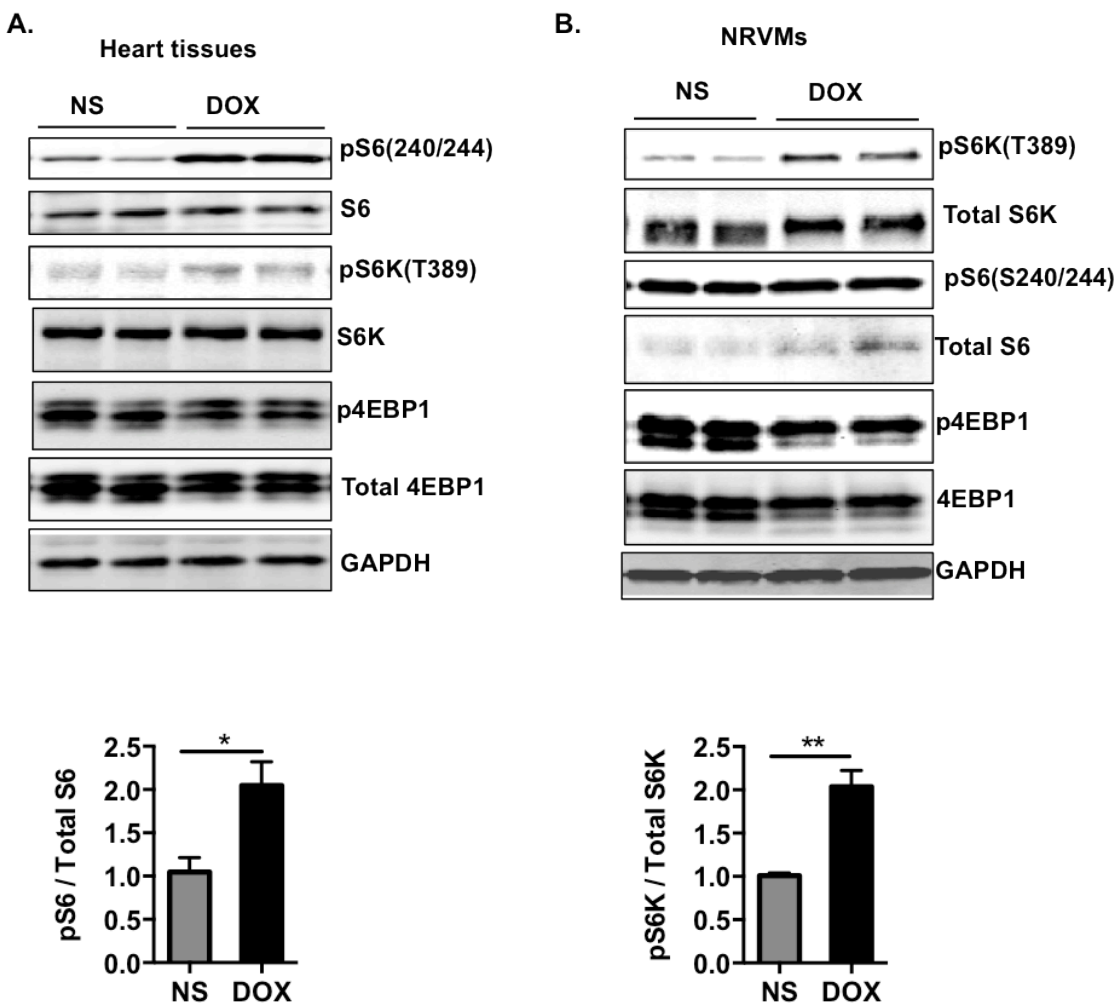


B.



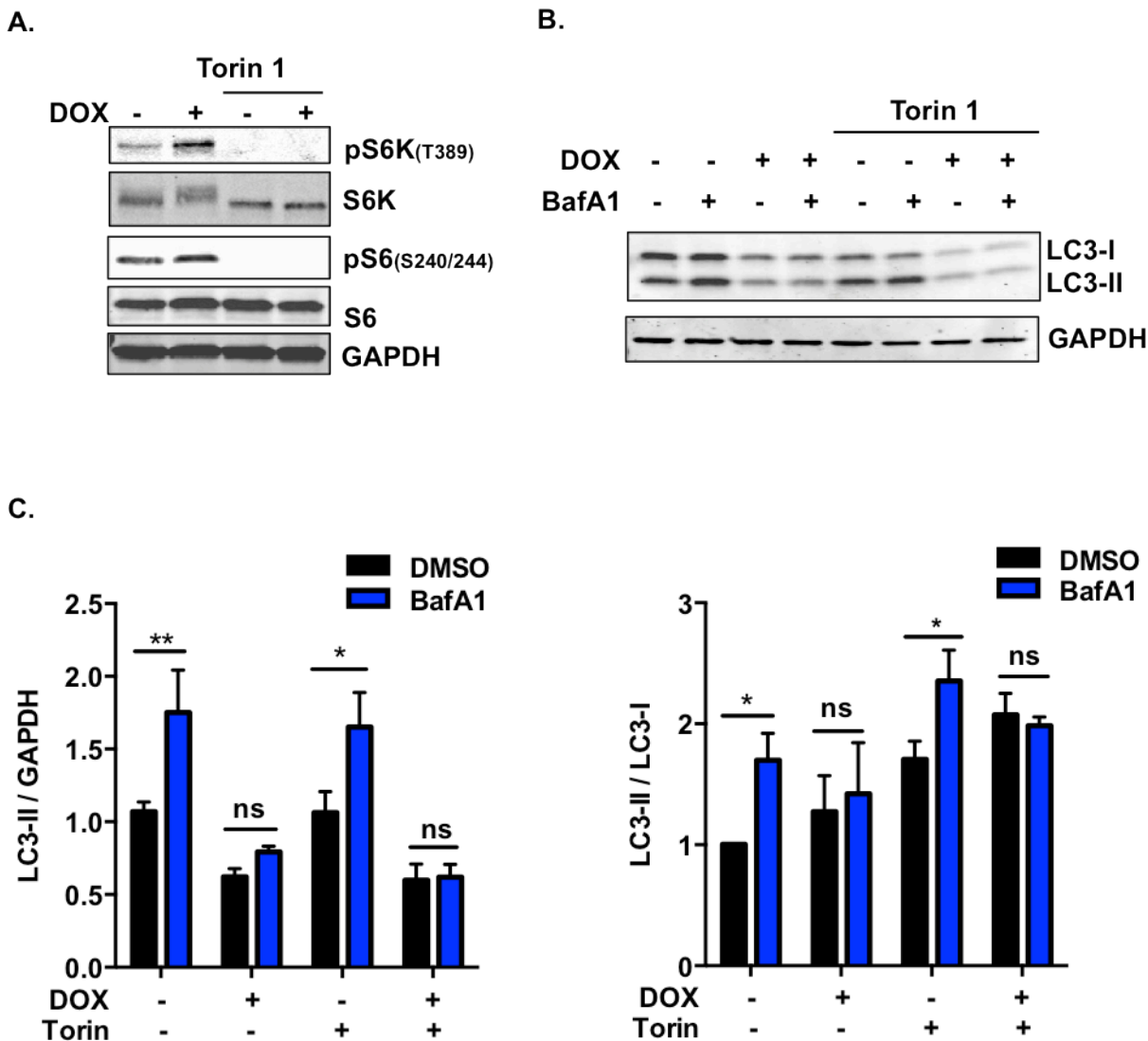
**Figure 2.8. Doxorubicin induces accumulation of autolysosomes in NRVMs.** (A) Representative fluorescent images of NRVMs expressing RFP-GFP-LC3 and treated with DOX for 8 hours. Nuclei were stained with DAPI. Numbers of autophagosomes and autolysosomes in each cell were quantified.  $N = 40-50$  cells per group. Scale bar,  $10\ \mu\text{m}$ . (B) Representative transmission electron microscopy images of cardiomyocytes treated with doxorubicin for overnight. Arrows, autolysosomes; arrowhead, autophagosome. Scale bars,  $1\ \mu\text{m}$  in left- and  $0.5\ \mu\text{m}$  right-side images respectively. \*\*,  $p < 0.01$ .

## Figure 2.9



**Figure 2.9. Doxorubicin induces mTORC1 activation in NRVMs.** (A) mTORC1 signaling pathway in hearts was activated 24 hours after doxorubicin injection. pS6/total S6 was quantified. N = 4 per group. (B) mTORC1 signaling pathway in NRVMs was activated by overnight doxorubicin treatment. pS6K/total S6K was quantified. N = 4 independent experiments. \*,  $p < 0.05$ ; \*\*,  $p < 0.01$ .

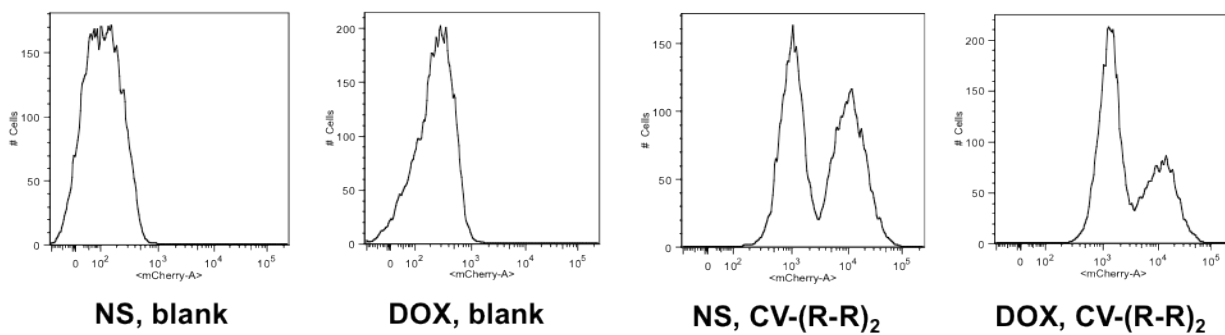
## Figure 2.10



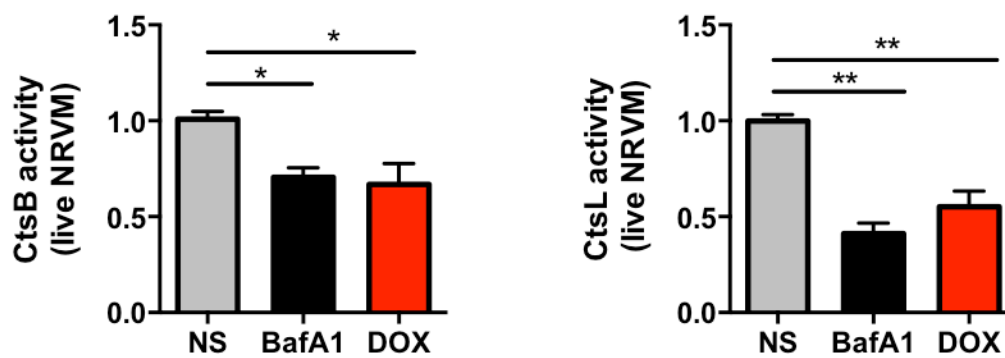
**Figure 2.10. Inhibition of autophagic flux by doxorubicin in NRVMs is independent of mTORC1 activation.** (A) Torin 1 (50 nM) inhibited basal and doxorubicin-induced mTORC1 activity. (B) Co-treatment with torin 1 failed to rescue the inhibition of autophagic flux by doxorubicin in cardiomyocytes. (C) Quantification of LC3-II /GAPDH and LC3-II /LC3-I in (B). N = 3 independent experiments. \*,  $p < 0.05$ ; \*\*,  $p < 0.01$ ; ns, not significant.

Figure 2.11

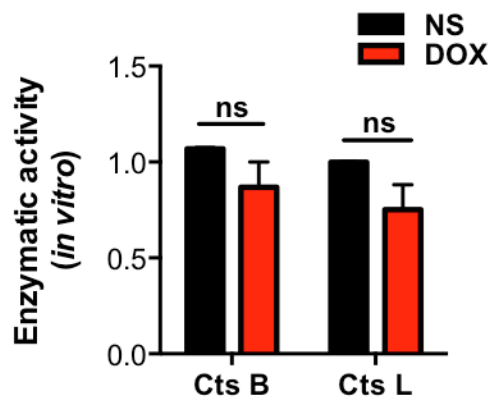
A.



B.



C.



D.

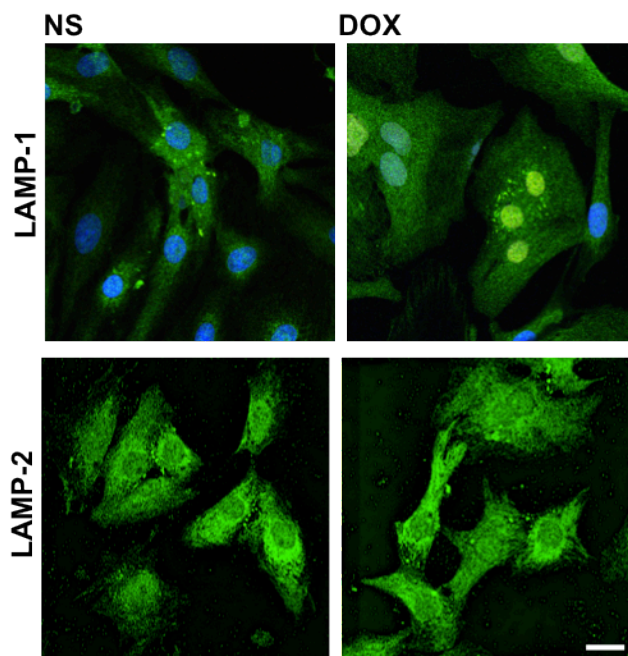


**Figure 2.11. Doxorubicin inhibits lysosomal function in NRVMs.** (A) Flow cytometry separating fluorescent signals from doxorubicin and from Cresyl violet (CV). Doxorubicin fluorescence was detected with Ex/Em 488/710 nm while CV fluorescence was collected with Ex/Em 561/610 nm. Signal in Ex/Em 561/610 nm was quantified as measurement of cathepsin B or L activity respectively. (B) Doxorubicin inhibited activities of lysosomal enzymes cathepsin B and cathepsin L in live cardiomyocytes, examined by FACS. N = 4. (C) *In vitro* enzyme activities of cathepsin B and cathepsin L isolated from lysosomes of cardiomyocytes treated with normal saline or doxorubicin. N = 3 independent experiments. (D) Representative immunofluorescent images of NRVMs with LAMP-1 and LAMP-2 immunostaining staining after 8-hour treatment of DOX or NS. Scale bar, 10  $\mu\text{m}$ . \*,  $p < 0.05$ ; \*\*,  $p < 0.01$ ; ns, not significant.

Figure 2.12

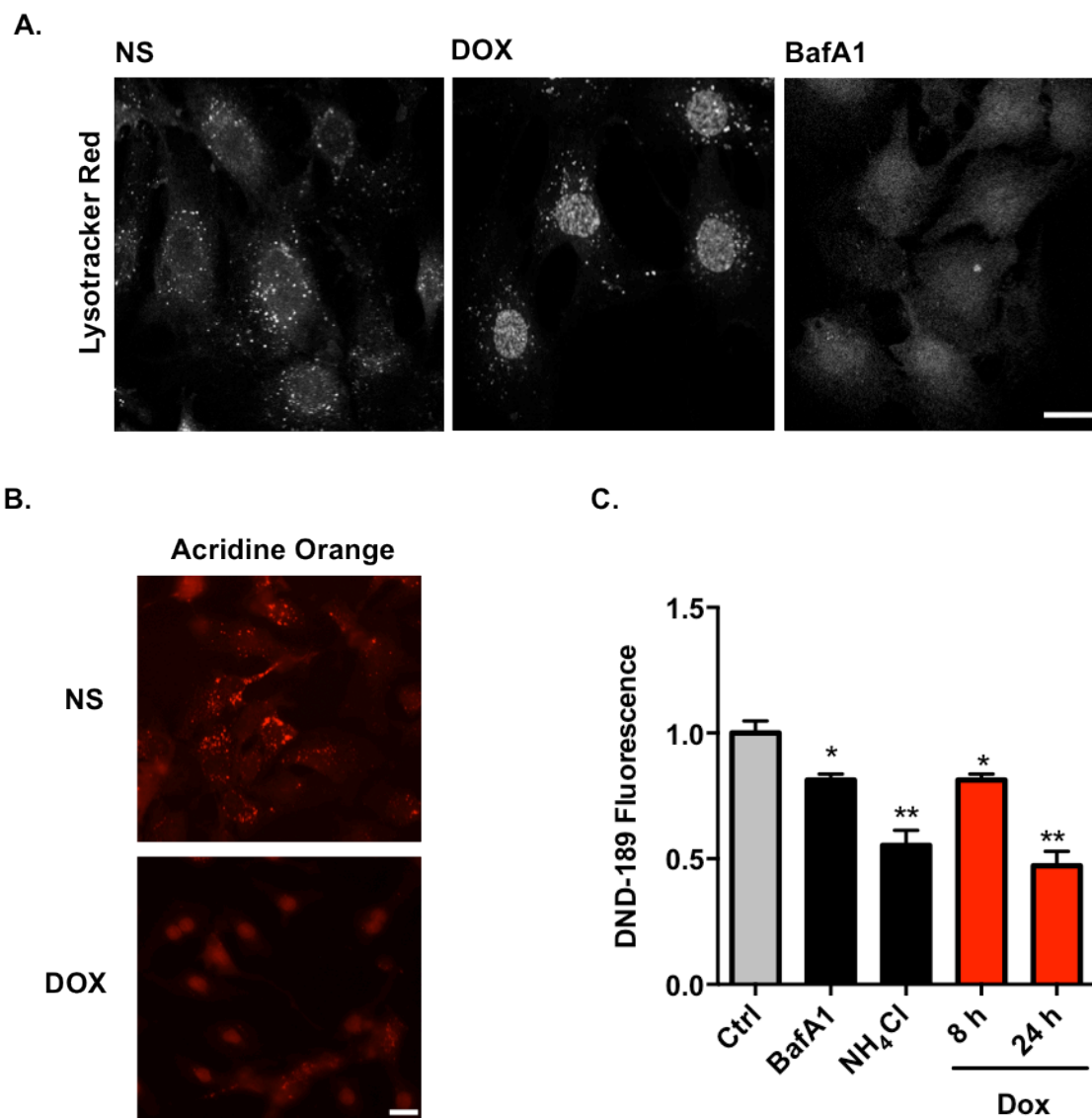
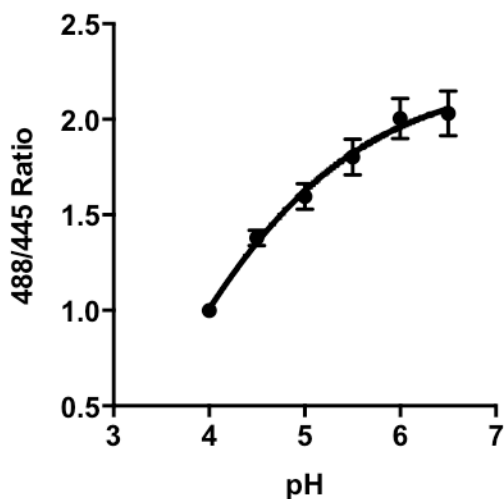


**Figure 2.12. Doxorubicin inhibits lysosomal acidification in NRVMs.** (A) Lysotracker Red (DND-99) positive puncta in the cytosol were significantly reduced after 8-hour doxorubicin treatment. Bafilomycin A1 served as a positive control. (B) Representative immunofluorescent images of NRVMs with Acridine Orange (1  $\mu$ M for 15 minutes) staining after 8-hour-treatment of DOX. (C) Doxorubicin decreased Lysosensor DND-189 fluorescence, determined by FACS. Bafilomycin A1 (100 nM for 2 hours) and NH<sub>4</sub>Cl (10 mM for 0.5 hour) are positive controls. N = 3 in duplicates. Scale bar, 10  $\mu$ m. \*,  $p < 0.05$ ; \*\*,  $p < 0.01$ .

## Figure 2.13

A.



B.

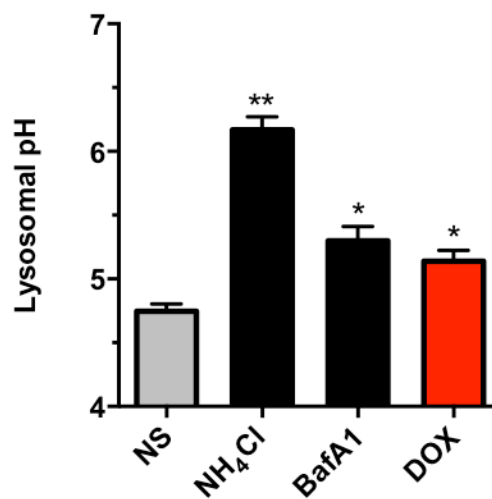
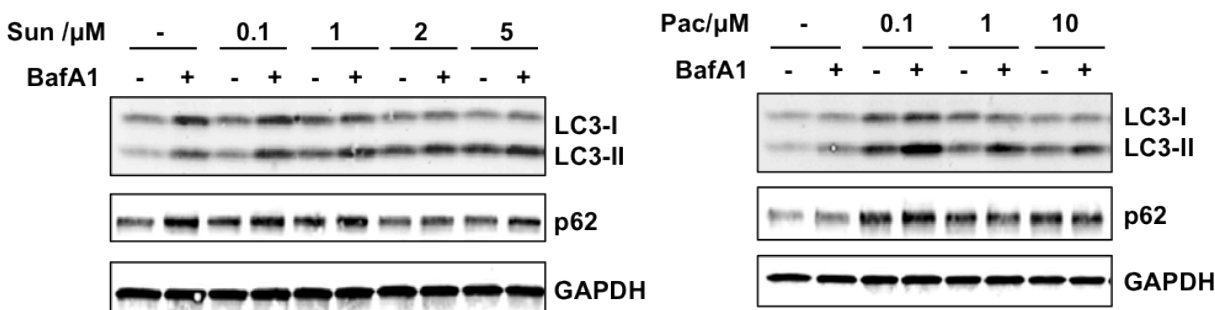


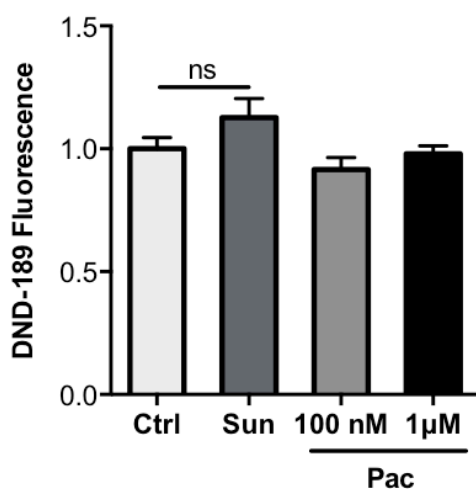
**Figure 2.13. Doxorubicin raises lysosomal pH in NRVMs.** (A) Standard curve for measuring of lysosomal pH using pH sensitive dextran (Dextran, Oregon Green 514) and radiometric imaging. An average of 10-20 cells was analyzed at each pH in each independent experiment. (B) Doxorubicin (overnight treatment) increased lysosomal pH. Lysosomal pH was examined using Dextran, Oregon Green 514. Bafilomycin A1 and NH<sub>4</sub>Cl are positive controls. Three independent experiments with a total of 100-120 cells were examined. \*,  $p < 0.05$ ; \*\*,  $p < 0.01$ .

## Figure 2.14

A.



B.



C.

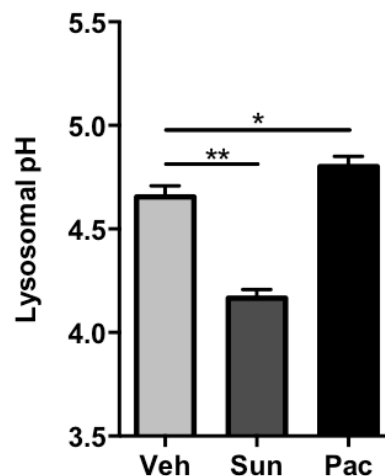
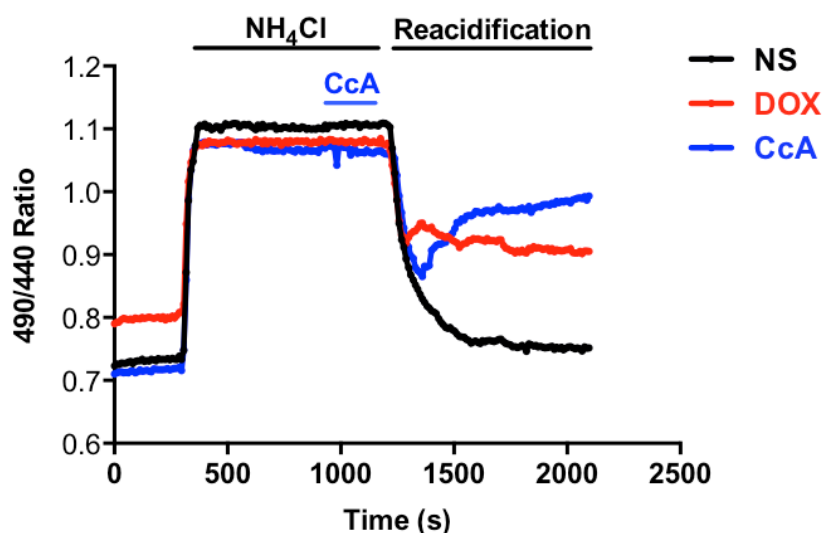


**Figure 2.14. Cardiomyocyte autophagic flux and lysosomal pH alteration by other cardiotoxic chemotherapeutic treatments.** (A) Cardiotoxic chemotherapeutic drugs sunitinib and paclitaxel induced autophagic flux in cardiomyocytes. Immunoblotting of LC3 after overnight incubation with different concentrations of sunitinib and paclitaxel are shown. (B) DND-189 fluorescence by FACS after overnight treatment of sunitinib (1  $\mu\text{M}$ ) and paclitaxel (100 nM and 1  $\mu\text{M}$ ). N = 3 independent experiments. (C) Lysosome pH measurement by Dextran, Oregon Green 514 in cardiomyocytes after treatment of sunitinib (1  $\mu\text{M}$ ) and paclitaxel (1  $\mu\text{M}$ ). N = 100 cells in 3 independent experiments. Sun, sunitinib. Pac, paclitaxel. \*,  $p < 0.05$ ; \*\*,  $p < 0.01$ ; ns, not significant.

## Figure 2.15

A.



B.

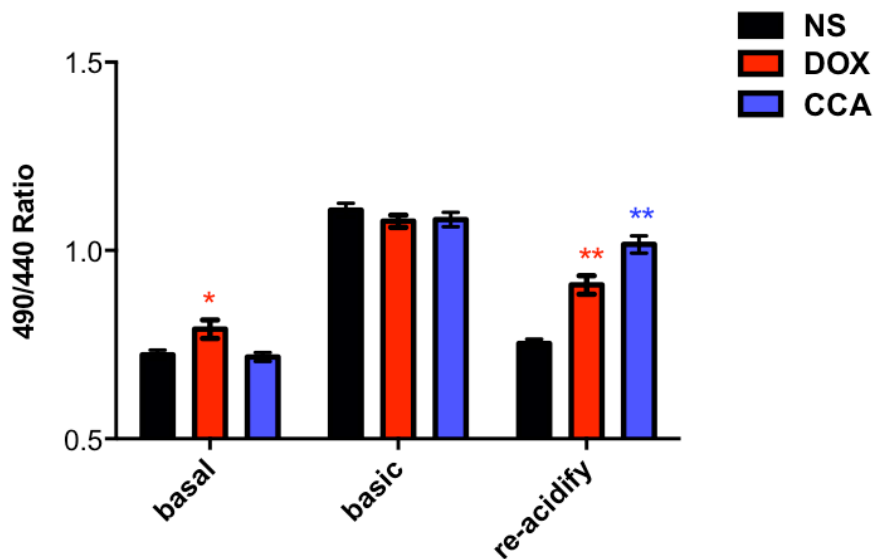
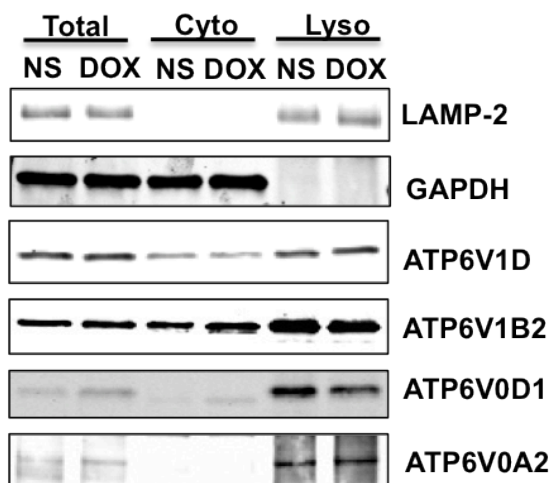


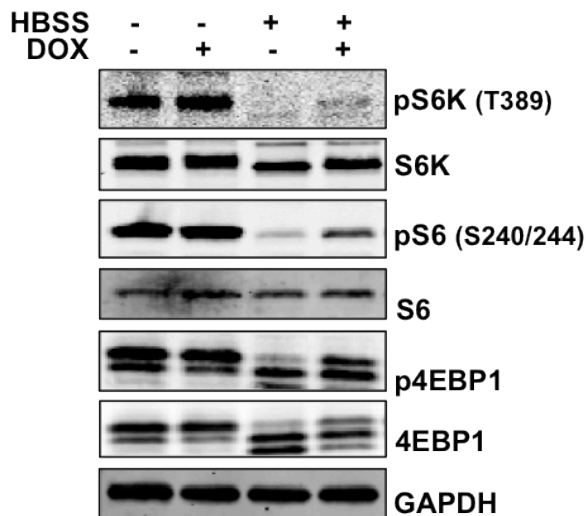
**Figure 2.15. Doxorubicin inhibits v-ATPase-dependent lysosomal acidification.** (A) Live NRVM lysosome re-acidification after  $\text{NH}_4\text{Cl}$ -induced alkalinization. Dextran, Oregon Green 514 was used to monitor relative change of lysosomal pH. Representative recordings of the fluorescence ratio are illustrated. (B) Fluorescence ratios of different groups were compared at different time points (t = 0 s, 1000 s, 2000 s) - basal condition, during lysosomal alkalinization, and during re-acidification. N = 22-25 cells in 5 independent experiments. \*,  $p < 0.05$ ; \*\*,  $p < 0.01$ .

## Figure 2.16

A.



B.



C.

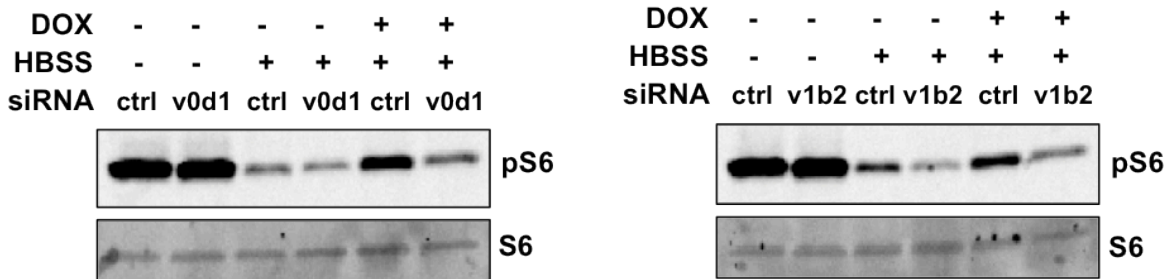
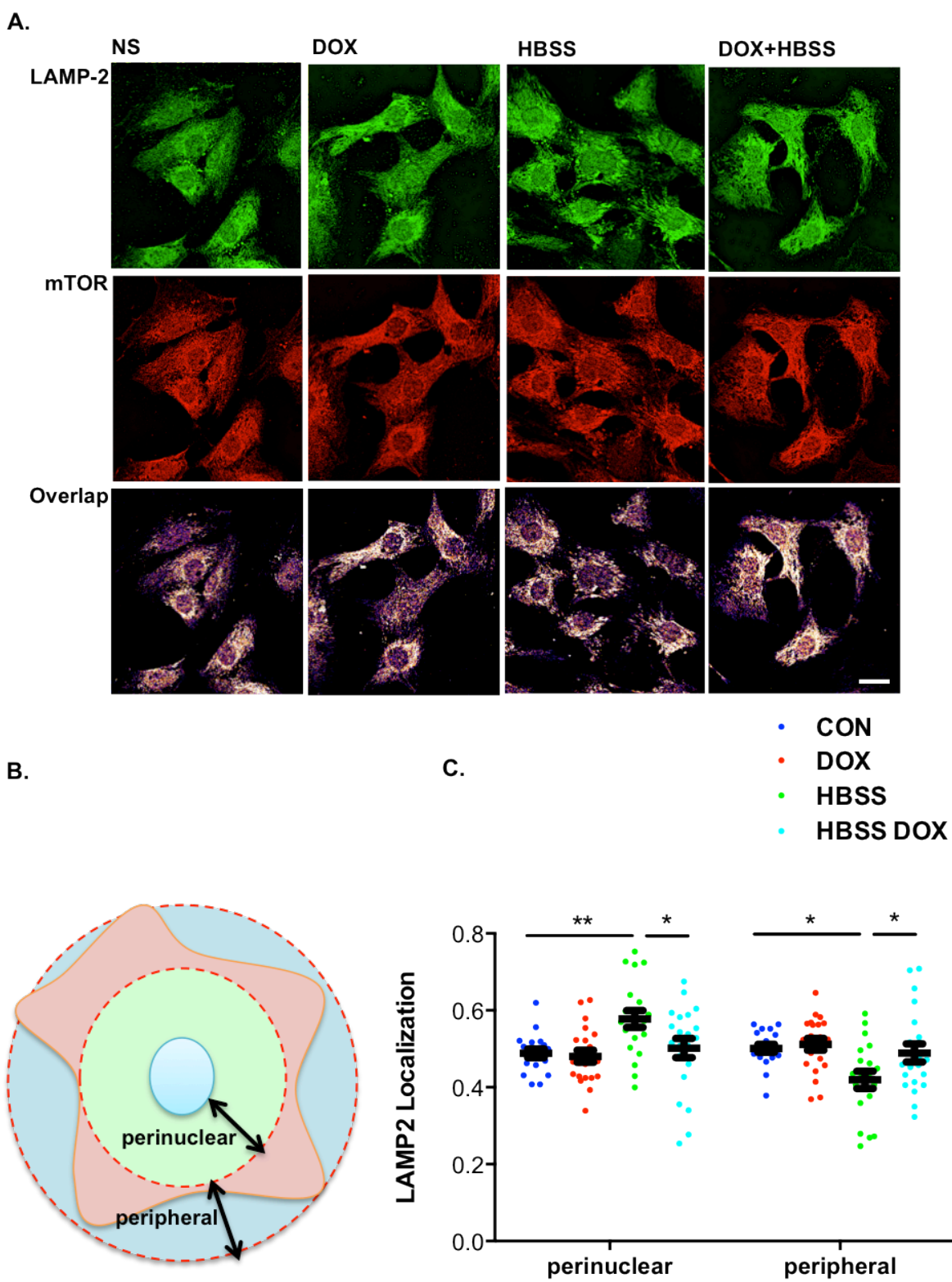


**Figure 2.16. Doxorubicin's effect on V-ATPase in NRVMs.** (A) Doxorubicin did not affect assembly of V1 and V0 subunit proteins in lysosomes. Lysosome-enriched compartments were isolated from NRVMs treated with DOX overnight. Immunoblotting of various subunits of V1V0 domains was shown. (B) Doxorubicin (8-hour treatment) increased mTORC1 activity even upon starvation in NRVMs. N = 3. (C) Knocking down of V-ATPase subunit ATP6V0D1 or ATP6V1B2, respectively, abolished doxorubicin-induced mTORC1 activation.

Figure 2.17



D.

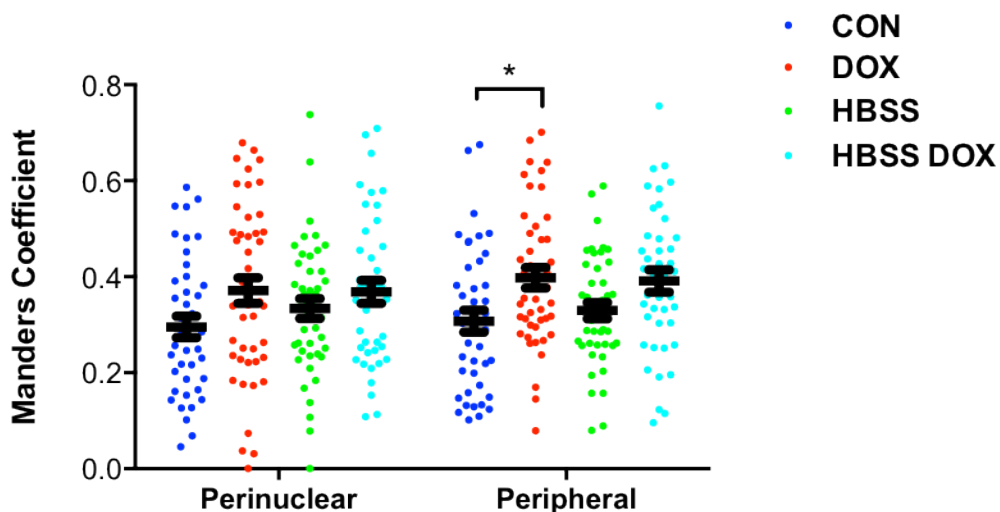


**Figure 2.17. Doxorubicin alters lysosomal subcellular localization and mTOR recruitment to lysosomes.** (A) Immunofluorescence study with anti-LAMP-2 antibody and mTOR antibody in NRVMs. NRVMs were treated with doxorubicin for 8 hours. HBSS starvation was treated in the last two hours. (B) Schematic showing the definition of perinuclear and peripheral region of a cardiomyocyte. (C) Doxorubicin (8-hour treatment) abolished starvation-induced perinuclear movement of lysosomes. N = 20-21 cells from 3 experiments. (D) Doxorubicin increased the colocalization of mTOR and LAMP-2. N=42-46 from 4 experiments. Scale bar, 10  $\mu$ m. \*,  $p < 0.05$ ; \*\*,  $p < 0.01$ .

Figure 2.18

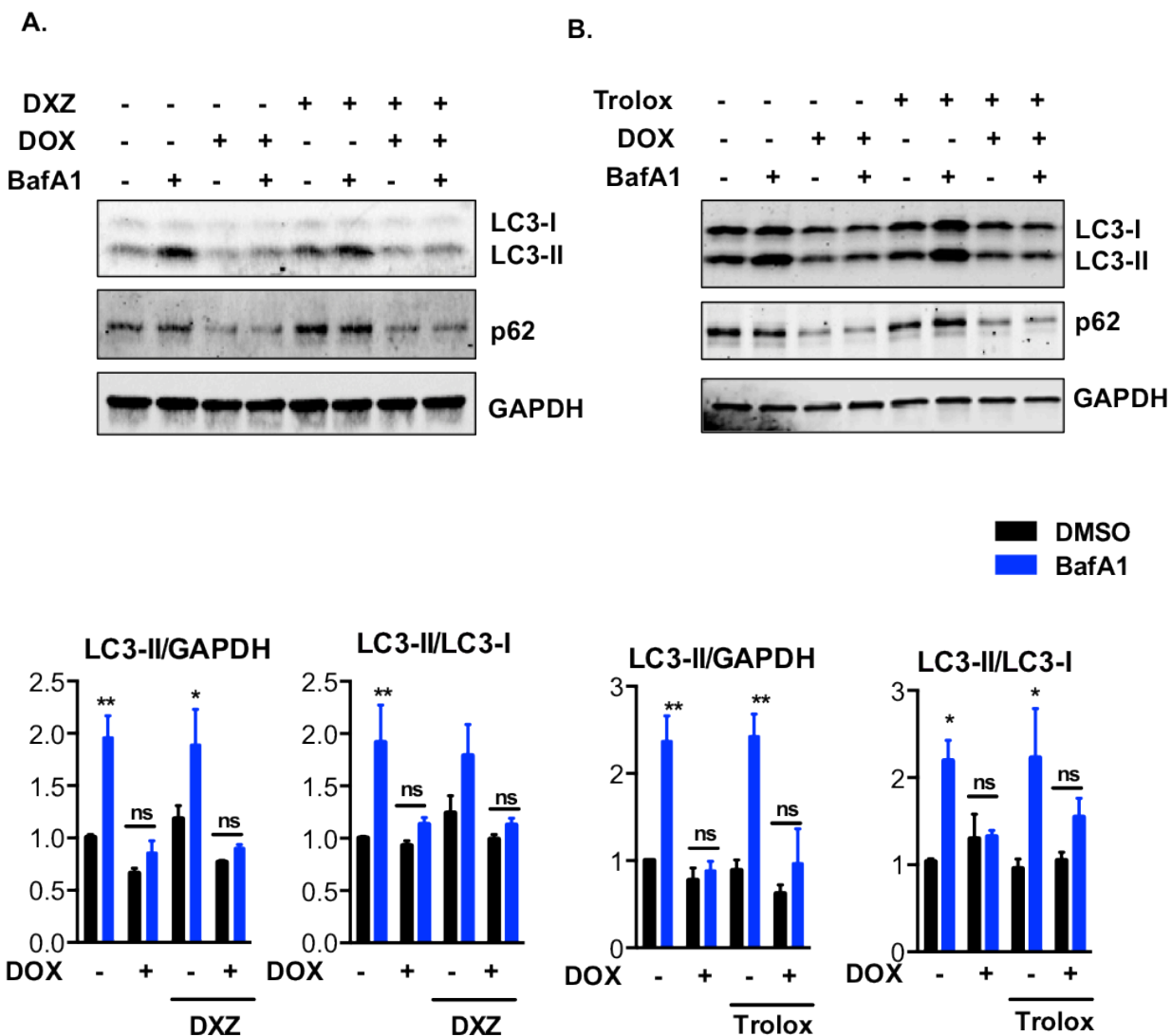


**Figure 2.18. ROS scavengers do not rescue the inhibition of cardiomyocyte autophagic flux by doxorubicin.** (A) NRVMs were co-incubated with Dexrazoxane (DXZ, 100 $\mu$ M) and doxorubicin for 18 hours and autophagic flux was examined by Western blotting. N = 3. (B) NRVMs were co-incubated with Trolox (10  $\mu$ M) and doxorubicin for 18 hours and autophagic flux was examined by Western blotting. N = 3. \*,  $p < 0.05$ ; \*\*,  $p < 0.01$ . ns, not significant.

**Table 2.1. Primers used in the study**

<b>Gene (Mouse)</b>	<b>Sequence</b>
<i>Beclin1</i>	5-CAGGAGCTGGAAGATGTGGA-3 5-GTGCCAGATATGGAAGGTCG-3
<i>Sqstm1</i>	5-CTTCAGCTTCTGCTTCA-3 5-GGCACTCCTTCTTCTTT-3
<i>Bnip3</i>	5-ATTGGTCAAGTCGGCCAGAA-3 5-AGTCGCTGTACGCTTTGGGT-3
<i>Gabarapl1</i>	5-CATCGTGGAGAAGGCTCCTA-3 5-ATACAGCTGTCCCATGGTAG-3
<i>Lc3b</i>	5-CGTCCTGGACAAGACCAAGT-3 5-AGTGCTGTCCCGAACGTCTC-3
<b>Gene (Rat)</b>	<b>Sequence</b>
<i>Atg5</i>	5-AGAAGCAGAGCCATACT-3 5-GCTGAGCTTGATGCAAGA-3
<i>Atg7</i>	5-GCAGCCAGCAAGCGAAAG-3 5-TCTCATGACAACAAAGGTGTCAA-3
<i>Atg12</i>	5-GGCCTCGGAGCAGTTGTTTA-3 5-CAGCATCAAACCTTCTCTGA-3
<i>Gabarapl1</i>	5-CATCGTGGAGAAGGCTCCTA-3 5-ATACAGCTGTCCCATGGTAG-3
<i>Lc3b</i>	5-CGTCCTGGACAAGACCAAGT-3 5-AGTGCTGTCCCGAACGTCTC-3
<i>Sqstm1</i>	5-CTTCAGCTTCTGCTTCA-3 5-GGCACTCCTTCTTCTTT-3
<i>Beclin1</i>	5-CAGGAGCTGGAAGATGTGGA-3 5-GTGCCAGATATGGAAGGTCG-3
<i>Lamp-1</i>	5-AGGATCAACCTTCCCCAACT-3 5-CACCTTCAGGGTCACCAACT-3

## METHODS

### *In vivo* model of chronic doxorubicin cardiomyopathy

C57/B6 mice were maintained on a 12-hour light/dark cycle from 6AM to 6PM. All protocols were approved by the Institutional Animal Care and Use Committee of UT Southwestern Medical Center. Eight to nine-week-old mice were injected via tail vein with doxorubicin (5 mg/kg) or normal saline once weekly for 4 weeks. Ventricular size and function were examined in acclimatized, unanesthetized mice by echocardiography (Vevo 2100, MS400C scanhead) 6 days after each injection and 4 weeks after the final injection.

### Cell culture

Neonatal rat ventricular myocytes (NRVMs) were isolated from 1- to 2-day-old Sprague-Dawley rats as previously described (25). Briefly, ventricles were harvested and digested. Fibroblasts were cleared by pre-plating the cell suspension for 2 hours. Cardiomyocytes were then plated at a density of 1,250 cells per 1 mm<sup>2</sup> in plating medium containing 10% fetal bovine serum with 100 μM bromodeoxyuridine. The culture contained >95% cardiomyocytes (data not shown). Twenty-four hours after plating, NRVMs were maintained in NRVM culture media (DMEM high glucose and Medium 199 in 3:1 ratio) containing 3% fetal bovine serum. On the fourth day after plating, experiments were initiated.

Adult rat ventricular myocytes (ARVMs) were isolated and cultured as previously described (26). Four hours after plating, ARVMs were maintained in culture medium (DMEM supplemented with 1x ITS, 10 mM 2,3-butanedione monoxime and 100 U/mL penicillin-streptomycin). On the second day after plating, experiments were initiated.

Cardiomyocytes were differentiated from H9 human embryonic stem cells as previously reported (27, 28). Briefly, embryonic stem cells (H9 cell line) were maintained on

matrigel in mTeSR culture medium. When H9 cells reached 85-90% confluency, the medium was changed to RPMI 1640 with B27 supplement, minus insulin (Life Technologies) (day 0 to 8), supplemented with CHIR99021 (6  $\mu$ M, Selleckchem) for the first 48 hours, and IWR-1 (5  $\mu$ M, Sigma) on day 4 for 48 hours. On day 8, the medium was switched to RPMI 1640 with B27 supplement, and the cells were metabolically selected for 10 days. Then, cells were replated and used for experiments after day 30.

H9c2 and C2C12 cells were cultured in Hyclone high glucose DMEM supplemented with 10% fetal bovine serum.

### **Immunoblot analysis**

Ventricular tissue (10-30 mg) was homogenized in 700  $\mu$ L T-PER lysis buffer (Thermo) supplemented with protease inhibitors and phospho-STOP (Roche). Lysates were centrifuged at 8,000g (15 min), and the supernatant was used for immunoblotting. For NRVMs, cells were washed once with cold PBS and lysed with T-PER buffer supplemented with protease inhibitors and phospho-STOP. Protein concentration was measured by Bradford assay (Bio-Rad). Protein lysates (10-15  $\mu$ g) were loaded for electrophoresis and transferred to nitrocellulose membrane. Then, the membrane was processed for immunoblotting and scanning using an Odyssey scanner (LI-COR).

### **Immunofluorescence study**

NRVMs were cultured on cover slips. After treatment, cells were fixed using 4% PFA for 15 minutes, followed by incubation with 0.1% Triton/PBS for 10 minutes to permeate the cell membrane. Cover slips were washed with PBS and blocked with 3% FBS/PBS for 1 hour. Next, cover slips were incubated with primary antibodies (1:100) overnight, followed by fluorescent

secondary antibodies (Life Sciences, 1:300) for 1 hour the next day. After washing, cover slips were mounted with ProLong Gold Antifade Mountant with DAPI (Life Sciences).

### **RNA isolation and PCR analysis**

Total RNA was isolated from ventricular tissue using the Total RNA Fatty and Fibrous Tissue Kit (Bio-Rad). A total of 300 ng RNA was used for reverse transcription and subsequent real-time qPCR analysis (Roche). All primer sequences are provided (**Table 2.1**).

### **Long-lived protein degradation assay**

Our protocol was modified from that previously described (29). To label intracellular proteins, NRVMs were incubated with culture medium supplemented with 0.5  $\mu\text{Ci/mL}$  of leucine, L-[3,4,5  $^3\text{H(N)}$ ]- (specific activity 112 mCi/mmol) for 48 hours at 37°C. Unincorporated radioactive leucine was cleared by washing the cells three times with warm PBS. NRVMs were subsequently incubated with culture medium supplemented with 20 mM leucine (Sigma-Aldrich) for 24 hours. The cells were then treated with saline or doxorubicin overnight. Next, medium was removed, and NRVMs were incubated in either EBSS to stimulate autophagy or with culture medium for 3 hours. Bafilomycin A1 was added as a positive control.

At the end of treatment, TCA (100%) was added to the supernatant medium to a final concentration of 10%. The mixture was precipitated overnight followed by centrifuging for 10 minutes at 2,000 rpm (4°C). The acid-soluble radioactivity was measured by liquid scintillation counting using complete counting cocktail (Research Products International Corp). The cells were washed twice with cold PBS, and protein was precipitated with 10% TCA (30 minutes, 4°C). The precipitant was then washed twice with 95% ethanol and dissolved in 0.5 M NaOH at 37°C overnight. On the next day, 0.5 M HCl was added to neutralize the NaOH. Radioactivity was measured by liquid scintillation counting. The rate of long-lived protein degradation was

calculated from the ratio of the acid-soluble radioactivity in the medium to that in the acid-precipitated cell fraction.

### **Lysosome-enriched cell fraction isolation**

The protocol was modified from that previously described (30). Cells were washed twice with cold PBS and then harvested in isotonic buffer (200 mM mannitol, 70 mM sucrose, 1 mM EGTA, 10 mM HEPES, pH 7.5). Cytoplasmic membranes were disrupted by passing the cells through a G25 needle 50 times. Debris and nuclei were pelleted by centrifuging at 2,000 rpm for 10 minutes (4°C). The supernatant was next centrifuged at 10,000 g for 35 minutes to pellet lysosome-enriched components. Pellets were resuspended in the isotonic buffer, and lysosomal membranes were disrupted by free-thaw three times. The supernatant was further spun at 100,000 g for 1 hour to eliminate microsomes. The final supernatant was collected as the cytosolic fraction.

### **Cathepsin B/L activity measurement**

Cathepsin B and cathepsin L activities in living cardiomyocytes were measured using the Magic Red Cathepsin B/L activity kit (Immunochemistry Technologies). By using BD FACSCanto II, Cresyl Violet fluorescence was excited using a 561 nm laser, and signal was collected with a 610 nm filter. Fluorescence from doxorubicin was collected with excitation at 488 nm and emission at 710 nm. Geometric mean of the fluorescence signal from Ex/Em 561/610 nm was calculated and corresponded to cathepsin B or cathepsin L activity.

For *in vitro* cathepsin B/L activity measurements, I employed a method that was described previously (30). Lysosome-enriched compartments were isolated as described earlier. Protein concentration was measured by Bradford assay, and 5 µg protein lysates from

the lysosomal fraction was added to a total of 200  $\mu$ L reaction buffer (50 mM sodium acetate, 8 mM EDTA, 8mM dithiothreitol, pH 5.0). Cathepsin B+L activity was measured by FLUOstar OPTIMA microplate reader (BMG Labtech, excitation 380 nm, emission 410 $\pm$ 20 nm) after being incubated with the substrate Z-Phe-Arg-AMC (50  $\mu$ M, Enzo life sciences) for 20 minutes at 37°C. Cathepsin B inhibitor CA-074 (5  $\mu$ M, Toris Biosciences) was added in parallel samples to measure cathepsin L activity. The difference between the two readings was calculated as cathepsin B activity.

### **Lysosomal pH measurement**

For qualitative lysosomal pH measurement using LysoSensor Green DND-189, cells were loaded with 2  $\mu$ M LysoSensor Green DND-189 for 30 minutes at 37°C. Then, the cells were washed with PBS three times and trypsinized for flow cytometry analysis (BD FACS scan, FL1 fluorescence, 10,000 cells collected for each sample).

For quantitative lysosomal pH measurement, methods were modified from that previously described (31). Briefly, NRVMs were plated in 35 mm MatTek dishes (MatTek) and loaded with 100  $\mu$ g/mL Dextran, Oregon Green 514 for 2 days before drug treatment. At the end of doxorubicin treatment, the cells were washed with PBS three times and incubated with physiological buffer (136 mM NaCl, 2.5 mM KCl, 2 mM CaCl<sub>2</sub>, 1.3 mM MgCl<sub>2</sub>, 5 mM glucose, 10 mM HEPES pH 7.4) for 1 hour in 37°C before imaging. Images were acquired using an Andor Spinning Disk confocal microscope with an Apo TIRF 60x/1.49 NA Oil lens, Nikon Ti stand and Nikon Perfect Focus system. Dextran, Oregon Green 514 was excited at 445 nm and 488 nm; the emitted light was selected with a 525  $\pm$  40 nm filter and captured by an Andor iXon Ultra EMCCD camera. Image acquisition was performed using Metamorph v7.8.6.0. To create a calibration curve, cells were sequentially bathed in isotonic K<sup>+</sup> solutions (145 mM KCl, 10 mM glucose, 1 mM MgCl<sub>2</sub>, and 20 mM HEPES) with pH ranging from 4.0-6.5, and containing 10

$\mu\text{g/mL}$  nigericin (Sigma). 488/525 and 445/525 fluorescence of each cell was analyzed (Image J Software), and the 488/445 emission fluorescence ratios were plotted as a function of pH fitting to a Boltzmann sigmoid using Prism (GraphPad Software). The ratios of samples were interpolated using the calibration curve. Measurements were performed in 3 independent experiments with a total 100-120 cells in each treatment group.

### **Lysosomal reacidification assay**

For the lysosomal re-acidification assay, cells grown on coverslips were loaded with Dextran, Oregon Green 514 and treated with normal saline or doxorubicin as described above. Cells were then washed with PBS three times and incubated with baseline buffer modified from previous protocols (31) (90 mM potassium glutamate, 50 mM KCl, 20 mM HEPES, 10 mM glucose, 1 mM EDTA, pH 7.4). Radiometric fluorescence recording was performed using the PTI (Photon Technology International) Fluorescence Imaging System (Birmingham, NJ) with an automated fluorescence microscope and CCD camera. The glass coverslip was inserted into the bottom of a perfusion chamber, and images were acquired by exciting Dextran, Oregon Green 514 alternately at 440 and 490 nm, and recording emitted fluorescence at 510 nm every 10 seconds. The ratio of 490/440 was calculated and represented as relative lysosomal pH. Cells were initially perfused in baseline buffer, and signals were recorded for 5 minutes. Lysosomes were then alkalinized by incubating cells with alkalization buffer (baseline buffer supplemented with 10mM  $\text{NH}_4\text{Cl}$ ) for 15 minutes. Re-acidification was initiated by replacing alkalization buffer with re-acidification buffer (90 mM potassium gluconate, 50 mM KCl, 3 mM  $\text{MgCl}_2$ , 20 mM HEPES, 10 mM glucose, 1 mM EDTA, pH 7.4) for another 15 minutes. Concanamycin A (500 nM, Santa Cruz) was supplemented in alkalization buffer for the last 5 minutes of the alkalization process to inhibit V-ATPase activity.

## **Histology and imaging**

For RFP/GFP analysis, hearts were harvested from anesthetized mice and fixed by overnight immersion in 4% paraformaldehyde/phosphate-buffered saline (PFA/PBS). Following fixation, hearts were sequentially cryoprotected with overnight incubations in 10% and 18% sucrose. Next, hearts were embedded in freezing matrix (TFM, Triangle Bioscience, Durham, NC), and 8  $\mu$ m frozen sections were prepared on a Leica CM3000 Cryostat (Leica Microsystems, Buffalo Grove IL) and stored at -80°C. For NRVMs, cells cultured and treated on coverslips were washed with ice-cold PBS twice and fixed with 4% PFA. Prior to imaging, slides were thawed and coverslipped with Prolong-Gold antifade mounting medium (Life Technologies). Images were acquired on a Leica Microsystems TCS SP5 confocal microscope.

## **Electron microscopy**

Hearts were transcardially perfused and fixed with 2.5% (v/v) glutaraldehyde in 0.1 M sodium cacodylate buffer. After three washes with 0.1 M sodium cacodylate buffer, hearts were post-fixed in 1% osmium tetroxide and 0.8% K<sub>3</sub> [Fe(CN<sub>6</sub>)] / 0.1 M sodium cacodylate buffer (1 hour, RT). After three rinses with water, specimens were dehydrated with increasing concentrations of ethanol, infiltrated with Embed-812 resin, and polymerized in a 60°C oven overnight. Blocks were sectioned with a diamond knife (Diatome) on a Leica Ultracut UC7 ultramicrotome (Leica Microsystems) and collected onto copper grids, post-stained with 2% uranyl acetate in water and lead citrate. Images were acquired on a Tecnai G2 spirit transmission electron microscope (FEI) equipped with a LaB6 source (120 kV).

## Echocardiography

Echocardiograms were performed on conscious, gently restrained mice (Vevo 2100 system, MS400C probe). M-mode images of the left ventricle were obtained at the level of papillary muscles. Left ventricular internal diameters at end-diastole (LVIDd) and end-systole (LVIDs) were measured from M-mode recordings. Fractional shortening (FS) was calculated  $(LVIDd - LVIDs)/LVIDd$  (%). Six representative contraction cycles were selected for analysis and average indexes (LVIDd, LVIDs, FS) were calculated for each mouse.

## Reagents

Doxorubicin was purchased from LC laboratories. Other reagents were purchased as follows: paclitaxel (Sigma Aldrich), torin 1 (Tocris Bioscience), bafilomycin A1 (LC laboratory), E64d, pepstatin (Sigma Aldrich), concanamycin A (Santa Cruz), Dexrazoxane (Sigma Aldrich), Trolox (Santa Cruz). LysoTracker Red (DND-99), lysosensor DND-189, acridine orange, Dextran, and Oregon Green 514 were purchased from Invitrogen. Antibodies: LC3 (previously developed (32)), p62 (Abnova), GAPDH (Fitzgerald Industries), pS6 (240/244), S6, pS6K (T389), S6K, p4EBP1, 4EBP1 (Cell Signaling), LAMP-1 (Hybridoma bank), LAMP-2 (Sigma Aldrich), ATP6V0D1, ATP6V0A2, ATPV1D, ATPV1B2 (Abcam).

## Data analysis

All data are reported as mean  $\pm$  standard error of the mean. The Student *t* test (2-tailed) was performed to compare two groups. One-way ANOVA analysis followed by Turkey *post hoc* test was used to compare multiple groups. Two-way ANOVA and subsequent Turkey tests were performed to analyze time course and concentration gradient studies. A *p* value of less than 0.05 was considered significant.

## CHAPTER 2 REFERENCES

1. Singal, P.K., Deally, C.M., and Weinberg, L.E. 1987. Subcellular effects of adriamycin in the heart: a concise review. *J Mol Cell Cardiol* 19:817-828.
2. Lipshultz, S.E., Colan, S.D., Gelber, R.D., Perez-Atayde, A.R., Sallan, S.E., and Sanders, S.P. 1991. Late cardiac effects of doxorubicin therapy for acute lymphoblastic leukemia in childhood. *N Engl J Med* 324:808-815.
3. Singal, P.K., and Iliskovic, N. 1998. Doxorubicin-induced cardiomyopathy. *N Engl J Med* 339:900-905.
4. Suliman, H.B., Carraway, M.S., Ali, A.S., Reynolds, C.M., Welty-Wolf, K.E., and Piantadosi, C.A. 2007. The CO/HO system reverses inhibition of mitochondrial biogenesis and prevents murine doxorubicin cardiomyopathy. *J Clin Invest* 117:3730-3741.
5. Doroshov, J.H., Locker, G.Y., and Myers, C.E. 1980. Enzymatic defenses of the mouse heart against reactive oxygen metabolites: alterations produced by doxorubicin. *J Clin Invest* 65:128-135.
6. Kuma, A., Hatano, M., Matsui, M., Yamamoto, A., Nakaya, H., Yoshimori, T., Ohsumi, Y., Tokuhiya, T., and Mizushima, N. 2004. The role of autophagy during the early neonatal starvation period. *Nature* 432:1032-1036.
7. Choi, A.M., Ryter, S.W., and Levine, B. 2013. Autophagy in human health and disease. *N Engl J Med* 368:651-662.
8. Nakai, A., Yamaguchi, O., Takeda, T., Higuchi, Y., Hikoso, S., Taniike, M., Omiya, S., Mizote, I., Matsumura, Y., Asahi, M., et al. 2007. The role of autophagy in cardiomyocytes in the basal state and in response to hemodynamic stress. *Nat Med* 13:619-624.
9. Tanaka, Y., Guhde, G., Suter, A., Eskelinen, E.L., Hartmann, D., Lullmann-Rauch, R., Janssen, P.M., Blanz, J., von Figura, K., and Saftig, P. 2000. Accumulation of autophagic vacuoles and cardiomyopathy in LAMP-2-deficient mice. *Nature* 406:902-906.
10. Mangieri, L.R., Mader, B.J., Thomas, C.E., Taylor, C.A., Luker, A.M., Tse, T.E., Huisinigh, C., and Shacka, J.J. 2014. ATP6V0C knockdown in neuroblastoma cells alters autophagy-lysosome pathway function and metabolism of proteins that accumulate in neurodegenerative disease. *PLoS One* 9:e93257.
11. Kim, Y.C., Park, H.W., Sciarretta, S., Mo, J.S., Jewell, J.L., Russell, R.C., Wu, X., Sadoshima, J., and Guan, K.L. 2014. Rag GTPases are cardioprotective by regulating lysosomal function. *Nat Commun* 5:4241.
12. Rifki, O.F., and Hill, J.A. 2012. Cardiac autophagy: good with the bad. *J Cardiovasc Pharmacol* 60:248-252.
13. Wen, X., Wu, J., Wang, F., Liu, B., Huang, C., and Wei, Y. 2013. Deconvoluting the role of reactive oxygen species and autophagy in human diseases. *Free Radic Biol Med* 65:402-410.
14. Li, L., Wang, Z.V., Hill, J.A., and Lin, F. 2014. New autophagy reporter mice reveal dynamics of proximal tubular autophagy. *J Am Soc Nephrol* 25:305-315.
15. Minotti, G., Menna, P., Salvatorelli, E., Cairo, G., and Gianni, L. 2004. Anthracyclines: molecular advances and pharmacologic developments in antitumor activity and cardiotoxicity. *Pharmacol Rev* 56:185-229.
16. Kim, J., Kundu, M., Viollet, B., and Guan, K.L. 2011. AMPK and mTOR regulate autophagy through direct phosphorylation of Ulk1. *Nat Cell Biol* 13:132-141.
17. Settembre, C., Zoncu, R., Medina, D.L., Vetrini, F., Erdin, S., Erdin, S., Huynh, T., Ferron, M., Karsenty, G., Vellard, M.C., et al. 2012. A lysosome-to-nucleus signalling

- mechanism senses and regulates the lysosome via mTOR and TFEB. *EMBO J* 31:1095-1108.
18. Yoshimori, T., Yamamoto, A., Moriyama, Y., Futai, M., and Tashiro, Y. 1991. Bafilomycin A1, a specific inhibitor of vacuolar-type H(+)-ATPase, inhibits acidification and protein degradation in lysosomes of cultured cells. *J Biol Chem* 266:17707-17712.
  19. O'Reilly, D.S. 1984. Increased ammoniogenesis and the renal tubular effects of potassium depletion. *J Clin Pathol* 37:1358-1362.
  20. Kim, A., Balis, F.M., and Widemann, B.C. 2009. Sorafenib and sunitinib. *Oncologist* 14:800-805.
  21. Rowinsky, E.K., Jiroutek, M., Bonomi, P., Johnson, D., and Baker, S.D. 1999. Paclitaxel steady-state plasma concentration as a determinant of disease outcome and toxicity in lung cancer patients treated with paclitaxel and cisplatin. *Clin Cancer Res* 5:767-774.
  22. Pillay, C.S., Elliott, E., and Dennison, C. 2002. Endolysosomal proteolysis and its regulation. *Biochem J* 363:417-429.
  23. Forgac, M. 2007. Vacuolar ATPases: rotary proton pumps in physiology and pathophysiology. *Nat Rev Mol Cell Biol* 8:917-929.
  24. Zoncu, R., Bar-Peled, L., Efeyan, A., Wang, S., Sancak, Y., and Sabatini, D.M. 2011. mTORC1 senses lysosomal amino acids through an inside-out mechanism that requires the vacuolar H(+)-ATPase. *Science* 334:678-683.
  25. Sancak, Y., Bar-Peled, L., Zoncu, R., Markhard, A.L., Nada, S., and Sabatini, D.M. 2010. Ragulator-Rag complex targets mTORC1 to the lysosomal surface and is necessary for its activation by amino acids. *Cell* 141:290-303.
  26. Korolchuk, V.I., Saiki, S., Lichtenberg, M., Siddiqi, F.H., Roberts, E.A., Imarisio, S., Jahreiss, L., Sarkar, S., Futter, M., Menzies, F.M., et al. 2011. Lysosomal positioning coordinates cellular nutrient responses. *Nat Cell Biol* 13:453-460.
  27. Kimura, S., Noda, T., and Yoshimori, T. 2008. Dynein-dependent movement of autophagosomes mediates efficient encounters with lysosomes. *Cell Struct Funct* 33:109-122.
  28. Wang, Z.V., Deng, Y., Gao, N., Pedrozo, Z., Li, D.L., Morales, C.R., Criollo, A., Luo, X., Tan, W., Jiang, N., et al. 2014. Spliced X-box binding protein 1 couples the unfolded protein response to hexosamine biosynthetic pathway. *Cell* 156:1179-1192.
  29. Xie, M., Kong, Y., Tan, W., May, H., Battiprolu, P.K., Pedrozo, Z., Wang, Z.V., Morales, C., Luo, X., Cho, G., et al. 2014. Histone deacetylase inhibition blunts ischemia/reperfusion injury by inducing cardiomyocyte autophagy. *Circulation* 129:1139-1151.
  30. Lian, X., Zhang, J., Azarin, S.M., Zhu, K., Hazeltine, L.B., Bao, X., Hsiao, C., Kamp, T.J., and Palecek, S.P. 2013. Directed cardiomyocyte differentiation from human pluripotent stem cells by modulating Wnt/beta-catenin signaling under fully defined conditions. *Nat Protoc* 8:162-175.
  31. Boheler, K.R., Bhattacharya, S., Kropp, E.M., Chuppa, S., Riordon, D.R., Bausch-Fluck, D., Burrige, P.W., Wu, J.C., Wersto, R.P., Chan, G.C., et al. 2014. A human pluripotent stem cell surface N-glycoproteome resource reveals markers, extracellular epitopes, and drug targets. *Stem Cell Reports* 3:185-203.
  32. Shang, L., Chen, S., Du, F., Li, S., Zhao, L., and Wang, X. 2011. Nutrient starvation elicits an acute autophagic response mediated by Ulk1 dephosphorylation and its subsequent dissociation from AMPK. *Proc Natl Acad Sci U S A* 108:4788-4793.
  33. Kreuzaler, P.A., Staniszewska, A.D., Li, W., Omidvar, N., Kedjouar, B., Turkson, J., Poli, V., Flavell, R.A., Clarkson, R.W., and Watson, C.J. 2011. Stat3 controls lysosomal-mediated cell death in vivo. *Nat Cell Biol* 13:303-309.

34. Steinberg, B.E., Huynh, K.K., Brodovitch, A., Jabs, S., Stauber, T., Jentsch, T.J., and Grinstein, S. 2010. A cation counterflux supports lysosomal acidification. *J Cell Biol* 189:1171-1186.
35. Zhu, H., Tannous, P., Johnstone, J.L., Kong, Y., Shelton, J.M., Richardson, J.A., Le, V., Levine, B., Rothermel, B.A., and Hill, J.A. 2007. Cardiac autophagy is a maladaptive response to hemodynamic stress. *J Clin Invest* 117:1782-1793.

**CHAPTER 3.**  
**ATTENUATED AUTOPHAGIC INITIATION AMELIORATES**  
**DOXORUBICIN CARDIOTOXICITY IN MICE**

## INTRODUCTION

Autophagy plays an important role in cardiac physiology (1-3). In addition, dysregulation of autophagy has been shown to contribute significantly to pathological cardiac hypertrophy (1, 4), ischemia/reperfusion injury (5, 6), and progression of heart failure (4).

Beclin 1 is an essential autophagy protein that regulates the initiation process of autophagy. It interacts with Vps34 and Atg14L, forming a complex that mediates the nucleation of the phagophore (7). Modulations of Beclin 1 levels have been shown to alter autophagic flux (8).

Using genetic mouse models (*Beclin 1*<sup>+/-</sup>, and  $\alpha$ -MHC-Beclin 1) to manipulate autophagic levels in heart, our group has previously shown that over-activated autophagy is detrimental in pressure-overload cardiomyopathy (4). We demonstrated that attenuation of autophagy (*Beclin 1*<sup>+/-</sup>) was protective against severe Transverse Aortic Constriction (sTAC) - induced pathologic hypertrophy and heart failure; by contrast, boosting autophagic initiation ( $\alpha$ -MHC-Beclin 1) exacerbated cardiac hypertrophy and progression to heart failure, despite the fact that  $\alpha$ -MHC-Beclin 1 mice did not manifest basal cardiac dysfunction.

On the other hand, we (9) and other groups (10) have reported that autophagy is beneficial for cardiomyocyte survival during ischemic injury. While controversy exists as to what role autophagy plays in reperfusion injury, it was shown that *Beclin 1*<sup>+/-</sup> mice were protected from ischemia/reperfusion injury (11). According to studies from Decker et al. (11) and Ma et al. (6), cardiomyocyte autophagic flux might be blocked during the reperfusion stage. Therefore, attenuation of autophagic initiation by Beclin 1 haplosufficiency might alleviate the downstream blockage of autophagic flux, and thereby be protective against reperfusion injury.

Here, I found that attenuation of autophagic initiation *in vivo* restored autophagic flux in heart, reduced doxorubicin-induced ROS production, and preserved cardiac function. In contrast, over-stimulation of autophagic initiation by overexpressing Beclin 1 further increased autolysosome accumulation, increased ROS production and exacerbated cardiac toxicity.

## RESULTS

### ***Attenuated autophagy initiation restores cardiac autophagic flux after doxorubicin exposure***

My data suggest that doxorubicin impairs autophagic flux by perturbing lysosomal acidification and autolysosomal processing. With no existing effective approach *in vivo* to rescue late processing events in the autophagic cascade, I investigated whether autophagic initiation could alter the cardiac response to doxorubicin.

Mice with heterozygous deletion of the gene coding for Beclin 1 (*Beclin 1<sup>+/-</sup>*) display decreased autophagy in multiple tissues and reduced autophagic activation in heart under pressure-overload stress (4). I capitalized on this model to examine autophagic flux in doxorubicin-treated *Beclin 1<sup>+/-</sup>* mice. Mice were treated with NS or doxorubicin (5 mg/kg) and sacrificed 24 hours post-injection (+/- 2 hour BafA1 exposure). WT and *Beclin1<sup>+/-</sup>* mice manifested comparable levels of autophagic flux at baseline (**Figure 3.1A**). However, in contrast to WT mice, which displayed blockade of cardiomyocyte autophagic flux, autophagic flux was maintained in *Beclin 1<sup>+/-</sup>* mice after doxorubicin treatment (**Figure 3.1A**). In addition, the increase in p62 levels tended to decrease in doxorubicin-treated *Beclin 1<sup>+/-</sup>* mice in comparison with WT littermates (**Figure 3.1A**), albeit p62 protein level is affected by transcription, and more variability is presented in its increase by BafA1 treatment *in vivo*. In conclusion, *Beclin 1<sup>+/-</sup>* mice manifested restored cardiac autophagic flux upon doxorubicin treatment.

This evidence suggests that doxorubicin suppresses autolysosomal processing but does not completely abolish it. Thus, the intact autophagic flux in doxorubicin-treated *Beclin 1<sup>+/-</sup>* mice may be the result of decreased demand on the lysosomal system after doxorubicin treatment due to decreased autophagic initiation in the heterozygous animal. To confirm this, I crossed *Beclin 1<sup>+/-</sup>* with the autophagic flux-reporter mouse line CAG-RFP-GFP-LC3 and quantified the autophagic vacuoles induced by doxorubicin administration. I found that in comparison with

CAG-RFP-GFP-LC3 mice exposed to doxorubicin, *Beclin 1*<sup>+/-</sup>/CAG-RFP-GFP-LC3 mice harbored significantly fewer autolysosomes in heart tissues (**Figure 3.1B**). These data are consistent with a model in which *Beclin1*<sup>+/-</sup> mice maintain normal autophagic flux by decreasing the demand on lysosomal processing.

### ***Attenuated autophagy initiation protects from doxorubicin-induced cardiotoxicity***

The data suggest a model in which the decrease in autophagic flux induced by doxorubicin contributes to cardiotoxicity. To determine whether preserved autophagic flux after doxorubicin treatment in *Beclin 1* haplosufficient mice alters the extent of cardiac injury by doxorubicin, I examined ventricular function in *Beclin 1*<sup>+/-</sup> mice exposed chronically to doxorubicin. In contrast to their WT littermates, *Beclin 1*<sup>+/-</sup> mice manifested preserved systolic performance after long-term doxorubicin administration (**Figure 3.2A**). In addition, *Beclin 1*<sup>+/-</sup> mice manifested less ventricular dilatation provoked by doxorubicin (**Table 3.2**). Induction of fetal genes and fibrotic genes elicited by doxorubicin was also significantly reduced in *Beclin1*<sup>+/-</sup> mice (**Figure 3.2B**), suggesting less pathological remodeling of the heart. Furthermore, histological analysis revealed less interstitial and perivascular fibrosis in *Beclin 1*<sup>+/-</sup> mice after doxorubicin treatment (**Figure 3.2C**). In summary, *Beclin 1*<sup>+/-</sup> mice are protected from doxorubicin-induced chronic cardiotoxicity.

### ***Enhanced autophagy initiation exacerbates cardiac autolysosome accumulation by doxorubicin***

I next examined the cardiac response to doxorubicin in mice with amplified stress-induced cardiomyocyte autophagy from cardiomyocyte-specific over-expression of *Beclin 1* (*Beclin 1* Tg mice) (4). These mice manifest normal cardiac structure and function under baseline conditions but an amplified autophagic response to disease-related stress (4). I first

examined the change in autophagic flux in doxorubicin-treated Beclin 1 Tg mice by Western blot. Beclin 1 Tg mice manifested increased autophagic initiation and flux in heart under baseline conditions, assayed as LC3-II levels by immunoblotting. Upon doxorubicin treatment, autophagic flux in Beclin1 Tg mice was again blunted. Interestingly, the accumulation of LC3-II protein after BafA1 treatment was similar between WT and Beclin1 Tg mice (**Figure 3.3A**). The reason for this observation is not yet clear.

In order to further quantify autophagic flux in doxorubicin-treated heart, I crossed the Beclin 1 Tg mouse line with the autophagic flux reporter line. I observed that reporter mice on the Beclin 1 Tg background presented a trend toward increased numbers of both autophagosomes and autolysosomes relative to WT at baseline (**Figure 3.3B**), consistent with the Western blot result that Beclin 1 Tg mice have higher autophagic flux. Upon doxorubicin treatment, Beclin 1 Tg mice showed further increased numbers of autolysosomes compared to wild-type littermates, suggesting that Beclin 1 Tg mice have exacerbated accumulation of autolysosomes (**Figure 3.3B**). There was also an increase in autophagosomes in doxorubicin-treated Beclin 1 Tg mouse hearts compared with the WT mice (**Figure 3.3B**), again suggesting that Beclin 1 Tg mice manifest an additional increase in autolysosome accumulation upon doxorubicin exposure via upregulating initiation of autophagy.

### ***Enhanced autophagy initiation exacerbates doxorubicin cardiotoxicity***

To determine whether the increased demand on lysosomal processing in the Beclin 1 Tg mice resulted in increased sensitivity to doxorubicin-induced cardiomyopathy, I subjected them to long-term doxorubicin treatment. Serial echo analysis revealed that ventricular systolic function declined faster in the Beclin 1 Tg mice after doxorubicin treatment when compared with WT mice (**Figure 3.4A**). Cardiac function remained significantly lower in these animals weeks after completion of serial doxorubicin administration (**Figure 3.4A**). Doxorubicin-treated Beclin

1 Tg mice also manifested exacerbated ventricular dilatation (**Table 3.3**), more robust induction of both fetal genes and fibrotic genes (**Figure 3.4B**), and increased cardiac fibrosis (**Figure 3.4C**). Together, these findings support a model in which enhanced autophagic initiation, without correcting dysfunctional autolysosomal processing, exacerbates doxorubicin cardiomyopathy.

### **Modulation of autophagic initiation alters doxorubicin-elicited increases in ROS**

Reactive Oxygen Species (ROS) have been considered an important contributor to the pathogenesis of doxorubicin cardiomyopathy. I tested whether the level of doxorubicin-elicited ROS in heart would be affected by different levels of autophagic initiation. Dihydroethidium (DHE) staining of heart 24 hours after one dose of doxorubicin (5 mg/kg) revealed that doxorubicin-induced ROS production was significantly reduced in *Beclin 1*<sup>+/-</sup> mice (**Figure 3.5A**). By contrast, *Beclin 1* Tg mice manifested increased levels of ROS in heart after doxorubicin administration (**Figure 3.5B**). My data suggest that reduced autophagic initiation decreases acutely the ROS induced by doxorubicin via restoring cardiomyocyte autophagic flux, while enhanced autophagic initiation exacerbated ROS production as a result of accumulation of undigested autolysosomes, further burdening the autophagic machinery and impairing its capacity to eliminate damaged proteins and organelles.

### **Beclin 1 modulates cardiac autophagic flux in the long term after doxorubicin treatment**

According to my data, *Beclin 1*<sup>+/-</sup> mice manifested recovered autophagic flux upon doxorubicin treatment, which correlated with acute reduction of ROS generation and protection of cardiac function in the long term. By contrast, *Beclin 1* Tg mice presented with exacerbated accumulation of autolysosomes and increased ROS generation upon acute doxorubicin treatment. They also presented with early cardiac dysfunction during the serial doxorubicin

injections. Taken together, these data argue strongly that cardiac injury caused by doxorubicin happens early during doxorubicin exposure. The different extents of cardiac injury induced by doxorubicin in *Beclin 1<sup>+/-</sup>* and *Beclin 1 Tg* suggest the level of autophagic flux inhibition could also dictate the long-term cardiac outcome.

Earlier (Chapter 2) I revealed the dynamic changes in autophagic flux in our chronic mouse model of doxorubicin cardiomyopathy, *i.e.* autophagic flux was blocked by doxorubicin 24 hours after one injection and four serial injections, while it became increased 4 weeks after the final injection. As discussed earlier, the increase in autophagic flux was likely due to secondary pathological remodeling rather than the direct effect of doxorubicin. Since cardiac dysfunction persisted weeks after doxorubicin injections, I asked the question how *Beclin 1* level affects autophagic flux changes in the remodeling phase of doxorubicin cardiomyopathy. Using Western blot to assess autophagic flux, I found that autophagic flux in *Beclin 1<sup>+/-</sup>* mice showed no significant increase 4 weeks after doxorubicin treatment (**Figure 3.6A**); in contrast, *Beclin 1 Tg* mice showed consistently an even higher autophagic flux than WT long after doxorubicin treatment (**Figure 3.6B**).

Although it is not known whether the increase in autophagic flux in the remodeling phase also contribute to the progression of doxorubicin cardiomyopathy, from our previous study (4), it appears that excessive autophagic flux is detrimental for cardiac pathological remodeling under pressure overload and contributes to the progression of heart failure. So the possibility exists that blockage of autophagic flux during the injury phase (serial-doxorubicin injection period) accelerates the ROS generation by doxorubicin, while the upregulation of autophagy in the remodeling phase (weeks after serial injections) exacerbates pathological remodeling. Attenuation of autophagic initiation by reducing *Beclin 1* levels could recover the autophagic flux acutely and inhibit the long-term upregulation of autophagy, effectively blunting doxorubicin cardiotoxicity both short-term and long-term.

### **Beclin1 levels and cardiac apoptotic activity in chronic doxorubicin cardiomyopathy**

A large body of literature suggests that doxorubicin causes cardiomyocyte apoptosis. Therefore we also tested the apoptotic level in my chronic doxorubicin cardiomyopathy model. I did not detect an increase of caspase 3/7 activity in heart 24 hours after one small dose (5 mg/kg) of doxorubicin injection (**Figure 3.7A**). In comparison, I also measured caspase 3/7 activity after one single large dose of doxorubicin, and again failed to detect any significant changes at different time points after doxorubicin treatment (**Figure 3.7B**). These results are consistent with previous reports (12, 13) that adult cardiomyocytes possess very low caspase activities and are relatively resistant to apoptosis.

Next I examined apoptosis via TUNEL staining and did not detect positive signals after one small dose of doxorubicin injection; however, I detect TUNEL positive signals weeks after multiple doxorubicin injections, and more frequently in atria (**Figure 3.7C**). Further, the TUNEL-positivity was attenuated in doxorubicin-treated *Beclin 1<sup>+/-</sup>* mice, and amplified in doxorubicin-treated Beclin 1 Tg mice (**Figure 3.7D, E**). However, closer observation revealed that the TUNEL signals came from non-cardiomyocytes. Previously, Zhang et al (14) also pointed out that the TUNEL positive sites in their chronic doxorubicin cardiomyopathy rat model were confined to endothelial cells, interstitial cells and macrophages, but not cardiomyocytes. On the other hand, the increase in apoptotic signals in non-cardiomyocytes might still reflect cardiac injury and pathological cardiac remodeling. Therefore, the reduction of TUNEL positivity in *Beclin 1<sup>+/-</sup>* mice and amplification of TUNEL positivity in Beclin 1 Tg mice suggest that *Beclin 1<sup>+/-</sup>* mice are protected from, while Beclin 1 Tg mice are at increased risk for doxorubicin cardiotoxicity.

### ***In vitro* modulation of Beclin1 levels failed to affect doxorubicin-cytotoxicity in NRVMs**

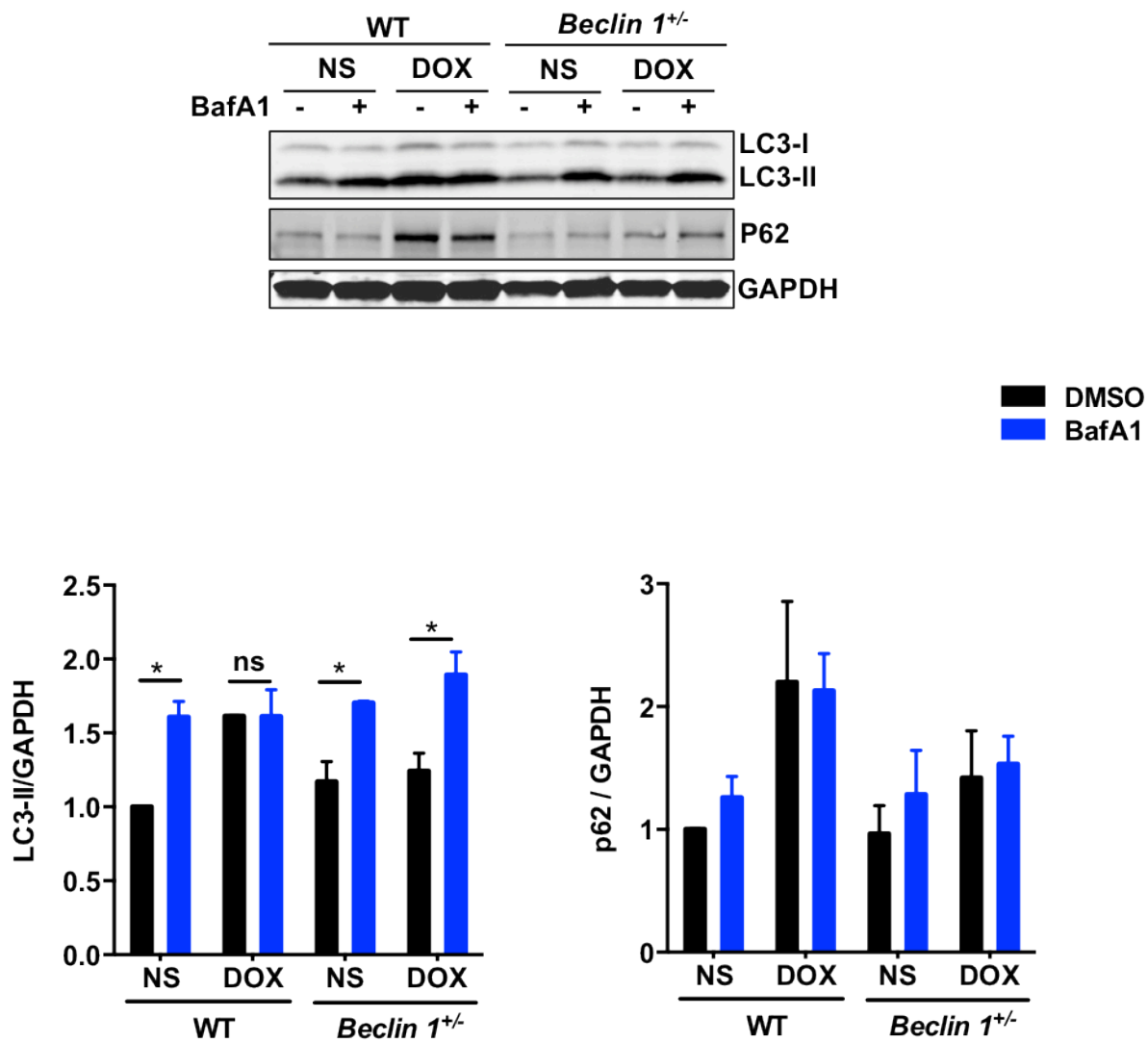
I first examined *in vitro* whether knock-down or overexpression of Beclin 1 affected doxorubicin's inhibition of autophagic flux in NRVMs. I did not detect a restoration of autophagic

flux in NRVMs with knocking down Beclin 1 by siRNA (**Figure 3.8A**). In addition, overexpression of Beclin 1 yielded no changes to the inhibition of autophagic flux by doxorubicin either (**Figure 3.8B**). Given this, it was not surprising that neither reducing nor overexpressing Beclin 1 affected doxorubicin-elicited NRVM death (**Figure 3.8C**).

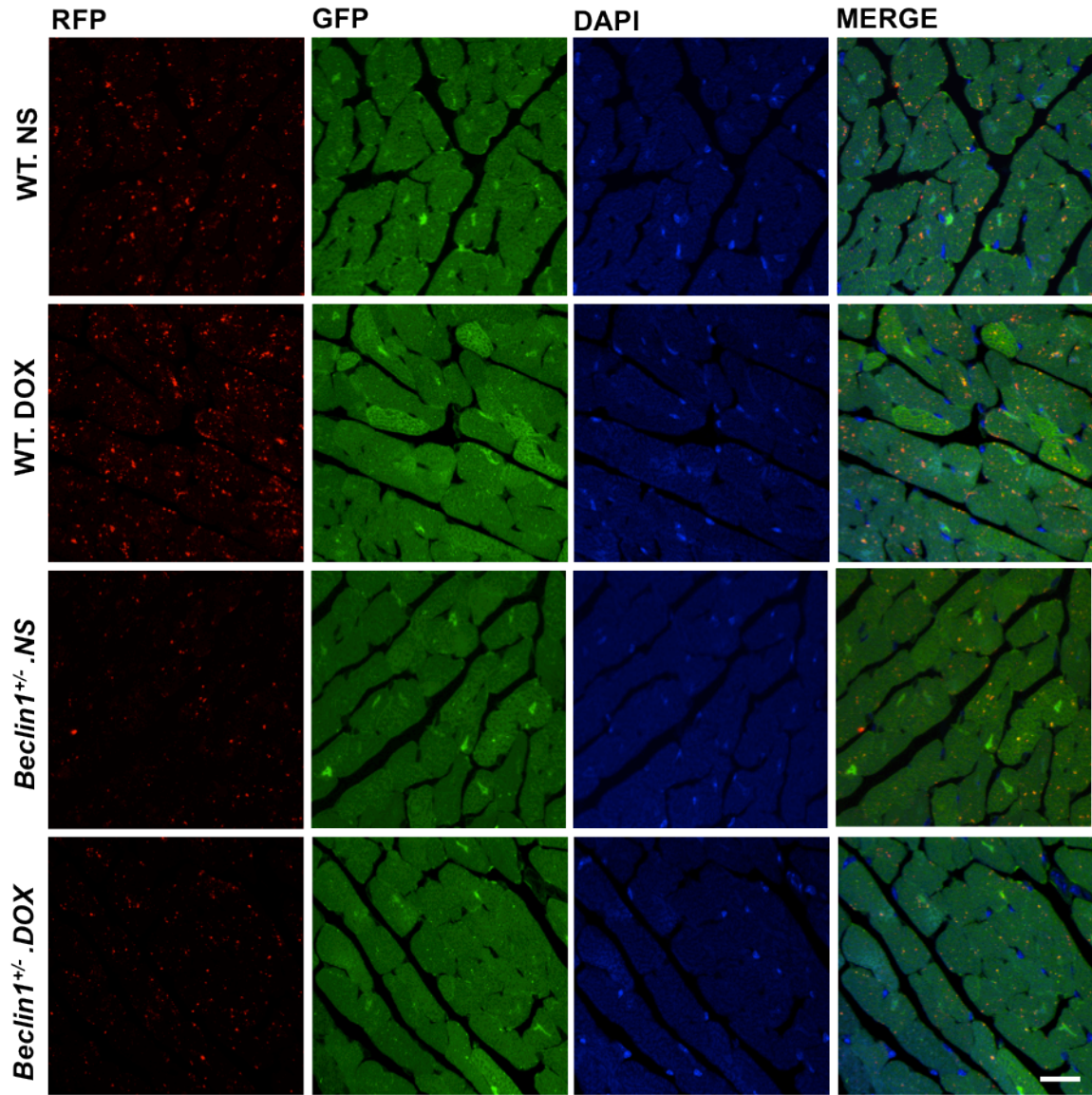
These observations were not consistent with my *in vivo* data. However, significant differences exist between *in vivo* and *in vitro* cardiomyocyte responses to doxorubicin. While I observed a consistent increase in LC3-II levels in doxorubicin-treated heart, this was not the case in *in vitro* cultured cells. I reasoned that while autophagic initiation machinery is intact in the *in vivo* system, it is impaired by doxorubicin in cultured cardiomyocytes. This disparity might stem from the fact that the *in vivo* system also involves influences from hepatic metabolism of doxorubicin, circulatory factors, neurohormonal regulation and paracrine mechanisms between cardiomyocytes and non-cardiomyocytes.

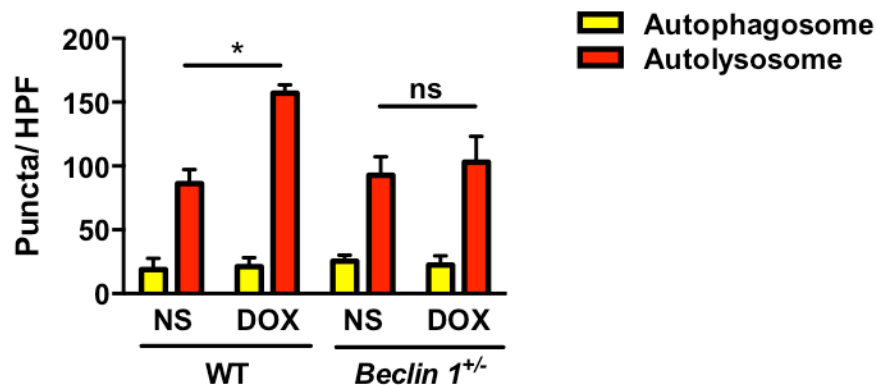
Figure 3.1

A.



B.

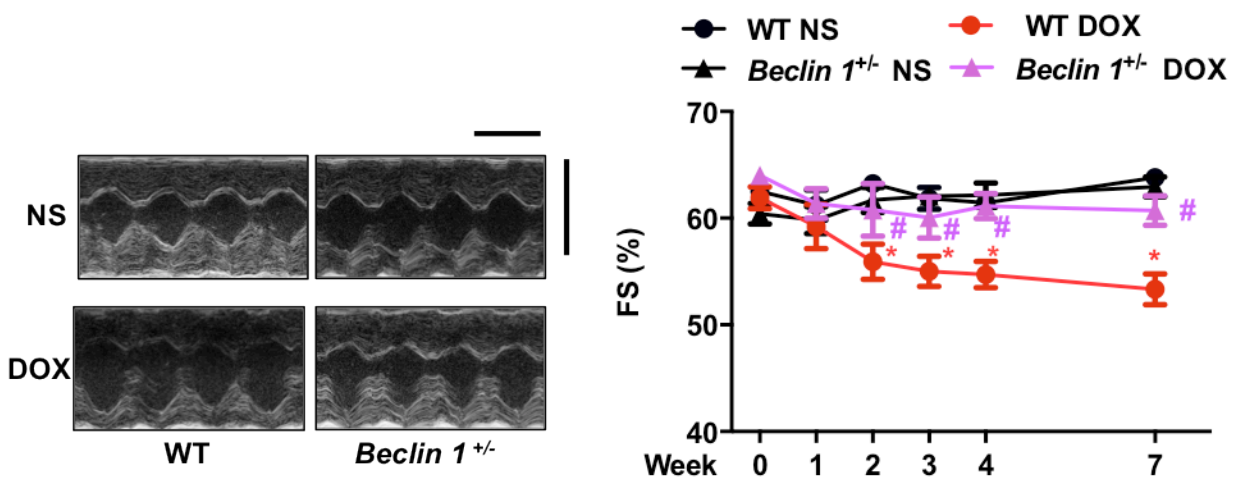




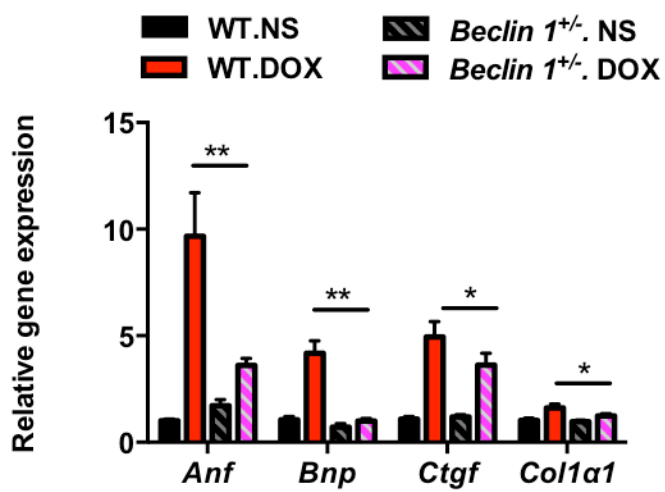
**Figure 3.1. Attenuated autophagy initiation restores cardiac autophagic flux after doxorubicin exposure.** (A) Autophagic flux inhibition by doxorubicin was rescued in *Beclin1<sup>+/-</sup>* mouse hearts, determined by immunoblotting LC3 and p62 with or without bafilomycin A1 treatment. N = 4 per group. (B) Representative fluorescence imaging of heart tissue sections from CAG-RFP-GFP-LC3 transgenic mice or *Beclin1<sup>+/-</sup>/CAG-RFP-GFP-LC3* 24 hours after DOX injection. Autophagosome (yellow puncta) and autolysosome numbers (red puncta) were quantified with 6 microscopic fields (14,000  $\mu\text{m}^2$ ) per heart section. N = 4 mice per group. Scale bar, 20  $\mu\text{m}$ . \*,  $p < 0.05$ ; ns, not significant.

Figure 3.2

A.



B.



C.

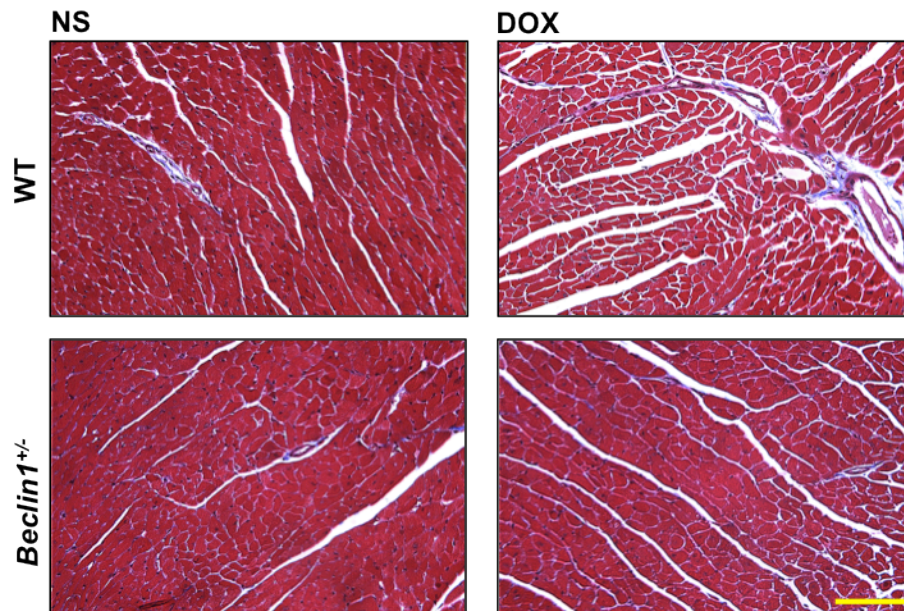
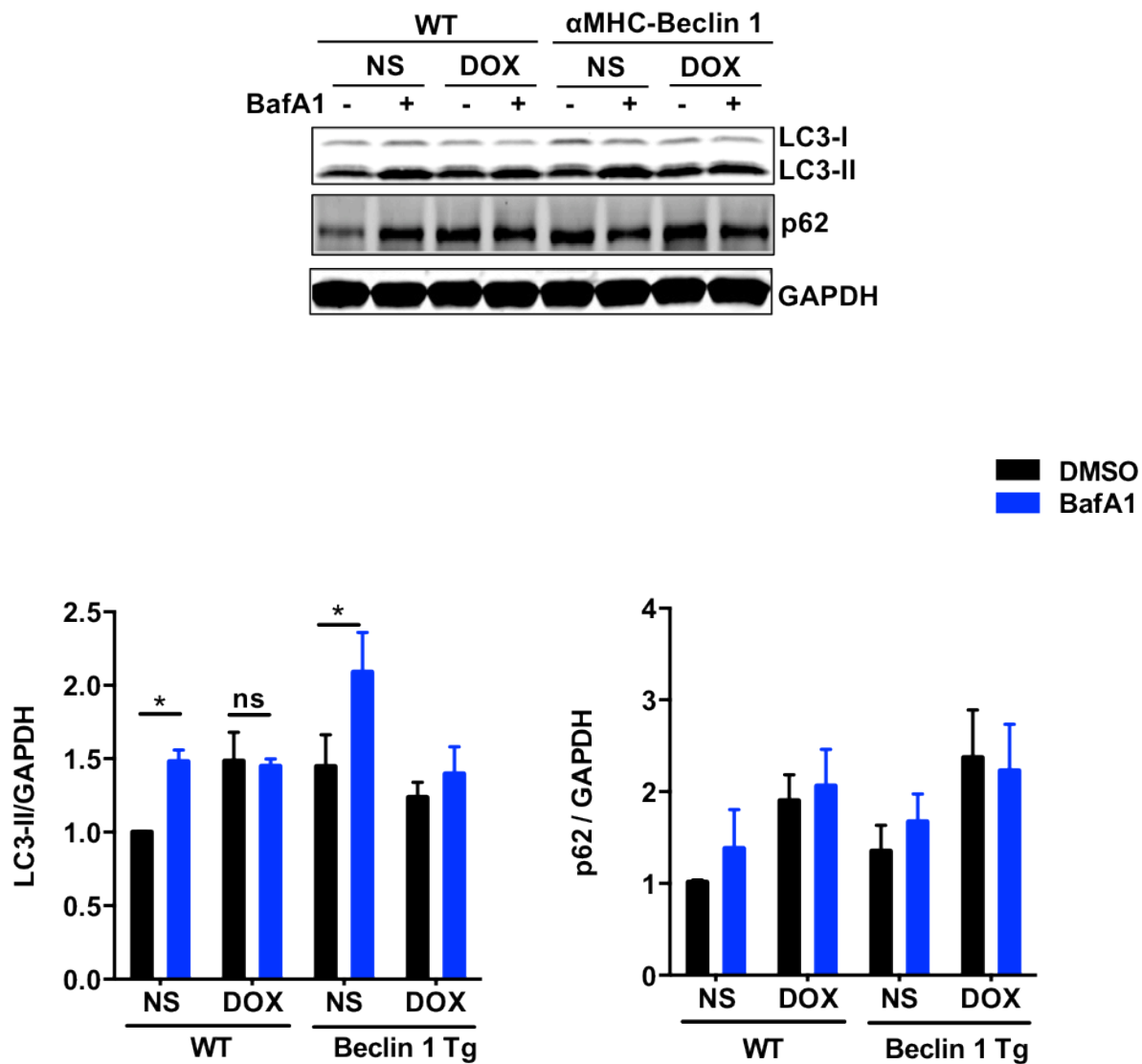


**Figure 3.2. Attenuated autophagy initiation is cardioprotective against doxorubicin.**

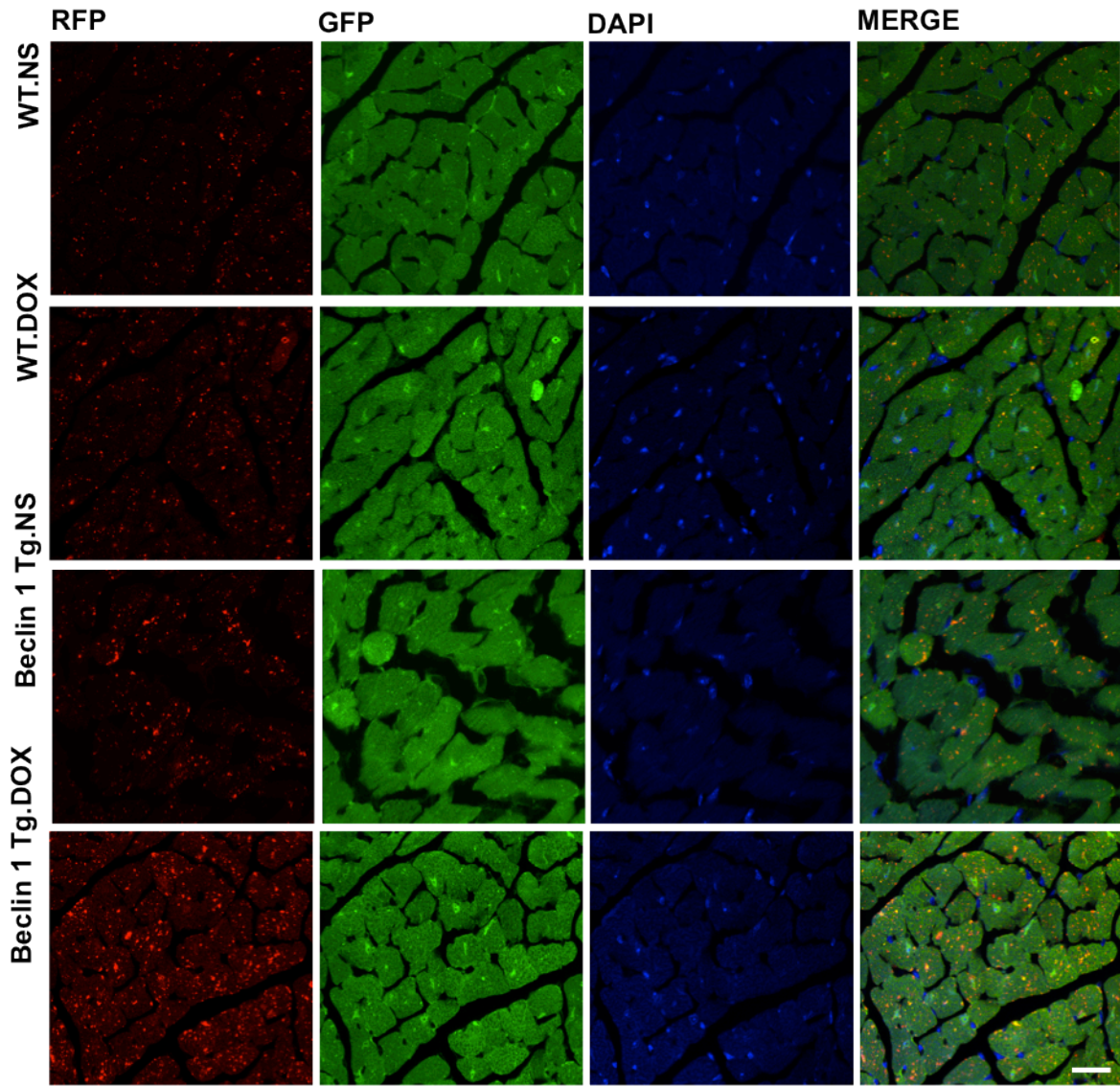
(A) Cardiac function was preserved in doxorubicin-treated *beclin1*<sup>+/-</sup> mice compared to WT mice. Representative echocardiograms from WT and *Beclin1*<sup>+/-</sup> mice treated with NS and DOX, taken 1 day before sacrifice, were shown. N = 7-8 mice per group. \*  $p < 0.05$ , DOX-treated WT mice compared to NS-treated WT mice. #  $p < 0.05$ , DOX-treated *Beclin1*<sup>+/-</sup> mice compared with DOX-treated WT mice. Scale bar, 0.1 s, 5 mm. (B) *Beclin1*<sup>+/-</sup> mice showed less pathological cardiac remodeling after chronic doxorubicin treatment, examined by relative mRNA levels of fetal genes and fibrotic genes. N = 6-7 per group. (C) Representative trichrome staining images of hearts from WT and *Beclin1*<sup>+/-</sup> mice treated with NS or DOX. *Beclin1*<sup>+/-</sup> mice presented with reduced interstitial fibrosis than WT mice after chronic doxorubicin treatment. Scale bar, 100  $\mu$ m. HPF, high-power field. \*,  $p < 0.05$ ; \*\*,  $p < 0.01$ ; ns, not significant.

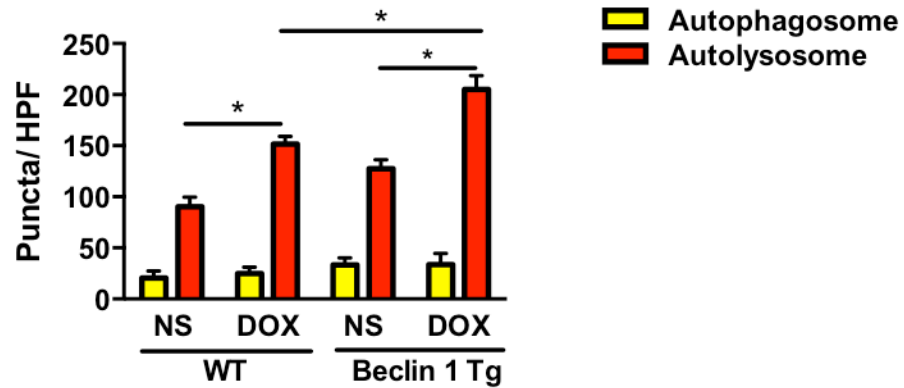
Figure 3.3

A.



B.

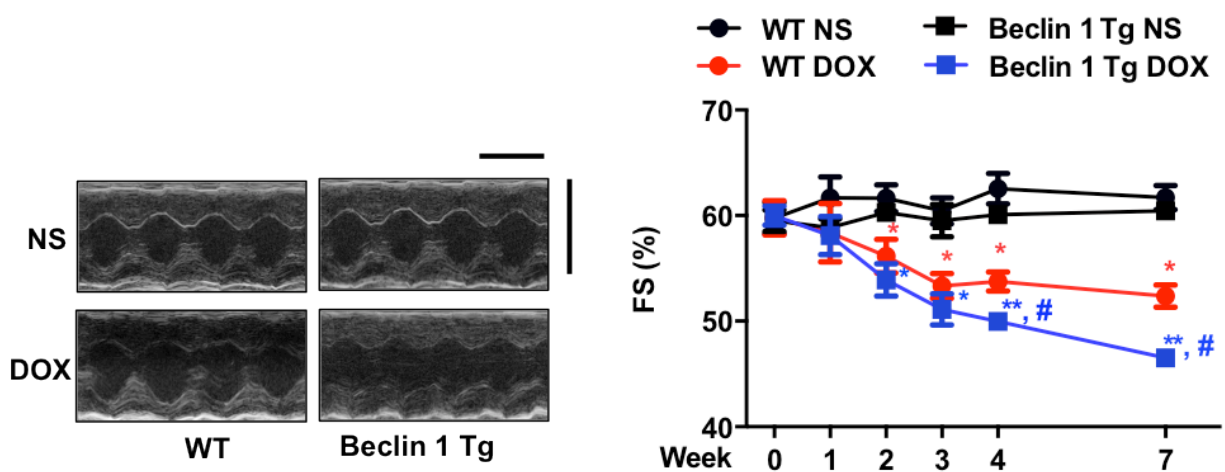




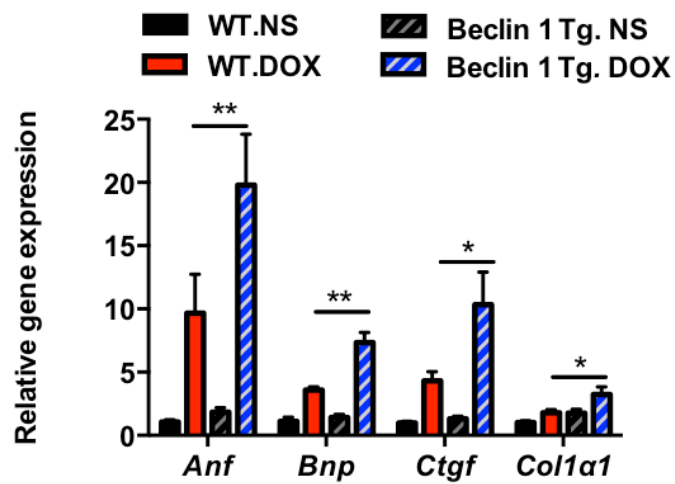
**Figure 3.3. Doxorubicin-induced autophagic flux blockage is exacerbated in  $\alpha$ MHC-Beclin1 mice.** (A) Autophagic flux in WT and  $\alpha$ MHC-Beclin1 (Beclin1 Tg) mouse hearts determined by immunoblotting LC3 with or without bafilomycin A1 treatment. N = 4 per group. (B) Representative fluorescent images of heart tissue sections from CAG-RFP-GFP-LC3 transgenic mice or  $\alpha$ MHC-Beclin1/CAG-RFP-GFP-LC3 mice. Quantification of autophagosome (yellow puncta) and autolysosome numbers (red puncta) was based on 6 microscopic fields ( $14,000 \mu\text{m}^2$ ) per heart section. N = 4 mice per group. Scale bar, 20  $\mu\text{m}$ . HPF, high-power field. \*,  $p < 0.05$ ; ns, not significant

Figure 3.4

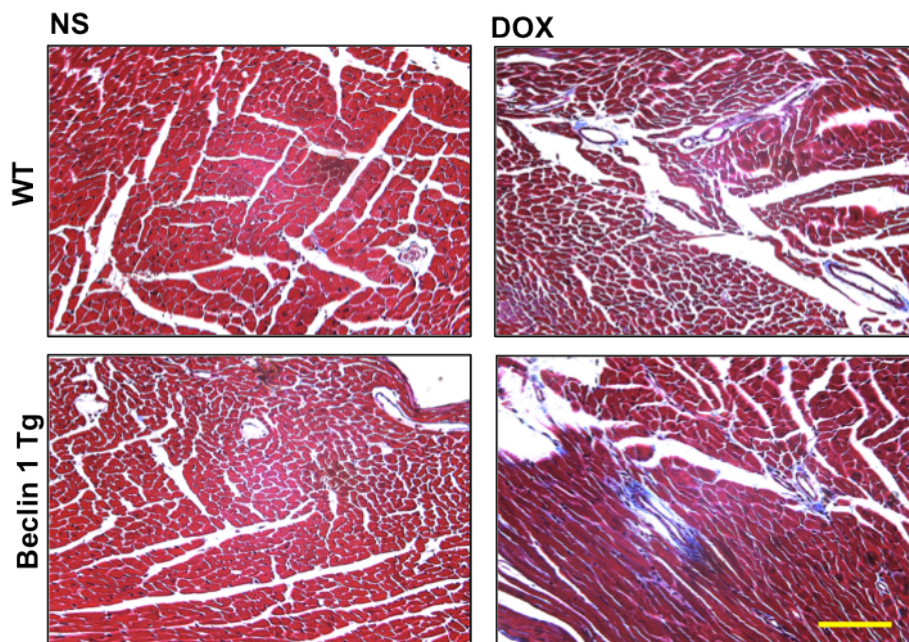
A.



B.



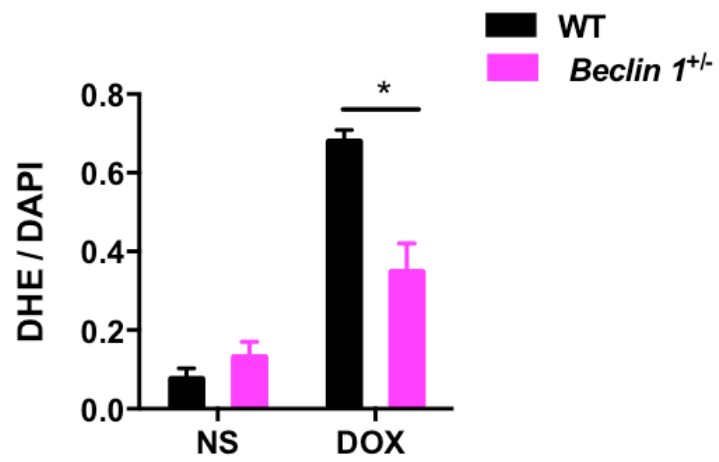
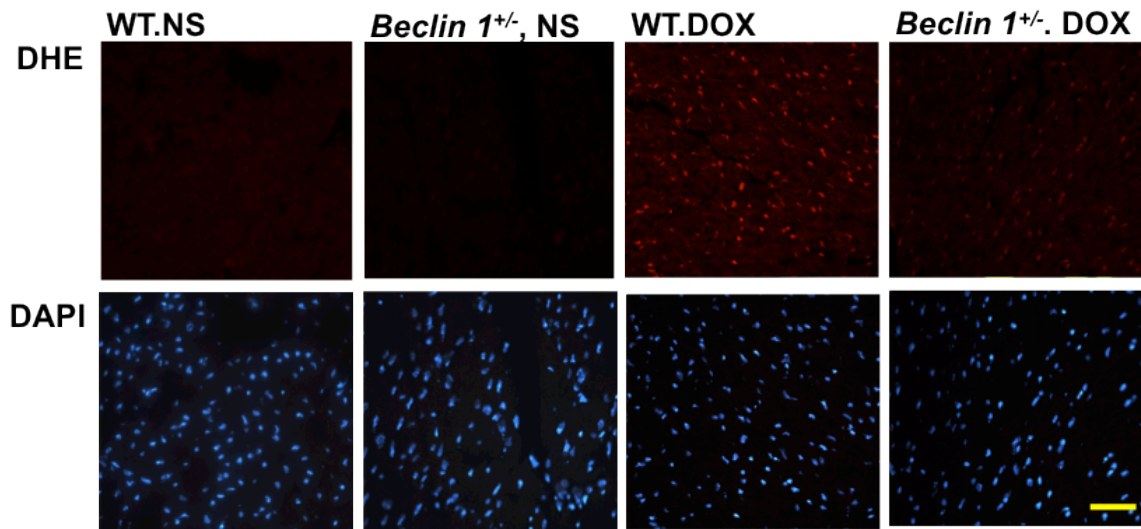
C.



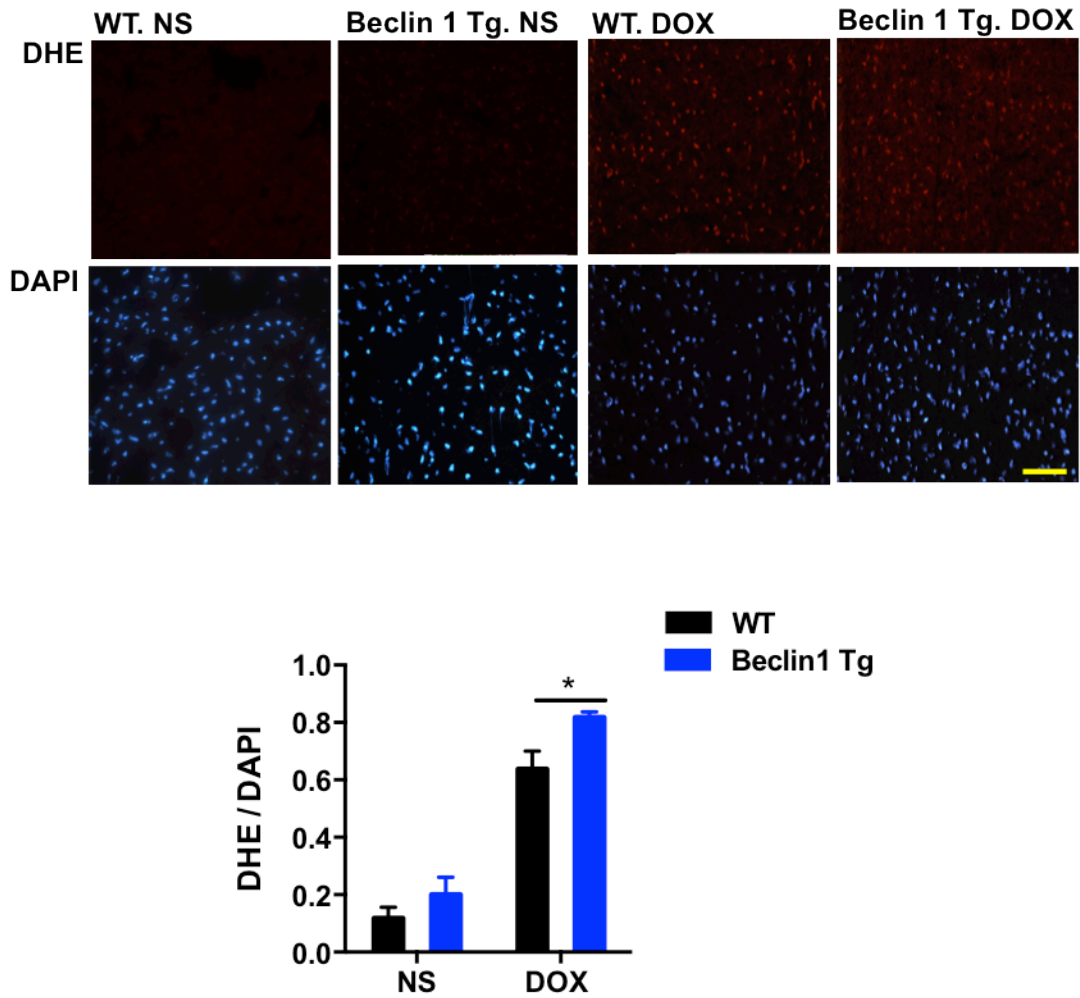
**Figure 3.4. Doxorubicin cardiotoxicity is exacerbated in  $\alpha$ MHC-Beclin1 mice.** (A) Cardiac function was exacerbated in doxorubicin-treated Beclin1 Tg mice compared to WT mice. Representative echocardiograms from WT and Beclin1 Tg mice treated with NS and DOX were shown. Scale bar, 0.1 s, 5 mm. N = 8 mice per group. \*,  $p < 0.05$ , DOX-treated WT mice compared to NS-treated WT mice; #,  $p < 0.05$ , DOX-treated Beclin1 Tg mice compared with DOX-treated WT mice. (B) Beclin1 Tg mice showed exacerbated pathological cardiac remodeling after chronic doxorubicin treatment, examined by relative mRNA levels of fetal genes and fibrotic genes. N = 6 per group. (C) Representative trichrome staining images of hearts from WT and Beclin1 Tg mice treated with NS and DOX. Beclin1 Tg mice showed increased perivascular and interstitial fibrosis than WT mice after chronic doxorubicin treatment. Scale bar, 100  $\mu$ m.

Figure 3.5

A.



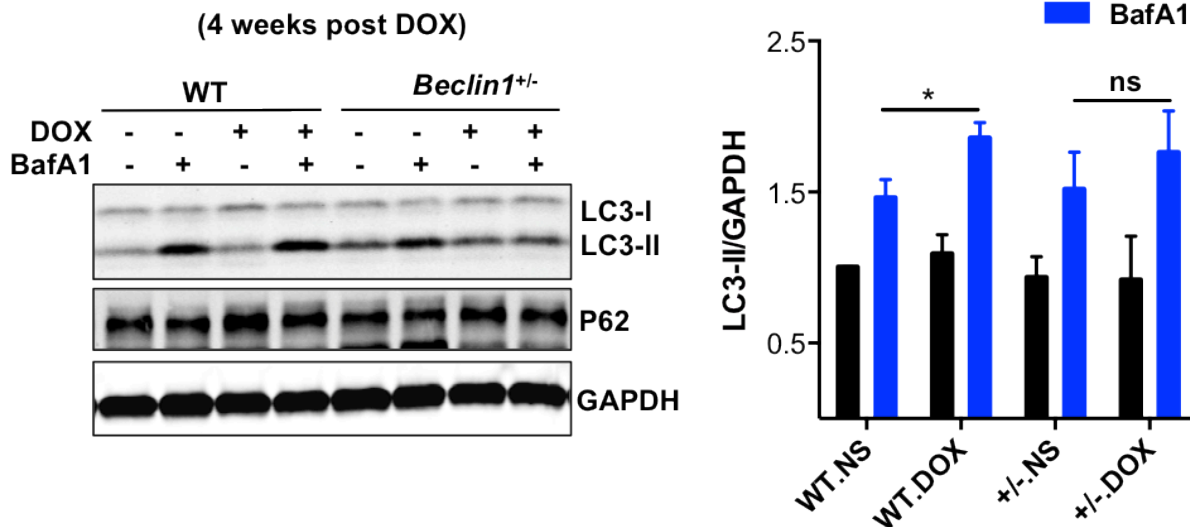
B.



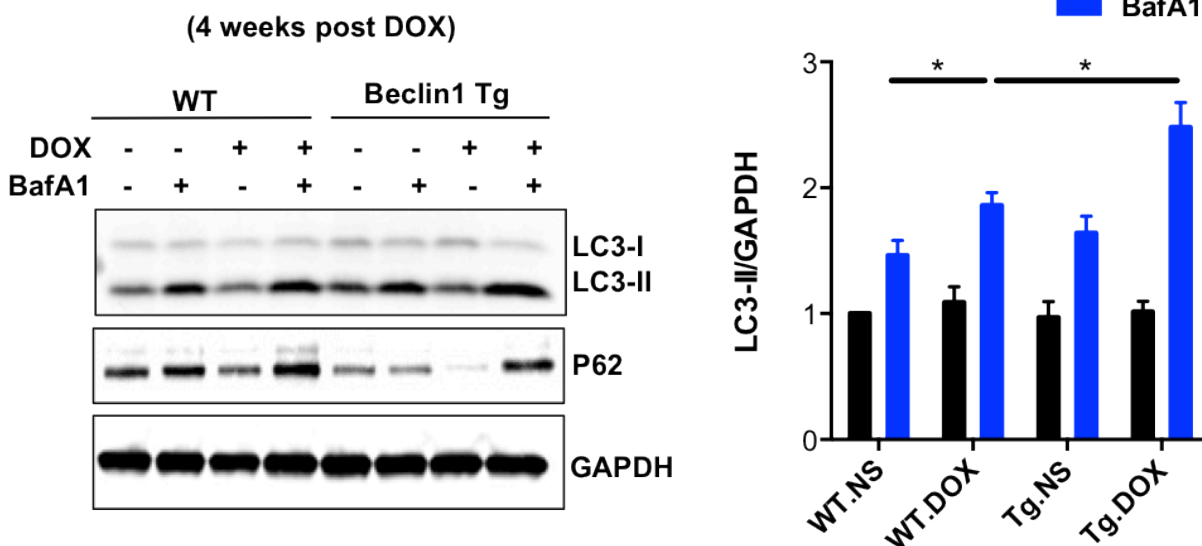
**Figure 3.5. Modulation of autophagic initiation affects cardiac ROS levels elicited by doxorubicin.** (A) Doxorubicin-induced ROS formation (by DHE staining) was decreased in *Beclin 1*<sup>+/-</sup> mice. N = 3 mice per group. (B) Doxorubicin-induced ROS formation (determined by DHE staining of hearts treated with DOX for 20 hours) was decreased in Beclin 1 Tg mice. N = 4 mice per group. Scale bar, 100  $\mu$ m. HPF, high-power field. \*,  $p < 0.05$ ; \*\*,  $p < 0.01$ ; ns, not significant.

## Figure 3.6

A.



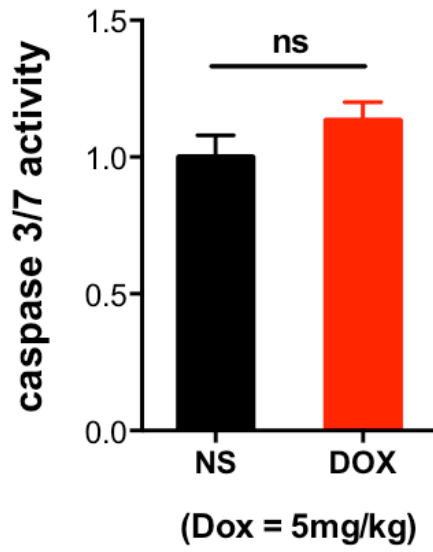
B.



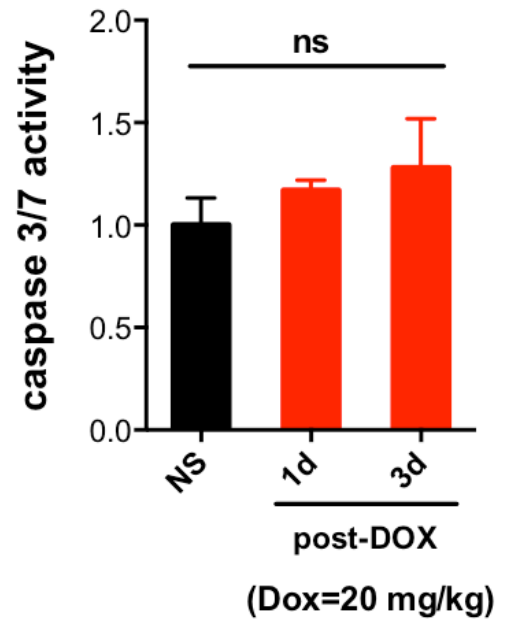
**Figure 3.6. Beclin1 levels modulate cardiac autophagic flux in the remodeling phase of chronic doxorubicin cardiomyopathy.** (A) Cardiac autophagic flux was measured by Western blotting of LC3 and p62 4 weeks after completion of serial doxorubicin treatment. *Beclin1*<sup>+/-</sup> showed a similar autophagic response as WT. N = 4 per group. (C) Cardiac autophagic flux was measured by Western blotting of LC3 and p62 4 weeks after completion of serial doxorubicin treatment. Beclin1 Tg mice showed a higher autophagic flux compared to WT. N = 5 per group. . \*,  $p < 0.05$ ; ns, not significant.

Figure 3.7

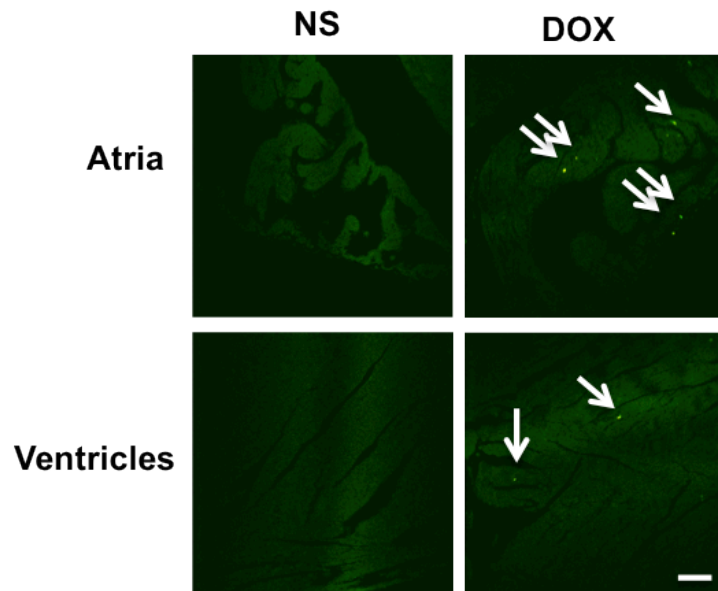
A.



B.



C.





E.

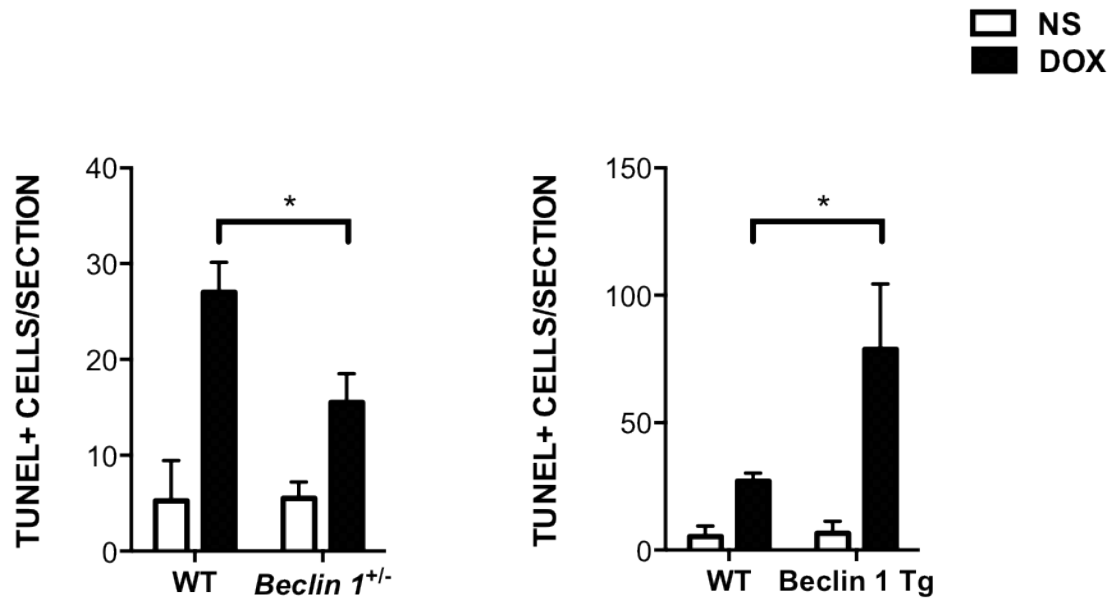


**Figure 3.7. Cardiac apoptotic activity in chronic doxorubicin cardiomyopathy model.** (A) Caspase 3/7 activities were measured in heart lysates from mice 24 hours after 5 mg/kg doxorubicin injection. N = 4 per group. (B) Caspase 3/7 activities were measured in heart lysates from mice 1 day and 3 days after a single 20 mg/kg doxorubicin injection. N = 3 per group. (C) TUNEL positivity was detected in chronic doxorubicin cardiomyopathy model. Heart tissues were harvested 4 weeks after completion of chronic doxorubicin treatments. (D) TUNEL positivity in doxorubicin-treated WT, *Beclin 1*<sup>+/-</sup>, and *Beclin 1* Tg mouse hearts. Quantifications were based on 3-4 animals per group, with 3 different sections per heart. Scale bar, 100  $\mu$ m. \*,  $p < 0.05$ ; ns, not significant.

Figure 3.8

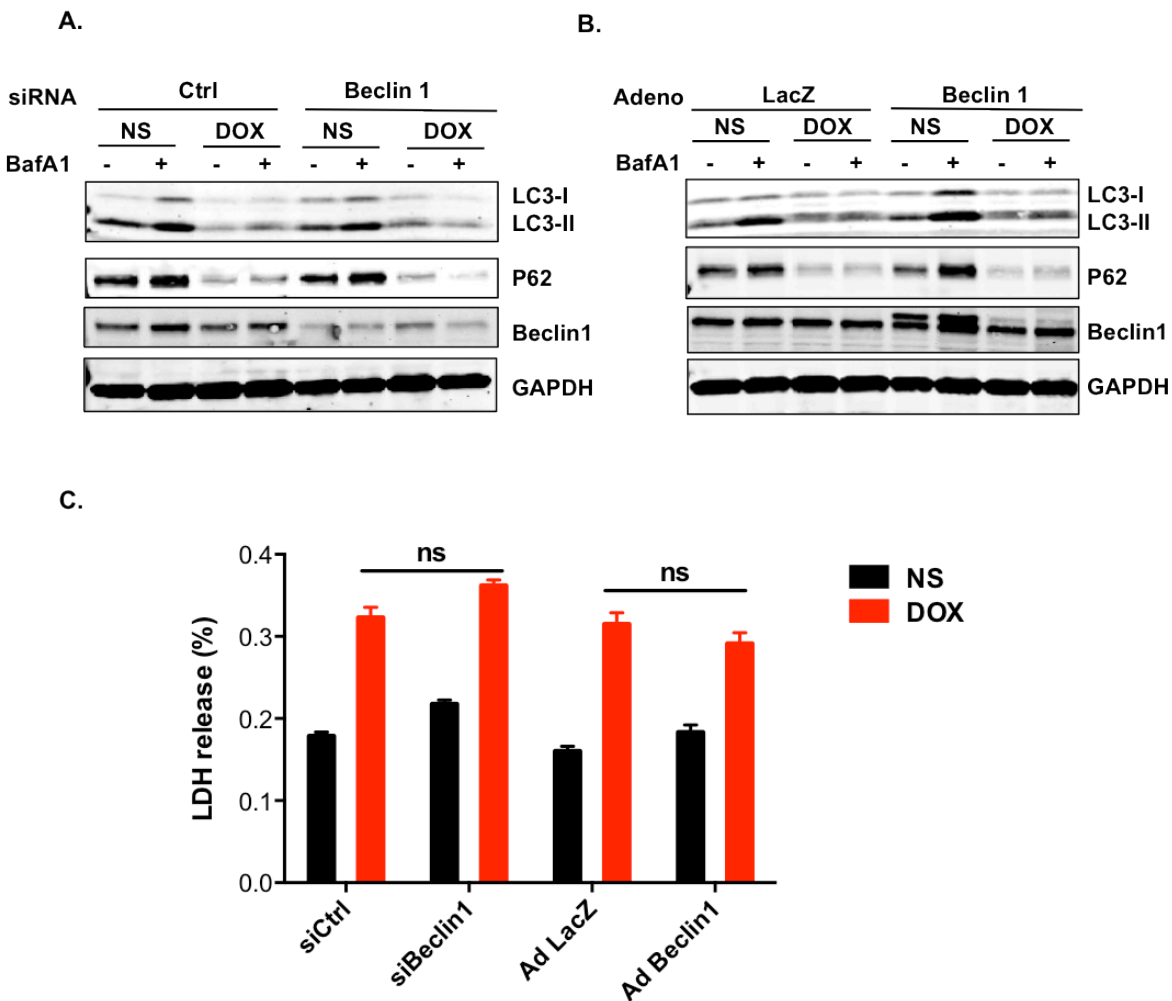


**Figure 3.8. *In vitro* modulations of Beclin1 expression fail to affect doxorubicin-induced cell death.** (A) Knock-down of Beclin1 in NRVMs failed to rescue autophagic inhibition by doxorubicin. (B) Overexpression of Beclin1 in NRVMs did not alter autophagic inhibition by doxorubicin. (C) LDH release measuring cell death revealed that beclin1 protein levels did not affect doxorubicin-induced NRVM death. N = 3. ns, not significant.

**Table 3.1. Echocardiography of WT and *Beclin1*<sup>+/-</sup>**

Genotype	Treatment	LVIDd(mm)	LVIDs(mm)	FS(%)	HR(bpm)
WT	NS	2.658±0.061	1.029±0.052	61.24±2.25	666±16
<i>Beclin1</i> <sup>+/-</sup>	NS	2.706±0.085	1.080±0.073	60.38±1.66	706±12
WT	DOX	2.909±0.037 *	1.413±0.065 *	51.49±2.93 *	675±14
<i>Beclin1</i> <sup>+/-</sup>	DOX	2.698±0.075	1.128±0.067 #	58.31±3.42 #	685±6

\*,  $p < 0.05$  WT-NS group VS WT-DOX group. #,  $p < 0.05$  WT-DOX group VS *Beclin1*<sup>+/-</sup> -DOX group

**Table 3.2. Echocardiography of WT and *Beclin1* Tg**

Genotype	Treatment	LVIDd(mm)	LVIDs(mm)	FS(%)	HR(bpm)
WT	NS	2.666±0.058	1.028±0.026	61.34±2.52	722±9
<i>Beclin1</i> Tg	NS	2.730±0.060	1.037±0.03	62.08±3.44	717±11
WT	DOX	2.836±0.042	1.361±0.068 *	51.78±3.33 *	680±11
<i>Beclin1</i> Tg	DOX	3.134±0.083 #	1.715±0.108 #	44.94±2.83 #	668±9

\*,  $p < 0.05$  WT-NS group VS WT-DOX group. #,  $p < 0.05$  WT-DOX group VS *Beclin1* Tg -DOX group

**Table 3.3. Primers used in the study**

Gene (Mouse)	Sequence
<i>Anf</i>	5-CTTCTTCCTCTTCCTGGCCT-3 5-TTCATCGGTCTGCTCGCTCA-3
<i>Bnp</i>	5-TCCTTAATCTGTCGCCGCTG-3 5-AGGCGCTGTCTTGAGACCTA-3
<i>Col1a1</i>	5-TGGCCAAGAAGACATCCCTGAAGT-3 5-ACATCAGGTTTCCACGTCTCACCA-3
<i>Ctgf</i>	5-GTTGATGAGGCAGGAAGG-3 5-AACTGAATGGAGTCCTAC-3

## METHODS

### ***In vivo* model of chronic doxorubicin cardiomyopathy**

*Beclin 1*<sup>+/-</sup>, αMHC-*Beclin 1* mice and their WT littermates on C57/B6 background were maintained on a 12-hour light/dark cycle from 6AM to 6PM. All protocols were approved by Institutional Animal Care and Use Committee of UT Southwestern Medical Center. Eight to nine-week-old mice were injected via tail vein with doxorubicin (5 mg/kg) or normal saline once weekly for 4 weeks. Ventricular size and function were examined in acclimatized, unanesthetized mice by echocardiography (Vevo 2100, MS400C scanhead) 6 days after each injection and 4 weeks after the final injection.

### **Cell culture**

Neonatal rat ventricular myocytes (NRVMs) were isolated from 1- to 2-day-old Sprague-Dawley rats as previously described (15). NRVMs were maintained in NRVM culture media (DMEM high glucose and Medium 199 in 3:1 ratio) containing 3% fetal bovine serum. On the fourth day after plating, experiments were initiated.

### **Cell survival Measurement**

LDH permeability was measured using the CytoTox 96 Non-Radioactive Cytotoxicity assay kit (Promega) – a measurement of plasma membrane integrity. LDH activity in live cells and in culture media at the end of experiments were measured; the percentages of LDH activity in media over the added amount of LDH activity in media plus attached cells were calculated as percentage of LDH permeability, correlating with cell death.

### **Immunoblot analysis**

Ventricular tissue (10-30 mg) was homogenized in 700 μL T-PER lysis buffer (Thermo) supplemented with protease inhibitors and phospho-STOP (Roche). Lysates were centrifuged at 8,000g (15 min), and the supernatant was used for immunoblotting. For NRVMs, cells were washed once with cold PBS and lysed with T-PER buffer supplemented with protease inhibitors and phospho-STOP. Protein concentration was measured by Bradford assay (Bio-Rad). Protein lysates (10-15 μg) were loaded for electrophoresis and transferred to nitrocellulose membrane. Then, the membrane was processed for immunoblotting and scanning using an Odyssey scanner (LI-COR).

## **RNA isolation and PCR analysis**

Total RNA was isolated from ventricular tissue using the Total RNA Fatty and Fibrous Tissue Kit (Bio-Rad). A total of 300 ng RNA was used for reverse transcription and subsequent real-time qPCR analysis (Roche). All primer sequences are provided (**Table 3.1**).

## **Histology and imaging**

For RFP/GFP analysis, hearts were harvested from anesthetized mice and fixed by overnight immersion in 4% paraformaldehyde/phosphate-buffered saline (PFA/PBS). Following fixation, hearts were sequentially cryoprotected with overnight incubations in 10% and 18% sucrose. Next, hearts were embedded in freezing matrix (TFM, Triangle Bioscience, Durham, NC), and 8  $\mu\text{m}$  frozen sections were prepared on a Leica CM3000 Cryostat (Leica Microsystems, Buffalo Grove IL) and stored at  $-80^{\circ}\text{C}$ . Prior to imaging, slides were thawed and coverslipped with Prolong-Gold antifade mounting medium (Life Technologies). Images were acquired on a Leica Microsystems TCS SP5 confocal microscope.

For TUNEL staining, heart were harvested from anesthetized mice and fixed by overnight immersion in 4% paraformaldehyde/phosphate-buffered saline (PFA/PBS). Next, hearts were embedded in freezing matrix (TFM, Triangle Bioscience, Durham, NC), and 8  $\mu\text{m}$  frozen sections were prepared on a Leica CM3000 Cryostat (Leica Microsystems, Buffalo Grove IL). TUNEL stain was followed on the slides later.

## **Detection of reactive oxygen species (ROS)**

Anesthetized mice were transcordially perfused with ice-cold heparinized PBS. Hearts were dissected from the animals and cryoembedded in TFM. Frozen sections (8  $\mu\text{m}$ ) were prepared from the resulting cryoblocks, and sections were stained with dihydroethidium (DHE, Invitrogen) for 15 minutes followed by sealing with Prolong Gold Antifade Mountant with DAPI. Sections were immediately examined with a Leica DM2000 epifluorescence photomicroscope. Three microscopic fields ( $6.00 \times 10^4 \mu\text{m}^2$ ) were acquired per heart section, and three differing level heart sections per mouse were analyzed.

## Reagents

Doxorubicin was purchased from LC laboratories. Other reagents were purchased as follows: bafilomycin A1 (LC laboratory), siRNA for Beclin 1 are purchased from Sigma-Aldrich. Antibodies: LC3 (previously developed (4)), p62 (Abnova), GAPDH (Fitzgerald Industries).

## Data analysis

All data are reported as mean  $\pm$  standard error of the mean. The Student *t* test (2-tailed) was performed to compare two groups. One-way ANOVA analysis followed by Turkey *post hoc* test was used to compare multiple groups. Two-way ANOVA and subsequent Turkey tests were performed to analyze time course and concentration gradient studies. A *p* value of less than 0.05 was considered significant.

## CHAPTER 3 REFERENCES

1. Nakai, A., Yamaguchi, O., Takeda, T., Higuchi, Y., Hikoso, S., Taniike, M., Omiya, S., Mizote, I., Matsumura, Y., Asahi, M., et al. 2007. The role of autophagy in cardiomyocytes in the basal state and in response to hemodynamic stress. *Nat Med* 13:619-624.
2. Tanaka, Y., Guhde, G., Suter, A., Eskelinen, E.L., Hartmann, D., Lullmann-Rauch, R., Janssen, P.M., Blanz, J., von Figura, K., and Saftig, P. 2000. Accumulation of autophagic vacuoles and cardiomyopathy in LAMP-2-deficient mice. *Nature* 406:902-906.
3. Taneike, M., Yamaguchi, O., Nakai, A., Hikoso, S., Takeda, T., Mizote, I., Oka, T., Tamai, T., Oyabu, J., Murakawa, T., et al. 2010. Inhibition of autophagy in the heart induces age-related cardiomyopathy. *Autophagy* 6:600-606.
4. Zhu, H., Tannous, P., Johnstone, J.L., Kong, Y., Shelton, J.M., Richardson, J.A., Le, V., Levine, B., Rothermel, B.A., and Hill, J.A. 2007. Cardiac autophagy is a maladaptive response to hemodynamic stress. *J Clin Invest* 117:1782-1793.
5. Decker, R.S., Poole, A.R., Crie, J.S., Dingle, J.T., and Wildenthal, K. 1980. Lysosomal alterations in hypoxic and reoxygenated hearts. II. Immunohistochemical and biochemical changes in cathepsin D. *Am J Pathol* 98:445-456.
6. Ma, X., Liu, H., Foyil, S.R., Godar, R.J., Weinheimer, C.J., Hill, J.A., and Diwan, A. 2012. Impaired autophagosome clearance contributes to cardiomyocyte death in ischemia/reperfusion injury. *Circulation* 125:3170-3181.
7. Choi, A.M., Ryter, S.W., and Levine, B. 2013. Autophagy in human health and disease. *N Engl J Med* 368:651-662.
8. He, C., and Levine, B. 2010. The Beclin 1 interactome. *Curr Opin Cell Biol* 22:140-149.
9. Xie, M., Kong, Y., Tan, W., May, H., Battiprolu, P.K., Pedrozo, Z., Wang, Z.V., Morales, C., Luo, X., Cho, G., et al. 2014. Histone deacetylase inhibition blunts ischemia/reperfusion injury by inducing cardiomyocyte autophagy. *Circulation* 129:1139-1151.
10. Yan, L., Vatner, D.E., Kim, S.J., Ge, H., Masurekar, M., Massover, W.H., Yang, G., Matsui, Y., Sadoshima, J., and Vatner, S.F. 2005. Autophagy in chronically ischemic myocardium. *Proc Natl Acad Sci U S A* 102:13807-13812.
11. Matsui, Y., Takagi, H., Qu, X., Abdellatif, M., Sakoda, H., Asano, T., Levine, B., and Sadoshima, J. 2007. Distinct roles of autophagy in the heart during ischemia and reperfusion: roles of AMP-activated protein kinase and Beclin 1 in mediating autophagy. *Circ Res* 100:914-922.
12. Zhang, Y.W., Shi, J., Li, Y.J., and Wei, L. 2009. Cardiomyocyte death in doxorubicin-induced cardiotoxicity. *Arch Immunol Ther Exp (Warsz)* 57:435-445.
13. Shi, J., Zhang, L., Zhang, Y.W., Surma, M., Mark Payne, R., and Wei, L. 2012. Downregulation of doxorubicin-induced myocardial apoptosis accompanies postnatal heart maturation. *Am J Physiol Heart Circ Physiol* 302:H1603-1613.
14. Zhang, J., Clark, J.R., Jr., Herman, E.H., and Ferrans, V.J. 1996. Doxorubicin-induced apoptosis in spontaneously hypertensive rats: differential effects in heart, kidney and intestine, and inhibition by ICRF-187. *J Mol Cell Cardiol* 28:1931-1943.
15. Wang, Z.V., Deng, Y., Gao, N., Pedrozo, Z., Li, D.L., Morales, C.R., Criollo, A., Luo, X., Tan, W., Jiang, N., et al. 2014. Spliced X-box binding protein 1 couples the unfolded protein response to hexosamine biosynthetic pathway. *Cell* 156:1179-1192

## **CHAPTER 4. DISCUSSION**

Despite extensive studies of doxorubicin cardiomyopathy in recent years, the underlying molecular mechanisms remain elusive. Here, my study shows that doxorubicin compromises lysosomal acidification and function, thereby inhibiting autophagic flux in cardiomyocytes. This, in turn, is associated with ROS accumulation and pathological cardiac remodeling. I also provide evidence that diminishing autophagic initiation to limit the accumulation of unprocessed autolysosomes ameliorates doxorubicin cardiotoxicity. Conversely, increasing autophagosome formation without correcting the downstream block exacerbates cardiotoxicity.

### **Mouse model for chronic doxorubicin cardiomyopathy**

An animal model of doxorubicin cardiomyopathy is an essential tool in studying doxorubicin cardiomyopathy and testing potential therapeutics. The mouse model is most commonly employed in the studies reported in the literature because of its feasibility, easy manipulation, and advantages of genetic manipulations. However, a mouse model of chronic doxorubicin cardiomyopathy is challenging because of the difficulties in multiple *i.v.* doxorubicin injections, local toxicity of doxorubicin if applying other routes of administration, and variability of cardiac phenotypes in individual mice, etc. A majority of studies used mice for acute doxorubicin cardiotoxicity models, which often involve one or two large doses of *i.p.* doxorubicin injections. While these studies have certain merits in revealing some molecular mechanisms of doxorubicin cardiotoxicity, they do not necessarily reflect clinical scenarios of chronic doxorubicin cardiotoxicity.

Therefore, I established several criteria in trying to create a mouse model of chronic doxorubicin cardiomyopathy: 1) consistent and repeatable evidence of cardiac function impairment; 2) no non-cardiac lethality; 3) little or no body weight loss and normal food intake.

In my attempt to create a mouse model, I first tried to repeat the acute and chronic doxorubicin models reported in the literature. Here, all models involved *i.p.* administration(s) of doxorubicin. Not only a single large dose of doxorubicin (20 mg/kg, most commonly applied in mouse studies in the literature) caused a mortality of 20-30% within a week of injection (**Figure 2.1F, G**), but even chronic models of multiple smaller doses of doxorubicin caused about 20-30% of mortality during a 2-month of study period (**Figure 2.1F, G**). The dying mice in the acute model often presented with slow heart rate (around 300 *bpm* versus 600 *bpm* in control group) but relatively preserved fractional shortening examined by echocardiography. In chronic *i.p.* models, mice continued to lose weight even after the completion of doxorubicin injections. Furthermore, the mortality rate seemed unrelated to the cumulative dose of doxorubicin exposure (**Figure 2.1F, G, protocol 2 V.S. protocol 3**). These observations raised suspicion that the lethality was not caused by heart failure but rather from non-cardiac reasons. After dissection of the dead/dying mice, I found that doxorubicin *i.p.* injection(s) caused peritoneal injury and bowel obstruction, leading to gastrointestinal complications and non-cardiac death.

In comparison, my new model of chronic doxorubicin cardiomyopathy involves four weekly doxorubicin injections through the tail vein. Monitoring of cardiac function was carried out extensively during and after the completion of four doses of injections. I observed some local injury (swelling, skin sloughing, pigmentation) at the sites of injection in about 30-40% of the doxorubicin-treated mice. The doxorubicin-treated group did not gain weight significantly during the three weeks of injection compared with the normal saline-treated control group. This seems unavoidable given the systemic toxicities of doxorubicin and possibly pain from tail injuries. However, doxorubicin-treated mice started to gain weight similar to controls upon the

completion of doxorubicin treatment. Food intake was also comparable between groups as well. In addition, no mortality was observed. In aggregate, I engineered a mouse model of doxorubicin cardiomyopathy that bypasses the problems in reported *i.p.* administration models while achieving the cardiac phenotype of chronic doxorubicin cardiomyopathy.

### **Doxorubicin's impact on cardiomyocyte autophagic flux**

Autophagy is an evolutionarily conserved biological process that involves delivery of cytosolic materials to lysosomes for degradation (1). Previous studies have addressed the possible contribution of changes in autophagic flux to doxorubicin cardiotoxicity; their findings, however, are conflicting (2, 3). Autophagy has been reported to be either increased (4-8) or decreased (4, 9, 10), based on *in vivo* and/or *in vitro* analyses. We suggest that the discrepancies result from several factors. First, a large proportion of the literature is based on acute, high-dose doxorubicin exposure. As discussed, these models do not accurately reflect the clinical scenario. Further, both high-dose doxorubicin administration and intraperitoneal administration entail a number of comorbidities, including anorexia, weight loss and even non-cardiac death, greatly confounding the analysis of both cardiotoxicity and autophagy. In comparison, I believe that my new model of chronic doxorubicin cardiomyopathy is a more faithful recapitulation of events seen clinically and avoids the numerous confounding comorbidities that plague other studies.

A second reason for the discrepancies is the lack of evaluation of autophagy as a flux cascade. Since autophagy is a dynamic process, a comprehensive evaluation of flux is required, as opposed to a "snapshot in time." Further, evidence reported here and elsewhere (11) indicates that p62, a *bona fide* autophagic target, is affected transcriptionally by stress, including doxorubicin; simply tracking the abundance of this protein is inadequate to query autophagic flux. My findings highlight the need to examine autophagy and flux using a number

of approaches. The addition of BafA1 to these assays and confirmation by examining turnover of long-lived proteins allowed us to uncover and identify the underlying lysosomal dysfunction.

Finally, the time point at which autophagic flux is studied varies across studies. I chose to focus on 24 hours after doxorubicin administration, as events occurring then are more likely to be a direct effect of doxorubicin, rather than a secondary systemic effect. I further confirmed the blockage of autophagic flux persisted even 24 hours after serial injections of doxorubicin. In addition, the evidence that cardiac function declined progressively during injection period, and that the extent of autophagic flux blockage correlated with the level of acute ROS generation, strengthened the model that inhibition of autophagic flux contributes to chronic cardiac injuries caused by doxorubicin.

While LC3-II accumulation was observed after doxorubicin, the level returned to baseline at later stages, weeks after doxorubicin injections. This is likely due to the metabolism and clearance of doxorubicin from the tissues. Therefore, I believe that the accumulation of LC3-II- a marker for autophagic flux inhibition in this case- is a doxorubicin-induced, reversible change. I reason that in the remodeling phase, upregulation of autophagic flux is not a direct response to doxorubicin injury, but rather secondary to pathological remodeling of the heart.

Although the blockage of autophagic flux appears to be transient and reversible, ROS production and cellular damage by doxorubicin can be enhanced by temporary blockage of autophagic flux. Multiple administrations of doxorubicin cause cumulative damages that eventually lead to decompensation and cardiomyopathy. Whether increased autophagic flux in the long-term after doxorubicin injections contributes to progression of cardiac dysfunction is not clear and warrants further investigation.

I found that in both *in vitro* and *in vivo* doxorubicin cardiotoxicity models, cardiomyocyte autophagic flux was inhibited, albeit differences exist between the two models. Accumulation of LC3-II by Western blotting was observed in doxorubicin-treated hearts, while in

NRVMs there was no increase in steady state LC3-II levels upon doxorubicin treatment. It raises the possibility that doxorubicin impairs the autophagic initiation machinery *in vitro* as well, which seems not the case in our *in vivo* study. The *in vivo* system could be affected by a host of other factors: secondary products of doxorubicin due to metabolism, fluctuation of tissue doxorubicin concentration, circulatory factors, neurohormonal and paracrine regulation, etc. However, the common features between *in vivo* and *in vitro* system- the blockage of autophagic flux and accumulation of autolysosomes – strongly suggest that doxorubicin blocks autolysosomal digestion in cardiomyocytes.

### **Impaired lysosome function by doxorubicin**

An early clue to localize the point of autophagic cascade impairment derived from the imaging studies, which revealed robust accumulation of autolysosomes. I went on to reveal that doxorubicin inhibits lysosomal acidification and suppresses lysosome function.

Early literature reported lysosomal changes in cardiomyocytes, both in numbers and morphology, induced by doxorubicin (12-14). In fact, lysosomal changes seem to appear early in response to doxorubicin treatment (14). Singal et al (14) measured activities of various lysosomal enzymes in rat heart lysates and found changes- either increased or decreased- after chronic doxorubicin treatment. However, the significance was less clear since the changes were bidirectional. In addition, It is reported that doxorubicin also increases lysosomal membrane leakage (15), although the changes seemed to be modest. Using live cell recording of fluorescent products resulting from cathepsin digestion, I was able to track the activities of two common lysosomal enzymes -cathepsin B and cathepsin L- in live cells. I found that both enzyme activities were downregulated by doxorubicin; however, enzymes isolated from cardiomyocytes treated with doxorubicin did not show significant defects in activities, suggesting that the lysosomal environment is a critical reason for doxorubicin-induced impairment of

enzyme activities. Further, my data, for the first time show that doxorubicin perturbs lysosomal function via inhibition of its luminal acidity.

Lysosomes are subcellular compartments that contain a plethora of hydrolases for degradation of proteins, lipids, and polysaccharides, within a low pH environment. The acidic luminal environment of lysosomes (pH 4-5) is of critical importance for the activities of most hydrolytic enzymes (16), as well as movement and maturation of lysosomes (17). I found that doxorubicin increases lysosomal pH from a basal level of pH 4.6 to pH 5.2. Given the sensitivity of lysosomal hydrolases to luminal pH, my data implicates a defect in lysosomal acidification that inhibits lysosomal enzyme activities.

Interestingly, autolysosomal accumulation has also been reported as a dramatic feature in neurons from Alzheimer's disease patients (18). Mutations of Alzheimer's disease-linked genes presenilin 1 (19) and ApoE4 (20) have been shown to affect lysosomal acidification and lysosomal membrane stabilization, respectively. Other factors such as oxidative stress (21) and amyloid accumulations (22) could also impair lysosomal acidification (21) and lysosomal proteolysis (22), leading to accumulation of undigested autolysosomes.

It has been reported in some cell types that an increase in lysosomal pH can impair the fusion of lysosomes with autophagosomes (23, 24). By contrast, I observed an increase in autolysosome number by doxorubicin. However, it remains controversial whether inhibition of autophagosome-lysosome fusion is solely dependent on increases in lysosomal pH. Events such as calcium release from the lysosome have been suggested to be required for autophagosome-lysosome fusion (25). It is also possible that the autophagosome-lysosome fusion event is inhibited only when lysosomal pH elevates to a certain level. Lastly, when examining autophagic flux by tandem fluorescent LC3, green fluorescence from GFP cannot be quenched when the lysosome pH exceeds 6. Therefore in some occasions, the accumulation of "autophagosomes" observed might actually be autolysosomes without an optimal luminal pH.

### **Lysosome V-ATPase and regulation of lysosomal pH**

Lysosomal acidification is dependent on the activity of the V-ATPase. To analyze V-ATPase-induced lysosomal acidification, lysosomes can be transiently alkalinized by  $\text{NH}_4\text{Cl}$  or FCCP (26, 27). However, lysosomes in NRVMs are relatively resistant to the protonophore FCCP (1  $\mu\text{M}$ ); protons dissipate more slowly than reported in other cell lines. In contrast,  $\text{NH}_4\text{Cl}$  induces rapid alkalization in NRVMs. Therefore, I used  $\text{NH}_4\text{Cl}$  for evaluating the lysosomal re-acidification process. My data strongly suggest that doxorubicin acts by inhibiting V-ATPase activity. However, other possibilities exist, such as alterations in counter ion exchanger activities, or increased lysosomal permeability to protons due to membrane lipid peroxidation.

Fourteen subunits are assembled into an ATP-hydrolytic domain (V1) and a proton-translocation domain (V0). Energy from ATP hydrolysis within the V1 sector is used to transport protons into the lysosomal lumen through the V0 sector. Abolishing the activity of the V-ATPase, by either deleting the subunit or inhibiting its activity, impairs lysosome acidification, and lysosomal pH rises as a consequence (28).

Mechanisms underlying doxorubicin-dependent inhibition of lysosome V-ATPase activity are presently unknown. Evidence collected to date suggests that doxorubicin affects V-ATPase activity through inhibiting the coupling of its two domains, V0 and V1. Yeast homologues of ATP6V0d and ATP6V0a have been shown to regulate the coupling of V0 and V1 activities (29, 30). The two subunits reside at the peripheral and central stalks of the pump respectively, connecting V1 to V0 domain. The ATP6V0a subunit is critical in regulating both the assembly and coupling of the two domains (29); by contrast, mutation in *vma6*, *Atp6v0d*'s homologue in yeast, results in compromised proton transport but not ATPase activity (30). I did

not detect a change in protein levels of the V0d subunit following doxorubicin treatment, however. Of note, the V0d subunit is the only protein in the V0 domain localized to the membrane periphery and hence prone to possible modification by doxorubicin, either directly or secondarily by ROS.

A study by Kim et al showed that a defect in V-ATPase assembly in cardiomyocyte caused an impairment in lysosomal acidification, hypertrophic cardiomyopathy and heart failure (31), highlighting the importance of V-ATPase in cardiomyocyte physiology. We believe that in our model, it is unlikely that doxorubicin targets cardiomyocyte V-ATPase specifically, as opposed to lysosome proton pumps in other cells. Rather, as cardiomyocytes are among the cells most highly dependent on high throughput autophagic flux (32), we suggest that these cells are uniquely susceptible to perturbations in downstream lysosomal processing events.

### **Impaired autophagy in doxorubicin cardiomyopathy**

Blockage of autophagic flux in the heart has been suggested to play an important role in chloroquine-induced cardiomyopathy in patients (33). Here, I demonstrate that doxorubicin inhibits cardiomyocyte autophagic flux by altering lysosomal function. As there is no effective means presently available to modify lysosomal function in order to rescue doxorubicin cardiotoxicity, I decided to modify autophagic flux at the stage of cascade initiation. I employed both gain- and loss-of-function models of Beclin 1 activity to alter the rate at which autophagosomes are delivered to the lysosome.

Previous studies reported disparate conclusions regarding whether autophagy is beneficial or detrimental in doxorubicin cardiotoxicity. Lu et al (8) reported that 3-MA treatment preserved cardiac function after exposure to high-dose doxorubicin. On the other hand, several studies (9, 10) reported that increasing autophagy in mice by either rapamycin or pre-fasting

blunts doxorubicin-induced cardiac dysfunction. However, both starvation and small molecules, such as 3-MA and rapamycin, have a wide range of other targets as well, especially in animals (34). In contrast, modulating Beclin 1 expression in cardiomyocytes is a more specific means of manipulating autophagy.

I observed that *Beclin 1*<sup>+/-</sup> mice were able to restore autophagic flux after doxorubicin treatment; meanwhile, ROS production caused by doxorubicin was significantly reduced. After chronic doxorubicin treatment, these mice manifested preserved cardiac function, blunted fetal gene reactivation and reduced fibrosis formation. On the other hand, cardiomyocyte-specific Beclin 1 transgenic mice presented with an increase of autolysosome accumulation in heart after doxorubicin treatment, correlating with increased levels of ROS production and exacerbated cardiac function chronically. This suggests that it is the levels of Beclin 1 protein in cardiomyocytes that are mediating the different responses to doxorubicin. It is not known why a further accumulation of LC3-II was not observed in Beclin 1 transgenic mice. In retrospect, I did not observe a further accumulation of LC3-II in the hearts of mice after starvation upon doxorubicin injection. One possibility might be that more severe blockage of downstream autophagic machinery leads to feedback inhibition of autophagy initiation in starved WT or Beclin 1 transgenic mice.

The ability of decreased Beclin 1 activity to rescue autophagic flux (and conversely increased Beclin 1 to exacerbate flux) may be due to the decreased (increased) demand on lysosomal processing. While lysosomal proteolytic function is blunted by doxorubicin, it is not completely abolished. One possibility is that the decreased demand allows for the proper processing of lysosomal content. An alternative explanation is that the block I observed is at the point of lysosome recycling. Inhibition of lysosomal recycling results in a similar accumulation of dysfunctional autophagosomes, as lysosomal maturation to a stage at which hydrolases can be

retrieved and reused is blocked (35). Regardless, my data show that the extent of autophagic flux perturbation correlated with the level of doxorubicin-induced cardiac dysfunction.

Aside from its essential role in autophagy, Beclin 1 may have other unknown functions. Studies have shown that Beclin 1 interacts with a variety of proteins, including Bcl-2 family members. It is a matter of controversy whether Beclin1 promotes or suppresses apoptosis. Maejima et al. (36) argued that Beclin 1, by sequestering Bcl-2 and Bcl-xL, could release pro-apoptotic protein Bax and stimulate apoptosis. However, on the other hand, the Ciechomska (37) group showed that Beclin 1-Bcl-2 interaction neither impaired the anti-apoptotic function of Bcl-2, nor modified apoptotic levels under apoptotic stimuli. Since doxorubicin has been reported to cause cardiomyocyte apoptosis, I examined apoptotic activities in doxorubicin-treated heart. Unchanged caspase activity and negative TUNEL staining shortly (24 hour) after doxorubicin treatment suggest the low possibility of doxorubicin's direct pro-apoptotic effect in cardiomyocytes. Mild increase of TUNEL positivity was detected in the remodeling phase (4 weeks after completion of serial doxorubicin injections); however, under higher magnification, the positivity did not localize to myocytes. Albeit *Beclin 1<sup>+/-</sup>* mice showed reduced levels of TUNEL positivity and Beclin 1 transgenic mice manifested a higher level of TUNEL positivity, the differences appeared unlikely due to Beclin 1-dependent changes in doxorubicin-induced apoptosis in cardiomyocytes.

While cardiomyocyte Beclin 1 protein levels modulated the autophagic response to doxorubicin and modified doxorubicin-induced cardiac injury, this was not seen *in vitro*. This discrepancy might derive from the differences in *in vitro* and *in vivo* systems regarding the possible effect of doxorubicin on autophagic initiation, as discussed above. Moreover, an *in vitro* system is ideal for studying direct cellular responses to doxorubicin in a short time frame. Cytotoxicity caused by doxorubicin in NRVMs is not necessarily translated to *in vivo* doxorubicin

cardiotoxicity. In fact, animal models remain a more ideal tool in studying drug cardiotoxicity and potential protective therapies against cardiotoxicity (38, 39).

### **Autophagy, ROS and doxorubicin cardiomyopathy**

Despite controversies, excessive production of ROS remains widely accepted as key factor contributing to doxorubicin cardiotoxicity (40). The potential sites of ROS generation by doxorubicin include mitochondria, sarcoplasmic reticulum, and cytoplasmic compartments (41). On the other hand, the abundance and activity of anti-oxidant enzymes SOD and catalase in heart are much lower than other organs (42). Therefore, high autophagy levels in heart might serve as an important defense mechanism against doxorubicin-induced ROS (32, 43). My findings suggest that doxorubicin impairs cardiomyocyte autophagy, thereby compromising the defense system against ROS-induced cell injury.

At this time, the mechanism underlying correlation between autolysosomal accumulation and ROS is unclear. The source of ROS might be the defective autolysosomes or from dysfunctional mitochondria not effectively degraded by autophagy. Damaged mitochondria are a major source for ROS production in cardiomyocytes (44). At the same time, it has been suggested that lysosomal dysfunction and substrate accumulation also promote ROS production (45, 46). Intriguingly, whereas persistently high levels of intracellular ROS trigger cellular damage, it can also induce autophagosome formation (43), potentially initiating a vicious cycle that promotes cell injury and cardiac dysfunction.

### ***Future directions in autophagic flux inhibition and doxorubicin cardiomyopathy***

Mitochondrial injury is a prominent feature of chronic doxorubicin cardiomyopathy in animal studies. Defects in mitophagy could potentially lead to accumulation of damaged

mitochondria, which are major sources of ROS production. Indeed, the severity of mitochondrial damage correlates with decline of cardiac function (12, 47). Mitochondrial oxidative phosphorylation appears to be compromised by doxorubicin (47, 48). Incubation of doxorubicin with isolated mitochondria *in vitro* resulted in increased state 4 respiration (basal respiration) but inhibition of state 3 (ADP-stimulated) respiration (47). Mitochondria isolated from large-dose doxorubicin-treated mice showed significantly decreased respiration (48). In my *in vivo* chronic doxorubicin cardiomyopathy model, swollen mitochondria were commonly observed (**Figure 4.1A**), consistent with previous findings (47). In cultured NRVMs, doxorubicin treatment (18 hours) caused mitochondrial morphological changes: fragmentation and/or mitochondrial fission (**Figure 4.1B**). To further examine functional changes in mitochondria, tetramethylrhodamine, methyl ester (TMRM) was used to measure mitochondrial membrane potential. It is a cell-permeable, cationic, fluorescent dye that is sequestered by active mitochondria. By contrast, mitotracker green marks all the mitochondria within the cell regardless of mitochondrial membrane potential. Using these two dyes, I found that doxorubicin reduced mitochondrial membrane potential but did not affect total mitochondrial volume in NRVMs (**Figure 4.1C**). However, manipulation of Beclin 1 levels in NRVMs did not affect mitochondrial membrane potential with or without doxorubicin treatment (data not shown). Still, I am interested whether modulation of autophagy *in vivo* by Beclin 1 expression levels will affect mitochondrial function in the chronic doxorubicin cardiomyopathy model. Assessment of mitochondrial injury by doxorubicin can be achieved through morphological studies of mitochondria after chronic doxorubicin treatment, and through functional tests - respiration rate in mitochondria isolated from doxorubicin-treated mice.

My second future interest lies in exploring potential strategies to rescue autophagic flux in cardiomyocytes in an attempt to protect against doxorubicin cardiotoxicity. One possibility is to reduce the initiation of autophagy. One commonly used pharmacological inhibitor of autophagic initiation is 3-methyladenine (3-MA). As an inhibitor of PI3K, 3-MA suppresses

phagophore nucleation. One study (8) demonstrated the protective effect of 3-MA in a rat model of acute doxorubicin cardiotoxicity. However, 3-MA has other off-target actions such as effects on stress kinases and mPTP, which might affect the cellular response to doxorubicin. Therefore, exploring other more specific small molecular inhibitors of autophagic initiation is warranted.

Another possibility is to rescue lysosomal acidification and function. Transcription factor EB (TFEB) has been shown to drive the expression of multiple lysosomal genes and autophagic genes, therefore promoting lysosomal biogenesis and autophagic flux (49). My preliminary data showed that TFEB overexpression in cultured NRVMs rescued doxorubicin-induced suppression of lysosomal acidification, as assessed by lysosensor fluorescence (DND-189, **Figure 4.2A**). However, overexpression of TFEB failed to rescue the blockage of autophagic flux by doxorubicin in NRVMs (**Figure 4.2B**). Despite this, overexpression of TFEB still partially rescued mitochondrial dysfunction elicited by doxorubicin *in vitro*, shown as partial recovery of mitochondrial membrane potential (**Figure 4.2C**). These findings suggest several possibilities: 1) TFEB ameliorates the toxicity of doxorubicin in cardiomyocytes independent of autophagic flux. 2) LC3/p62 immunoblotting might not be sufficient to conclude the inhibition of autophagic flux in this case. 3) TFEB might affect selective autophagy such as mitophagy but not necessarily general autophagy in cardiomyocytes treated with doxorubicin. Future studies should test the role of autophagy/mitophagy in TFEB's mitochondrial protective effect against doxorubicin in NRVMs.

In addition, in collaboration with the Diwan lab (Washington University School of Medicine), we tested whether cardiomyocyte-specific overexpression of TFEB could rescue doxorubicin cardiotoxicity *in vivo*. The inducible TFEB transgenic mice were generated via Tet-Off system. The binding of Tetracycline transactivator (tTA) protein to a tetracycline response element (TRE) drives expression of the downstream gene *Tfeb*; in the presence of tetracycline or its derivative doxycycline, however, the binding of tTA and TRE is disrupted and TFEB overexpression is suppressed (**Figure 4.3A**). To turn on TFEB expression, doxycycline-

containing water was replaced by normal water at 8 weeks of age. Five days later, weekly doxorubicin delivery (5 mg/kg) started. Hearts were harvested one day after the fourth injection, following echocardiography. TFEB transgenic (TFEB Tg) mice showed robust TFEB overexpression in heart. However, TFEB Tg mice treated with doxorubicin presented with lower TFEB protein levels than normal saline-treated group (**Figure 4.3B**). Further study revealed the suppression of TFEB by doxorubicin in TFEB Tg mice was due to the inhibition of external TFEB gene transcription, while endogenous TFEB expression was not affected by doxorubicin (**Figure 4.3C**). Another hurdle I had in this *in vivo* study is that TFEB transgenic mice developed congestive heart failure within a month after doxycycline withdrawal (**Figure 4.3D**). Paradoxically, TFEB Tg mice treated with doxorubicin presented with better systolic function compared with TFEB Tg mice treated with NS (**Figure 4.3D**). This phenotype difference might be due to the suppression of TFEB overexpression in the doxorubicin-treated group. The cardiac phenotype observed in TFEB Tg mice may stem from excessive TFEB overexpression in the mouse line. I am currently working on generating an inducible cardiomyocyte-specific TFEB transgenic mouse line that harbors lower levels of TFEB expression. Whether modest overexpression of TFEB could affect doxorubicin cardiotoxicity *in vivo* remains to be studied in the future.

## Conclusion

In summary, here I have established a model that recapitulates the clinical reality of doxorubicin cardiomyopathy. With this model, I have revealed a novel mechanism of doxorubicin cardiotoxicity, *viz.* relative lysosome alkalinization and consequent inhibition of downstream autophagic flux. By titrating down the initiation of autophagosome initiation, doxorubicin cardiotoxicity is blunted, while by contrast, enhancing autophagic initiation aggravates doxorubicin cardiotoxicity (**Figure 4.4**). Together, these data uncover a novel

mechanism of disease pathogenesis and point to a unique strategy of limiting heart injury. Future studies of more bedside-translatable approaches to reverse cardiomyocyte autophagic flux by doxorubicin might shed light on preventing doxorubicin cardiomyopathy.

## Figure 4.1

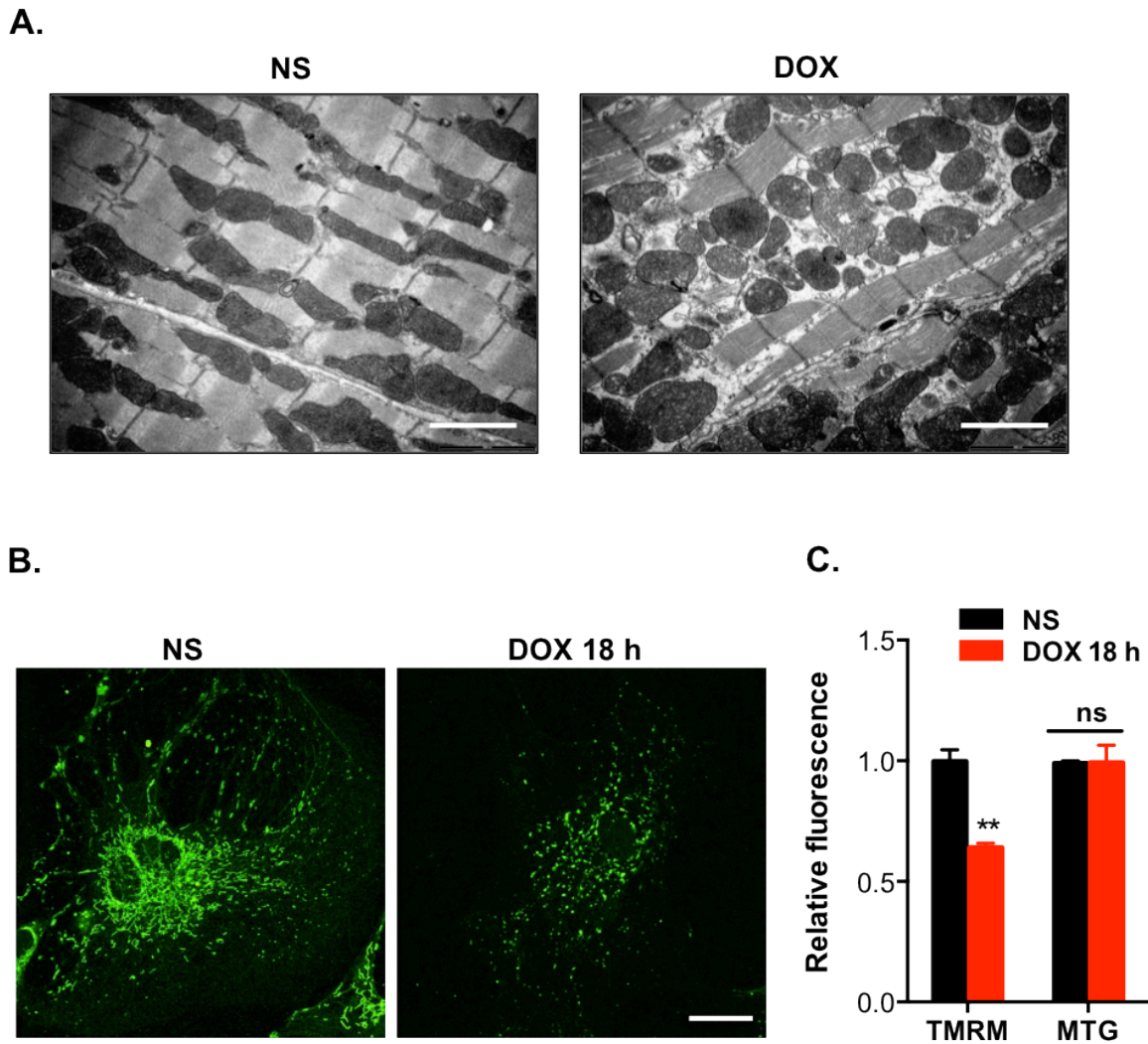


**Figure 4.1. Doxorubicin-elicited mitochondrial changes in heart and NRVMs (A)** Representative transmission electron microscopy images of hearts one day after serial doxorubicin injections. Scale bars, 2 $\mu$ m. **(B)** Representative immunofluorescence staining of mitochondria using anti-mitochondrial heat shock protein 70. Scale bars, 10 $\mu$ m. **(C)** Measurement of mitochondrial membrane potential (TMRM) and mitochondrial total volume (MTG) in NRVMs treated with NS or doxorubicin. TMRM, tetramethylrhodamine, methylester. MTG, mitotracker green. N = 5. \*\*, p < 0.01; ns, not significant.

## Figure 4.2

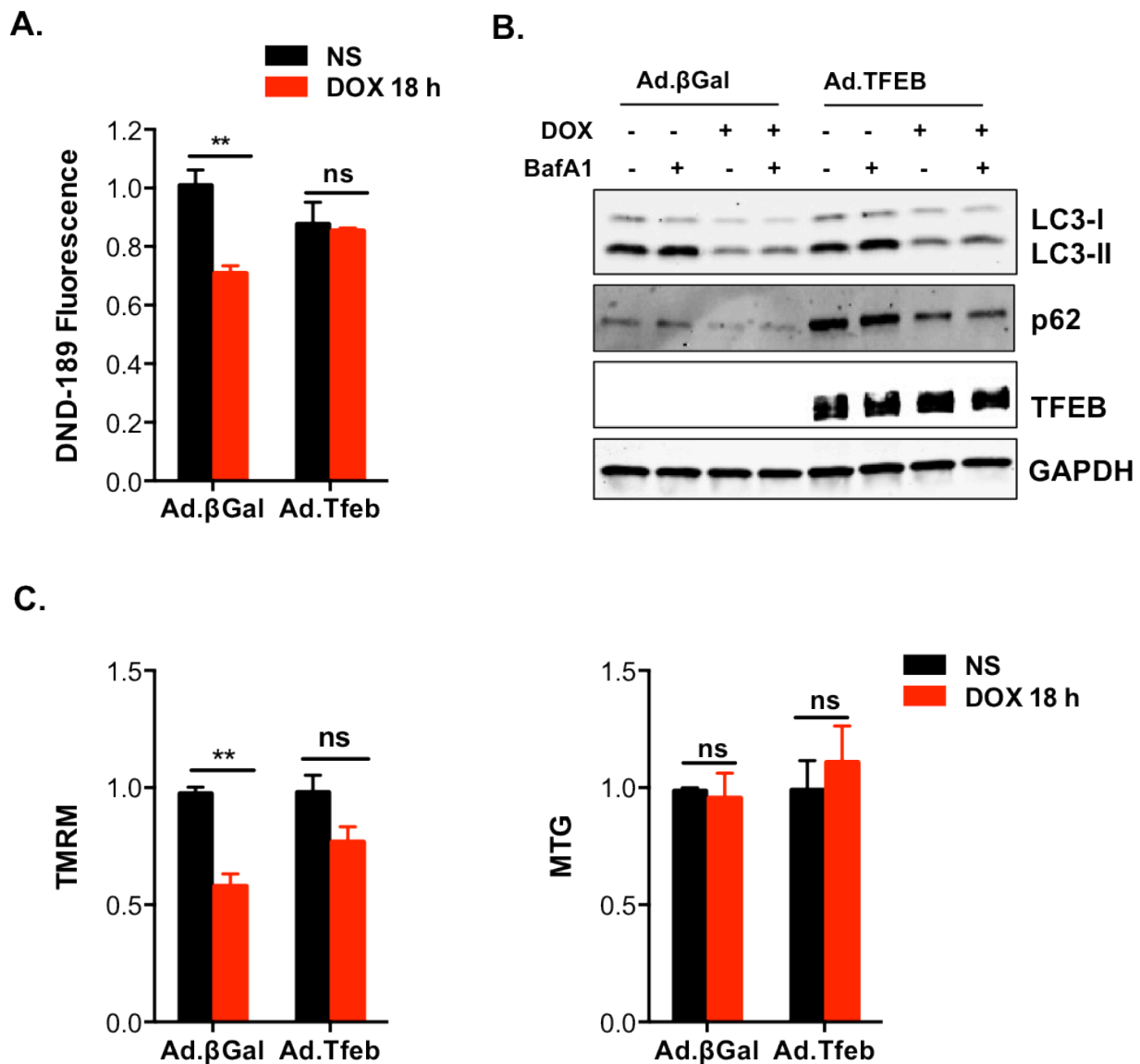


**Figure 4.2. The potential protective effect of TFEB in doxorubicin cardiotoxicity *in vitro*.** (A) Overexpression of TFEB rescues doxorubicin-induced decrease in lysosomal acidity. Measurement of lysosensor (DND-189) fluorescence via flow cytometry was used to indirectly measure lysosomal acidity. N = 4. (B) Western blot showing overexpression of TFEB does not rescue the blockage of autophagic flux in NRVMs. NRVMs were treated with doxorubicin for 18 hours. (C) Measurement of mitochondrial membrane potential (TMRM) and mitochondrial total volume (MTG) in NRVMs treated with NS or doxorubicin. Overexpression of TFEB partially rescues the decrease of mitochondrial membrane potential by doxorubicin. N = 5. Ad. βGal, adenovirus harboring CMV-βGal; Ad.Tfeb, adenovirus for overexpressing TFEB. \*\*,  $p < 0.01$ ; ns, not significant.

## Figure 4.3

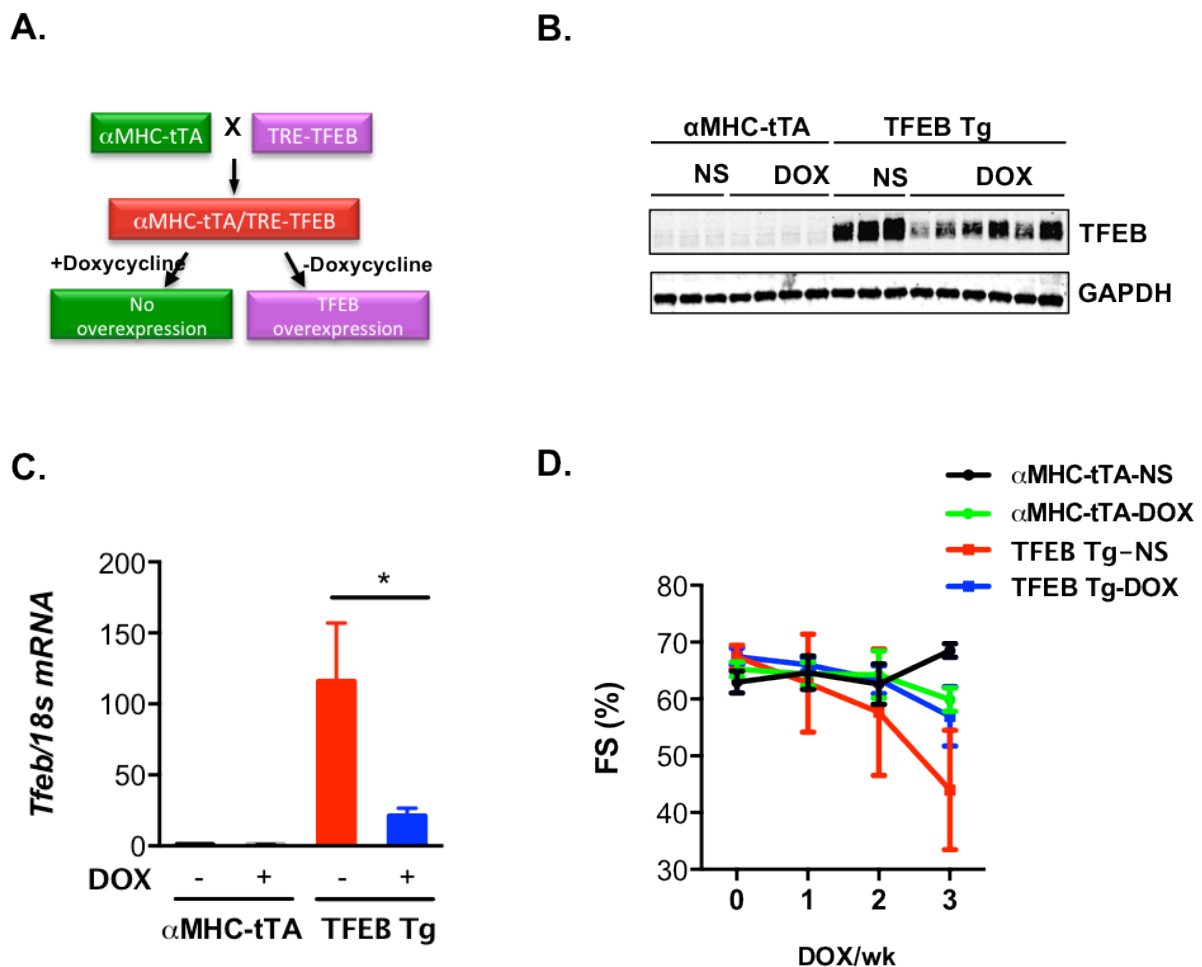


**Figure 4.3. Cardiomyocyte-specific TFEB transgenic mice develop heart failure.** (A) Inducible overexpression of TFEB in cardiomyocytes *in vivo*. Doxycycline suppresses TFEB expression. (B) Western blot showing overexpression of TFEB in αMHC-tTA/TRE-TFEB (TFEB Tg) mouse heart 4 weeks after replacing doxycycline-contained water to normal water. Five days after doxycycline withdrawal, four weekly doses of doxorubicin (5 mg/kg) were administered and hearts were harvested 24 hours after the last injection. Doxorubicin suppressed TFEB expression in TFEB Tg mice. (C) Doxorubicin suppresses TFEB transcription in TFEB Tg mice. TFEB mRNA levels were examined 24 hours after the 4<sup>th</sup> injection of doxorubicin. N = 3-6. (D) TFEB Tg mice develop heart failure after doxycycline withdrawal. Echocardiography was performed 1 day after the fourth doxorubicin injection. tTA, tetracycline controlled transcription activator. TRE, Tet-responsive element. FS, Fractional Shortening. \*,  $p < 0.05$ .

**Figure 4.4**

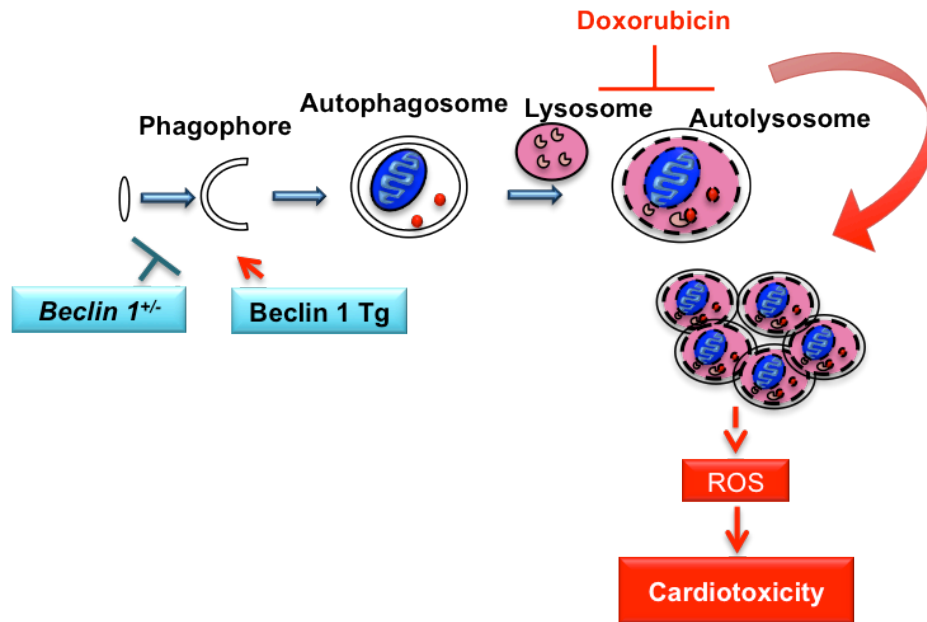


**Figure 4.4. Working Model.** Doxorubicin, by inhibiting lysosomal acidification and lysosomal function, blocks cardiomyocyte autophagic flux. Accumulation of autolysosomes leads to increased ROS production and cardiac injury. Slowing down autophagy initiation process by decreasing Beclin 1 partially rescues the autophagic flux blockage and protects heart from cardiotoxicity; while increasing autophagosome formation exacerbates autophagic flux inhibition and increases doxorubicin cardiotoxicity.

## CHAPTER 4 REFERENCES

1. Choi, A.M., Ryter, S.W., and Levine, B. 2013. Autophagy in human health and disease. *N Engl J Med* 368:651-662.
2. Li, D.L., and Hill, J.A. 2014. Cardiomyocyte autophagy and cancer chemotherapy. *J Mol Cell Cardiol* 71:54-61.
3. Dirks-Naylor, A.J. 2013. The role of autophagy in doxorubicin-induced cardiotoxicity. *Life Sci* 93:913-916.
4. Ding, Y., Sun, X., Huang, W., Hoage, T., Redfield, M., Kushwaha, S., Sivasubbu, S., Lin, X., Ekker, S., and Xu, X. 2011. Haploinsufficiency of target of rapamycin attenuates cardiomyopathies in adult zebrafish. *Circ Res* 109:658-669.
5. Kobayashi, S., Volden, P., Timm, D., Mao, K., Xu, X., and Liang, Q. 2010. Transcription factor GATA4 inhibits doxorubicin-induced autophagy and cardiomyocyte death. *J Biol Chem* 285:793-804.
6. Dimitrakis, P., Romay-Ogando, M.I., Timolati, F., Suter, T.M., and Zuppinger, C. 2012. Effects of doxorubicin cancer therapy on autophagy and the ubiquitin-proteasome system in long-term cultured adult rat cardiomyocytes. *Cell Tissue Res* 350:361-372.
7. Zhang, Y., Kang, Y.M., Tian, C., Zeng, Y., Jia, L.X., Ma, X., Du, J., and Li, H.H. 2011. Overexpression of Nr1h3 in the heart exacerbates doxorubicin-induced cardiac dysfunction in mice. *PLoS One* 6:e21104.
8. Lu, L., Wu, W., Yan, J., Li, X., Yu, H., and Yu, X. 2009. Adriamycin-induced autophagic cardiomyocyte death plays a pathogenic role in a rat model of heart failure. *Int J Cardiol* 134:82-90.
9. Kawaguchi, T., Takemura, G., Kanamori, H., Takeyama, T., Watanabe, T., Morishita, K., Ogino, A., Tsujimoto, A., Goto, K., Maruyama, R., et al. 2012. Prior starvation mitigates acute doxorubicin cardiotoxicity through restoration of autophagy in affected cardiomyocytes. *Cardiovasc Res* 96:456-465.
10. Sishi, B.J., Loos, B., van Rooyen, J., and Engelbrecht, A.M. 2013. Autophagy upregulation promotes survival and attenuates doxorubicin-induced cardiotoxicity. *Biochem Pharmacol* 85:124-134.
11. Jain, A., Lamark, T., Sjøttem, E., Larsen, K.B., Awuh, J.A., Overvatn, A., McMahon, M., Hayes, J.D., and Johansen, T. 2010. p62/SQSTM1 is a target gene for transcription factor NRF2 and creates a positive feedback loop by inducing antioxidant response element-driven gene transcription. *J Biol Chem* 285:22576-22591.
12. Singal, P.K., Deally, C.M., and Weinberg, L.E. 1987. Subcellular effects of adriamycin in the heart: a concise review. *J Mol Cell Cardiol* 19:817-828.
13. Solcia, E., Ballerini, L., Bellini, O., Magrini, U., Bertazzoli, C., Tosana, G., Sala, L., Balconi, F., and Rallo, F. 1981. Cardiomyopathy of doxorubicin in experimental animals, Factors affecting the severity, distribution and evolution of myocardial lesions. *Tumori* 67:461-472.
14. Singal, P.K., Segstro, R.J., Singh, R.P., and Kutryk, M.J. 1985. Changes in lysosomal morphology and enzyme activities during the development of adriamycin-induced cardiomyopathy. *Can J Cardiol* 1:139-147.
15. Gebbia, N., Leto, G., Gagliano, M., Tumminello, F.M., and Rausa, L. 1985. Lysosomal alterations in heart and liver of mice treated with doxorubicin. *Cancer Chemother Pharmacol* 15:26-30.

16. Pillay, C.S., Elliott, E., and Dennison, C. 2002. Endolysosomal proteolysis and its regulation. *Biochem J* 363:417-429.
17. Sun-Wada, G.H., Wada, Y., and Futai, M. 2003. Lysosome and lysosome-related organelles responsible for specialized functions in higher organisms, with special emphasis on vacuolar-type proton ATPase. *Cell Struct Funct* 28:455-463.
18. Nixon, R.A., Wegiel, J., Kumar, A., Yu, W.H., Peterhoff, C., Cataldo, A., and Cuervo, A.M. 2005. Extensive involvement of autophagy in Alzheimer disease: an immunoelectron microscopy study. *J Neuropathol Exp Neurol* 64:113-122.
19. Lee, J.H., Yu, W.H., Kumar, A., Lee, S., Mohan, P.S., Peterhoff, C.M., Wolfe, D.M., Martinez-Vicente, M., Massey, A.C., Sovak, G., et al. 2010. Lysosomal proteolysis and autophagy require presenilin 1 and are disrupted by Alzheimer-related PS1 mutations. *Cell* 141:1146-1158.
20. Ji, Z.S., Mullendorff, K., Cheng, I.H., Miranda, R.D., Huang, Y., and Mahley, R.W. 2006. Reactivity of apolipoprotein E4 and amyloid beta peptide: lysosomal stability and neurodegeneration. *J Biol Chem* 281:2683-2692.
21. Wang, Y., and Floor, E. 1998. Hydrogen peroxide inhibits the vacuolar H<sup>+</sup>-ATPase in brain synaptic vesicles at micromolar concentrations. *J Neurochem* 70:646-652.
22. Lipinski, M.M., Zheng, B., Lu, T., Yan, Z., Py, B.F., Ng, A., Xavier, R.J., Li, C., Yankner, B.A., Scherzer, C.R., et al. 2010. Genome-wide analysis reveals mechanisms modulating autophagy in normal brain aging and in Alzheimer's disease. *Proc Natl Acad Sci U S A* 107:14164-14169.
23. Yamamoto, A., Tagawa, Y., Yoshimori, T., Moriyama, Y., Masaki, R., and Tashiro, Y. 1998. Bafilomycin A1 prevents maturation of autophagic vacuoles by inhibiting fusion between autophagosomes and lysosomes in rat hepatoma cell line, H-4-II-E cells. *Cell Struct Funct* 23:33-42.
24. Kawai, A., Uchiyama, H., Takano, S., Nakamura, N., and Ohkuma, S. 2007. Autophagosome-lysosome fusion depends on the pH in acidic compartments in CHO cells. *Autophagy* 3:154-157.
25. Coen, K., Flannagan, R.S., Baron, S., Carraro-Lacroix, L.R., Wang, D., Vermeire, W., Michiels, C., Munck, S., Baert, V., Sugita, S., et al. 2012. Lysosomal calcium homeostasis defects, not proton pump defects, cause endo-lysosomal dysfunction in PSEN-deficient cells. *J Cell Biol* 198:23-35.
26. Lu, Y., Hao, B.X., Graeff, R., Wong, C.W., Wu, W.T., and Yue, J. 2013. Two pore channel 2 (TPC2) inhibits autophagosomal-lysosomal fusion by alkalinizing lysosomal pH. *J Biol Chem* 288:24247-24263.
27. Steinberg, B.E., Huynh, K.K., Brodovitch, A., Jabs, S., Stauber, T., Jentsch, T.J., and Grinstein, S. 2010. A cation counterflux supports lysosomal acidification. *J Cell Biol* 189:1171-1186.
28. Forgac, M. 2007. Vacuolar ATPases: rotary proton pumps in physiology and pathophysiology. *Nat Rev Mol Cell Biol* 8:917-929.
29. Kawasaki-Nishi, S., Bowers, K., Nishi, T., Forgac, M., and Stevens, T.H. 2001. The amino-terminal domain of the vacuolar proton-translocating ATPase a subunit controls targeting and in vivo dissociation, and the carboxyl-terminal domain affects coupling of proton transport and ATP hydrolysis. *J Biol Chem* 276:47411-47420.
30. Owegi, M.A., Pappas, D.L., Finch, M.W., Jr., Bilbo, S.A., Resendiz, C.A., Jacquemin, L.J., Warriar, A., Trombley, J.D., McCulloch, K.M., Margalef, K.L., et al. 2006. Identification

- of a domain in the V0 subunit d that is critical for coupling of the yeast vacuolar proton-translocating ATPase. *J Biol Chem* 281:30001-30014.
31. Kim, Y.C., Park, H.W., Sciarretta, S., Mo, J.S., Jewell, J.L., Russell, R.C., Wu, X., Sadoshima, J., and Guan, K.L. 2014. Rag GTPases are cardioprotective by regulating lysosomal function. *Nat Commun* 5:4241.
  32. Kuma, A., Hatano, M., Matsui, M., Yamamoto, A., Nakaya, H., Yoshimori, T., Ohsumi, Y., Tokuhisa, T., and Mizushima, N. 2004. The role of autophagy during the early neonatal starvation period. *Nature* 432:1032-1036.
  33. Soong, T.R., Barouch, L.A., Champion, H.C., Wigley, F.M., and Halushka, M.K. 2007. New clinical and ultrastructural findings in hydroxychloroquine-induced cardiomyopathy--a report of 2 cases. *Hum Pathol* 38:1858-1863.
  34. Kroemer, G., and Levine, B. 2008. Autophagic cell death: the story of a misnomer. *Nat Rev Mol Cell Biol* 9:1004-1010.
  35. King, J.S., Gueho, A., Hagedorn, M., Gopaldass, N., Leuba, F., Soldati, T., and Insall, R.H. 2013. WASH is required for lysosomal recycling and efficient autophagic and phagocytic digestion. *Mol Biol Cell* 24:2714-2726.
  36. Maejima, Y., Kyoi, S., Zhai, P., Liu, T., Li, H., Ivessa, A., Sciarretta, S., Del Re, D.P., Zablocki, D.K., Hsu, C.P., et al. 2013. Mst1 inhibits autophagy by promoting the interaction between Beclin1 and Bcl-2. *Nat Med* 19:1478-1488.
  37. Ciechomska, I.A., Goemans, G.C., Skepper, J.N., and Tolkovsky, A.M. 2009. Bcl-2 complexed with Beclin-1 maintains full anti-apoptotic function. *Oncogene* 28:2128-2141.
  38. Herman, E.H., and Ferrans, V.J. 1998. Preclinical animal models of cardiac protection from anthracycline-induced cardiotoxicity. *Semin Oncol* 25:15-21.
  39. Force, T., and Kolaja, K.L. 2011. Cardiotoxicity of kinase inhibitors: the prediction and translation of preclinical models to clinical outcomes. *Nat Rev Drug Discov* 10:111-126.
  40. Singal, P.K., and Iliskovic, N. 1998. Doxorubicin-induced cardiomyopathy. *N Engl J Med* 339:900-905.
  41. Sterba, M., Popelova, O., Vavrova, A., Jirkovsky, E., Kovarikova, P., Gersl, V., and Simunek, T. 2013. Oxidative stress, redox signaling, and metal chelation in anthracycline cardiotoxicity and pharmacological cardioprotection. *Antioxid Redox Signal* 18:899-929.
  42. Doroshov, J.H., Locker, G.Y., and Myers, C.E. 1980. Enzymatic defenses of the mouse heart against reactive oxygen metabolites: alterations produced by doxorubicin. *J Clin Invest* 65:128-135.
  43. Wen, X., Wu, J., Wang, F., Liu, B., Huang, C., and Wei, Y. 2013. Deconvoluting the role of reactive oxygen species and autophagy in human diseases. *Free Radic Biol Med* 65:402-410.
  44. Chen, Y.R., and Zweier, J.L. 2014. Cardiac mitochondria and reactive oxygen species generation. *Circ Res* 114:524-537.
  45. Nakanishi, H., and Wu, Z. 2009. Microglia-aging: roles of microglial lysosome- and mitochondria-derived reactive oxygen species in brain aging. *Behav Brain Res* 201:1-7.

46. Kubota, C., Torii, S., Hou, N., Saito, N., Yoshimoto, Y., Imai, H., and Takeuchi, T. 2010. Constitutive reactive oxygen species generation from autophagosome/lysosome in neuronal oxidative toxicity. *J Biol Chem* 285:667-674.
47. Wallace, K.B. 2003. Doxorubicin-induced cardiac mitochondrionopathy. *Pharmacol Toxicol* 93:105-115.
48. Dhingra, R., Margulets, V., Chowdhury, S.R., Thliveris, J., Jassal, D., Fernyhough, P., Dorn, G.W., 2nd, and Kirshenbaum, L.A. 2014. Bnip3 mediates doxorubicin-induced cardiac myocyte necrosis and mortality through changes in mitochondrial signaling. *Proc Natl Acad Sci U S A* 111:E5537-5544.
49. Settembre, C., Di Malta, C., Polito, V.A., Garcia Arencibia, M., Vetrini, F., Erdin, S., Erdin, S.U., Huynh, T., Medina, D., Colella, P., et al. 2011. TFEB links autophagy to lysosomal biogenesis. *Science* 332:1429-1433.